Magnetically induced currents and magnetic response properties of molecules

Dissertation for the degree of Doctor Philosophiae

Stefan Taubert
University of Helsinki
Faculty of Science
Department of Chemistry
Laboratory for Instruction in Swedish
P.O. Box 55 (A.I. Virtanens plats 1)
FI-00014 University of Helsinki, Finland

To be presented, with the assent of the Faculty of Science, University of Helsinki, for public discussion in Auditorium A129, Department of Chemistry (A.I. Virtanens plats 1, Helsinki), June the 21st, 2011, at noon.

Helsinki 2011

Supervised by

Prof. Dage Sundholm
Department of Chemistry
University of Helsinki
Helsinki, Finland

Prof. Juha Vaara
Department of Physics
University of Oulu
Oulu, Finland

Reviewed by

Doc. Antti Karttunen
Department of Chemistry
University of Eastern Finland
Joensuu, Finland

Prof. Stefano Pelloni
Dipirtimento di Chimica
Università degli studi di Modena e Reggio Emilia
Modena, Italy

Opponent

Prof. Trond Saue
Laboratoire de Chimie et Physique Quantiques
Universitié de Toulouse
Toulouse, France

ISBN 978-952-92-9143-4 (Paperback)
ISBN 978-952-10-7046-4 (PDF)
http://ethesis.helsinki.fi
Yliopistopaino Helsinki 2011

Acknowledgements

The research related to the thesis was conducted at the Department of Chemistry, University of Helsinki in the Molecular Magnetism group at the Laboratory of Physical Chemistry as well as in the Laboratory for Instruction in Swedish.

I am greatly indebted to my supervisors, Dage Sundholm and Juha Vaara, for the guidance and education I have had the privilege to receive during the years. Dage is an outstanding chemist with a broad knowledge and a deep understanding, still with the ability to explain involved phenomena in everyday words and his office door is always open when he is around. Juha is a physicist and expert on molecular properties. He has got an enormous patience in explaining both molecular physics and computer code technicalities, combined with an extremely careful attitude when it comes to scientific accuracy. The passion of one of you and the pragmatic attitude of the other one is striking, and I have tried to learn from both. Thank you for being great supervisors!

Without the undergraduate lectures and laboratory works under the guidance of the excellent teacher Henrik Konschin, I would probably not have walked into the exciting world of computational chemistry. Thank you, HK, for still being supportive. Pekka Pyykkö, thank you for good advice in several discussions and for the lectures in thermodynamics and relativistic quantum chemistry that have shown that chemistry indeed is beautiful. Also, thank you for reading and commenting on the thesis. During the chemistry lessons given by Stefan Gustafsson I realized I wanted to study chemistry at the university. Thank you for showing that natural sciences is a serious matter, and at the same time great fun.

I want to thank Michal Straka for collaboration and for all the discussions about endohedral fullerene chemistry and about life, and for the hospitality during my visit to Prague. Fabio Pichierri has been a source of many ideas and suggestions and he was a co-author on several papers. Antti Karttunen and Stefano Pelloni prereviewed the thesis and are thanked for valuable comments and suggestions. Thanks also to those who read and commented manuscripts on the coffee room table.

The Molecular Magnetism group was my working place for most of the time I worked on the thesis. I also spent quite much time at the Laboratory for Instruction in Swedish. The atmosphere there is really special — relaxed and scientifically inspiring, and above all, friendly. Much of the sunshine in the lab has been due to the previous secretary Susanne Lundberg and the present secretary Raija Eskelinen, who always were extremely helpful. Many thanks to the people at Svenska Kemen and in the Helsinki node of the Molecular Magnetism group: Helmi Liimatainen, Marja Hyvärinen, Sanna Kangasvieri, Jouni Karjalainen, Jelena Telenius, Sergio Losilla-Fernandez, Patryk Zaleski-Ejgierd, Cong Wang, Tommy Vänskä, Bertel Westermark, Anneka Tuomola, Nina Siegfrids, Janne Pesonen, Gustaf Boije af Gennäs, and all other past and present members of the lab. Especially thanks to Ying-Chan Lin, Heike Fliegl, Michael Patzschke, Olli Lehtonen, Perttu Lantto, Suvi Ikäläinen, Teemu O. Pennanen, Jonas Jusélius, Nergiz Özcan, Jirí Mares, Pekka Manninen, Ville Kaila, Nino Runeberg, Raphael Berger, and Mikael Johansson for many discussions and for sharing scripts, coordinates, expertise and ideas.

The computational resources provided by the CSC IT-Center for Science have been of importance in many of the projects and the Helpdesk-expertise has been essential to solve some problems. I acknowledge the financial support for the thesis and for traveling to conferences and summer schools from Magnus Ehrnrooth Foundation, Alfred Kordelin Foundation, Orion Research Foundation, the Chancellor of the University of Helsinki, Swedish Cultural Foundation in Finland, Oscar Öflund Foundation, Gust. Komppa Foundation, Academy of Sciences of the Czech Republic, and the LASKEMO Graduate School in Computational Chemistry and Molecular Spectroscopy.

I want to thank Johanna Virkkula for numerous metadiscussions in the commuter train, often related to research and sciences. I thank all my Friends in Scouting for shared experiences and for providing a counterweight to quantum chemistry.

A great support has come from my parents, Lisbeth and Håkan Taubert, and from my brothers Carl-Gustaf and Henrik and my sister Åsa. Tack ska ni ha! The encouragement from my dear in-laws and from the whole Arminen family means a lot. Kiitos!

Last, but not least, my own little family has a very special role in life. I want to express my deepest gratitude to my wife Paula Arminen and our son Juho. Your part in this thesis is greater than you might ever know.

Helsinki, 26th May 2011

Stefan Taubert

Contents

List of abbreviations

ACID	Anisotropy of the current-induced density
AIM	Atoms in molecules
AO	Atomic orbital
ARCS	Aromatic ring-current shieldings
ASE	Aromatic stabilization energy
B3LYP	The Becke-3 Lee-Yang-Parr hybrid density functional
BLA	Bond-length alternation
BP86	The Becke-Perdew 86 GGA density functional
CC2	Coupled-cluster with double excitations treated using perturbation theory
CCS	Coupled-cluster singles
CCSD	Coupled-cluster singles and doubles
CCSD(T)	CCSD with a perturbative treatment of the triple excitations
CCSDT	Coupled cluster singles, doubles and triples
CHF	Coupled Hartree-Fock
CP	Cycloparaphenylene
CSGT	Continuous set of gauge transformations
CTOCD	The Continuous transform of the current-density approach
DFT	Density-functional theory
ELF	Electron localization function
ESR	Electron spin resonance
GIAO	Gauge-including atomic orbitals
GIMIC	The Gauge-Including Magnetically Induced Current-method
GGA	Generalized gradient approximation
HF	Hartree-Fock
HMO	Hückel molecular orbital
HOMA	Harmonic oscillator model of aromaticity
IGAIM	Individual gauges for atoms in molecules
IUPAC	International union of pure and applied chemistry
LDA	Local density approximation
L_k	Linking number
MD	Molecular dynamics
MO	Molecular orbital
MP2	Møller-Plesset perturbation theory of the second order
NICS	Nucleus-independent chemical shift
NMR	Nuclear magnetic resonance
PBE	The Perdew-Becke-Ernzerhof GGA density functional
pNMR	Paramagnetic NMR
POAV	π-orbital axis vector
SCF	Self-consistent field
TPSS	The Tao-Perdew-Staroverov-Scuseria meta-GGA density functional
UCHF	Uncoupled Hartree-Fock
T_w	Twist
W_r	Writhe

List of publications

List of publications included in the thesis and the author's contributions

I S. Taubert, M. Straka, T. O. Pennanen, D. Sundholm, and J. Vaara, "Dynamics and magnetic resonance properties of $Sc_3C_2@C_{80}$ and its anion" *Phys. Chem. Chem. Phys.* 2008, **10**, 7158–7168.

S.T. performed all the calculations and wrote the first version of the manuscript.

II S. Taubert, D. Sundholm, J. Jusélius, W. Klopper, and H. Fliegl, "Calculation of magnetically induced currents in hydrocarbon nanorings" *J. Phys. Chem A.* 2008, **112**, 13584–13592.

S.T. performed all the NMR and GIMIC calculations and wrote the first version of the corresponding Results section.

III S. Taubert, D. Sundholm, and F. Pichierri, "Magnetically induced currents in Bianthraquinodimethane-stabilized Möbius- and Hückel [16]annulenes" *J.Org. Chem.* 2009, **74**, 6495–6502.

S.T. performed part of the geometry optimizations and all of the NMR and GIMIC calculations and wrote the first version of the corresponding Results sections.

IV H. Fliegl, D. Sundholm, S. Taubert, J. Jusélius, and W. Klopper, "Magnetically Induced Current Densities in Aromatic, Antiaromatic, Homoaromatic, and Nonaromatic Hydrocarbons" *J. Phys. Chem. A.* 2009, **113**, 8668–8676.

S.T. participated in setting up the GIMIC calculations and in the analysis of the results.

V H. Fliegl, D. Sundholm, S. Taubert, and F. Pichierri, "The aromatic pathways in twisted hexaphyrins" *J. Phys. Chem. A.* 2010, **114**, 7153–7161.

S.T. did the HOMA analysis and wrote the corresponding part of the manuscript and participated in the analysis of the results in the article.

VI S. Taubert, D. Sundholm, and F. Pichierri, "Magnetically induced currents in [n]cycloparaphenylenes." *J. Org. Chem.* 2010, **75**, 5867–5874.

S.T. performed part of the geometry optimizations and all the GIMIC calcula-

tions and wrote a large part of the manuscript.

VII S. Taubert, V. R. I. Kaila, and D. Sundholm, "Aromatic pathways in conjugated rings connected by single bonds." *Int. J. Quantum. Chem.* 2011, **111**, 848–857.

S.T. performed the majority of the GIMIC calculations. and wrote a large part of the Results section.

VIII S. Taubert, D. Sundholm, and J. Jusélius, " Calculation of spin-current densities using gauge-including atomic orbitals" *J. Chem. Phys.* 2011, **134**, 054123:1-12.

S.T. did the calculations on the boron and aluminum trimers and all the NICS calculations; participated in the analysis of the results and wrote the first version of corresponding parts of the manuscript.

List of other publications

I S. Taubert, H. Konschin, and D. Sundholm, "Computational studies of C-13 chemical shifts of saccharides" *Phys. Chem. Chem. Phys.* 2005, **7**, 2561–2569.

II D. Sundholm, S. Taubert, and F. Pichierri, "Calculation of absorption and emission spectra of [n]cycloparaphenylenes: the reason for the large Stokes shift" *Phys. Chem. Chem. Phys.* 2010, **12**, 2751–2757.

III T. O. Pennanen, J. Machácek, S. Taubert, J. Vaara, and D. Hnyk, "Ferrocene-like iron bis(dicarbollide), $[3\text{-}Fe^{III}\text{-}(1,2\text{-}C_2B_9H_{11})_2]^-$. The first experimental and theoretical refinement of a paramagnetic ^{11}B NMR spectrum" *Phys. Chem. Chem. Phys.* 2010, **12**, 7018–7025.

1 Introduction

The response of molecules to external fields, that can be measured in different spectroscopies, provides a vast amount of data. Analysis of the data yields detailed information about molecular properties. In a nuclear magnetic resonance (NMR) or an electron spin resonance (ESR) experiment the molecule is subjected to a magnetic field. The NMR and ESR spectra give information about geometry, electronic structure, spin state, spin localization, etc [1–4]. When an electron situated in the region around a nucleus is subject to a magnetic field, classical electrodynamics predicts that a current is induced. This local atomic current induces a secondary magnetic field which causes the nucleus to become shielded or deshielded [5, 6]. Since the electronic structure in the vicinity of the nucleus depends on the character of the nearest chemical bonds, measurements of the nuclear shielding constants can be utilized to probe the molecular structure.

In molecules that possess one or several circular pathways with delocalized electrons, the external magnetic field can also give rise to ring currents along the molecular framework [7–11]. A further magnetic field is induced by the ring current. If this induced magnetic field is antiparallel to the external field, locally the magnetic field will be weaker than the external field and the nuclei are said to be shielded. If the induced magnetic field is parallel to the external field, thus giving a locally stronger magnetic field, the nuclei will be deshielded. The direction of the secondary magnetic field depends on the direction of the ring current. In compounds where the diatropic ring current dominates, the nuclei outside the molecular ring are deshielded while the region inside the ring is shielded. Such compounds are said to be aromatic, with benzene as an obvious example. In antiaromatic molecules, e.g., cyclobutadiene, a paratropic ring current is induced, and the nuclei on the outside of the ring are shielded while the inside of the ring is deshielded.

In this thesis, the current delocalization pathways in conjugated hydrocarbons, fullerenes and small metal clusters are investigated. The concept of aromaticity is closely related to the existence of ring currents. Aromaticity is, however, a concept lacking an unequivocal definition, and this work will not provide one either. Instead, the ring currents themselves together with NMR chemical shifts are the main topic. The aromaticity of the investigated systems will be discussed in light of the magnetic properties. The results have been published in eight papers, referred to as Paper I-VIII in the text. In addition, some previously unpublished results on the ring currents in $Sc_3C_2@C_{80}$ and in coronene are presented. Paper I describes the

magnetic resonance parameters and the dynamical nature of $Sc_3C_2@C_{80}$. In Paper II, the ring-current strengths in a series of nano-sized hydrocarbon rings are related to static polarizabilities and to ^{1}H NMR shieldings; a direct relationship between ring-current strengths and ^{1}H NMR shieldings is confirmed. Paper III is a case study on the possible aromaticity of a novel Möbius-shaped [16]annulene. In Paper IV, aromatic, homoaromatic, antiaromatic, and nonaromatic ring-shaped hydrocarbons are characterized from the ring-current point of view. Paper IV provides a validation of the GIMIC method as a probe for possible aromaticity. The case studies on hexaphyrins and [n]cycloparaphenylenes in Papers V and VI show that explicit calculations are needed to unravel the ring-current delocalization pathways in complex multiring molecules. In Papers VII and VIII, the total ring currents and the spin currents are calculated for single-ring and bi-ring molecules with open shells.

2 Molecular magnetic properties and aromaticity

The International Union of Pure and Applied Chemistry (IUPAC) has defined aromaticity within the framework of theoretical organic chemistry as a property of systems that are thermodynamically stabilized as a consequence of cyclic electron delocalization [12]. This suggests that aromaticity is primarily to be defined based on the observable energy, and that the underlying reasons for the stabilization of so called aromatic compounds is the electron delocalization. Bond length equalization as well as the "existence of the diamagnetic ring current induced in a conjugated cyclic molecule by an external magnetic field and manifested by an exaltation and anisotropy of magnetic susceptibility", are complementary criteria of aromaticity, according to IUPAC. In this thesis, the magnetic criterion is adopted in a pragmatic manner: A molecule that has a net diatropic ring current may be aromatic. Similarly, a net paratropic ring current is descriptive for possibly antiaromatic molecules, whereas molecules with a zero ring current are considered nonaromatic. The correlation between diatropic ring currents and aromatic character is not exclusive, which is evident by considering cyclopropane that has a ring current as a consequence of the forced overlap of σ orbitals due to ring strain.

The stabilization of aromatic molecules can be realized by considering the phenomenon of resonance. Slater used the term "shared valence" to describe how the structure of the benzene molecule appears to be a combination of two Kekulé structures [13]. Pauling and Wheland considered all the canonical structures of benzene and naphthalene and obtained a measure of the resonance energy [14]. As a consequence of the "shared valence", the total energy of the benzene molecule will be lower than that of any single Lewis structure [15]. Although benzene is an obvious example, the same phenomenon is naturally observed in more complex molecules, too. Pauling writes, regarding higher condensed ring systems, that "The stabilization of the molecules by resonance gives them aromatic character in the same way as for benzene" [15].

The delocalized electronic structure of aromatic compounds also yields enhanced planarity, equalized bond lengths, enhanced stability due to resonance, favoring of substitution instead of addition that would be typical for isolated double bonds, and the ability to sustain ring currents when exposed to external magnetic fields. In this thesis, the focus is not so much on the nature of the aromaticity, but on the

ring currents. Ring currents are not observed directly in the experiment but the effect thereof is seen in many experimental observables, as discussed below. The nuclear magnetic shieldings and NMR chemical shifts of the hydrogen nucleus play a special role in assessing ring currents. There is generally a small electron density around the protons and therefore the ^{1}H NMR chemical shifts are sensitive to external factors such as ring currents. In the following Sections, different methods to assess aromaticity will be discussed with emphasis on approaches related to ring currents.

2.1 Ring currents and delocalization

The modern understanding of the ring currents in aromatic molecules is based on the Pauling-Lonsdale-London model. Pauling [7] and Lonsdale [8] calculated magnetic susceptibilities of benzene and condensed conjugated hydrocarbon molecules, assuming that the π electrons were able to move independently from the bonding electrons in the σ framework. The theory was built upon the molecular orbital theory by Hückel [16–18]. London presented the first quantum mechanical description of the ring current [9].

It is not only derivatives of benzene and condensed hydrocarbons that can have ring currents. Compounds such as Al_4^{2-} [19], the golden fullerene Au_{32} [20], B_3^- [21], and the B_{20} toroid [22] have been shown to be able to have time-independent ring currents that arise due to electron delocalization.

Pople showed in 1956 that the increased ^{1}H NMR chemical shifts in benzene and its derivatives can be explained by a diamagnetic current circulating around the benzene ring [23]. A molecular orbital theory of ring currents was subsequently published in 1958 by Pople [11].

Musher [24, 25] argued against the connection between ring currents and electron delocalization. Musher showed that the anisotropic susceptibilities for 16 aromatic hydrocarbons could be reliably calculated from anisotropic Pascal's constants for aromatic carbon atoms. Fleischer *et al* [26] showed that the NMR shielding tensors and magnetic susceptibility tensors for benzene and cyclohexatriene give evidence for a ring-current effect in benzene. They used the individual gauge for localized orbitals (IGLO) method in the calculations. The shortcomings of Musher's anti-theory have also been analyzed by Lazzeretti [27]. The ring-current effect on the proton NMR shieldings has been questioned by proposing that the deshielding of the protons in benzene is due to the σ electrons [28, 29]. On the other hand, the σ electrons do cause deshielding of the benzene protons, even though the ring current of the π electron cloud is the major contribution to the deshielding [30]. In Paper II, we show a direct relationship between the shielding of inner hydrogens in large delocalized hydrocarbon ring-shaped molecules and the size of the ring-current susceptibility. In the studied molecules, the effects on the shieldings caused by the molecular framework can be expected to be the same. Although the ring currents have a notable impact on ^{1}H NMR shieldings, also structural effects, solvent, and non-bonded interactions must be taken into account when analyzing anomalous NMR chemical shifts of protons, as shown in Paper V and elsewhere [31, 32].

The London-type theories for ring current came short in not accounting for the electron repulsion. This was a deficiency of the Hückel theory that the London model was built upon. An improvement was to introduce the coupled and uncoupled Hartree-Fock methods in the calculation of ring-current contributions to magnetic susceptibilities and nuclear shieldings [33, 34]. Later on, semiempirical methods based on the Biot-Savart law have been used by Haddon [35, 36]. In this thesis, the gauge including magnetically induced current (GIMIC) method [37] is used to calculate the magnetically induced ring-current susceptibilities explicitly.

In Figures 2.1 and 2.2 the ring current in benzene obtained from GIMIC calculations is visualized in three different ways. The signed modulus of the ring-current density vectors gives the three-dimensional scalar distribution of the ring current. The isocurve cut-through of the 3D-current density shows that a large part of the ring current flows in the ring plane and not only in the π space as traditionally claimed [38]. The gradient of the ring-current with respect to the x coordinate is shown in Figure 2.2. The ring-current gradient along the x axis gives an idea about the distribution of the paratropic and the diatropic ring currents. When the x axis is turned in the xy plane so that it is at an angle of 10° to the nearest C–H bond, the diatropic ring current can be seen to take the path around the hydrogen. The paratropic ring current profile for the axis cutting the C–C bond at the middle and for the axis cutting the C–C bond close to the carbon are very similar, which shows that the ring current is not merely a superposition of bond currents but it is delocalized along the ring. To get a quantitative measure of the ring current at any given bond in the molecule, one has to integrate the current density over a grid cutting that bond.

Although the GIMIC method strictly defined yields a susceptibility, in practice the term "current strength" will be used here. The relationship between the current strength and the current susceptibility is linear in the magnetic field strength in units of Tesla.

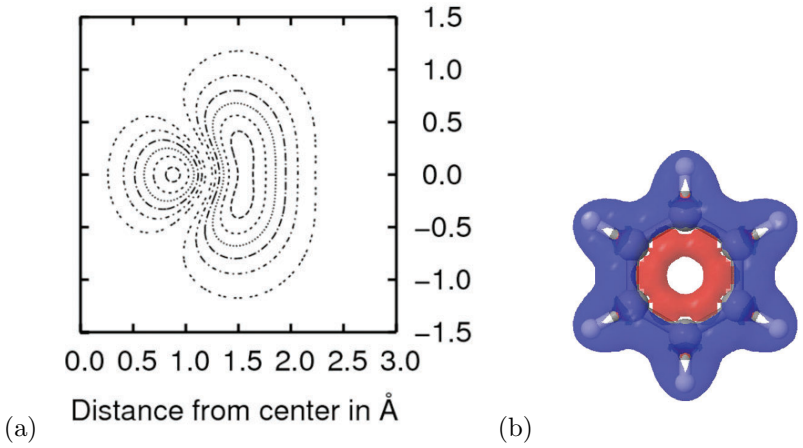

Figure 2.1: The ring current density in benzene consists of a paratropic current on the inside and a diatropic current on the outside of the ring. In the molecular plane the two contributions are equal and cancel while the diatropic component dominates above and below the ring. (a) The contour plot shows the cross section of the modulus of the ring current. The C–C bond of benzene is at (1.22,0.0) Å and it is perpendicular to the xy plane, and the center of the ring is at the origin. (b) The signed modulus of the ring current vector. The paratropic current is shown in red and the diatropic component is blue.

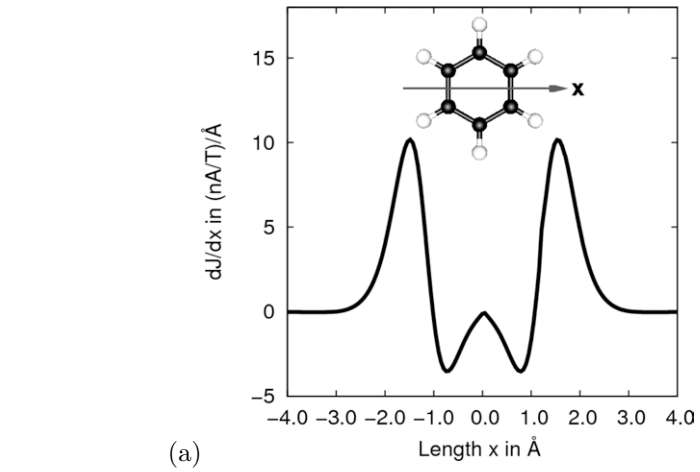

(a)

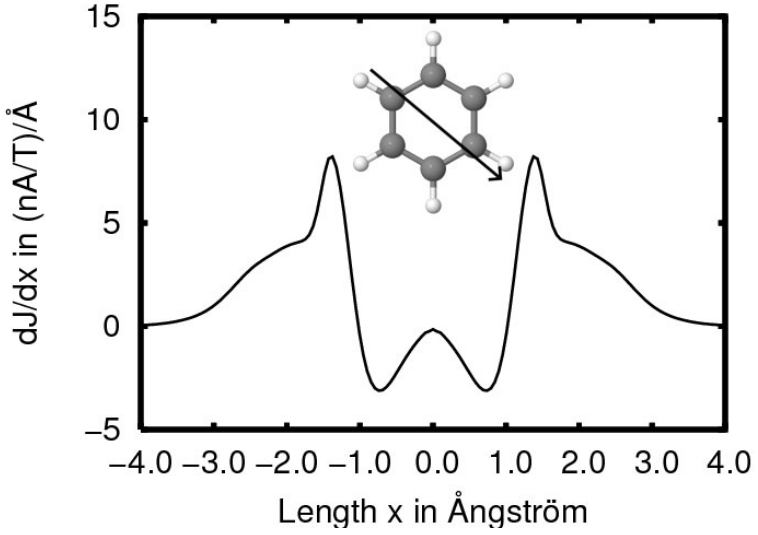

(b)

Figure 2.2: The ring current density in benzene consists of a paratropic current on the inside and a diatropic current on the outside of the ring. In the molecular plane the two contributions are equal and cancel while the diatropic component dominates above and below the ring. (a) The ring-current gradient along the arrow passing through the C–C bond in benzene gives the derivative $\partial J/\partial x$ of the cumulative integrated current strength J from the center of the ring outwards along the x direction. The ring-current region is extended to about 3.0 Å from the ring center. (b) The ring-current gradient along the axis passing close to a C nucleus. The angle between the axis and the closest C–H bond is 10 degrees.

The ring current induces a secondary magnetic field which in paratropic regions enhances the external magnetic field and in diatropic regions opposes the external field. Consequently, nuclei in the paratropic region become further shielded and, consequently, the chemical shift is smaller. The enhanced shielding in the paratropic current region is demonstrated in Figure 2.3, where the NMR shielding of protons residing inside the ring-current pathway is compared to the ring current strength.

Since it is not yet possible to directly measure the ring-current strength in molecules, the ring-current has to be observed indirectly through other observables.

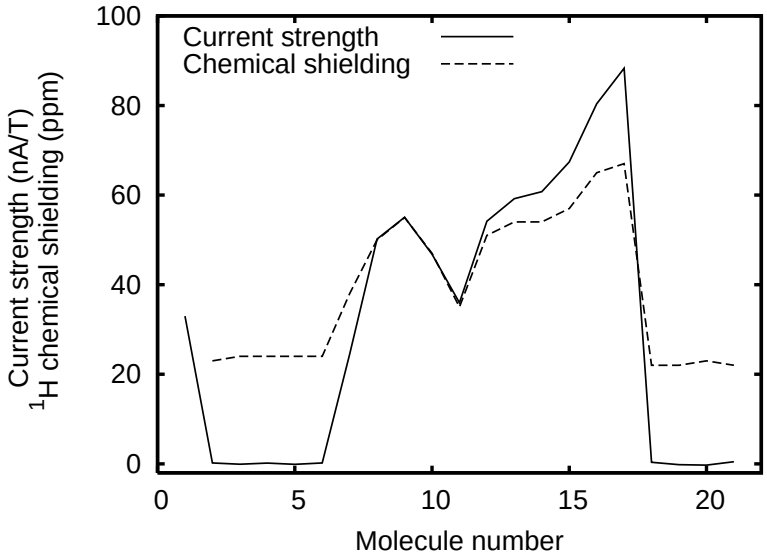

Figure 2.3: Comparison of the global ring current (in nA/T) and the ^{1}H NMR shieldings (in ppm) in the hydrocarbon nanorings of Paper II. The nuclear shieldings are calculated for the hydrogen in the corner group directed towards the center of the main ring. The molecules are shown in Figures 4.2-4.5.

The pioneering ring current models by Pauling [7], Lonsdale [8], London [9], and Pople [11] were constructed based on observations of magnetic susceptibilities and NMR chemical shifts. The magnetic susceptibility tensor χ and the NMR shielding tensor σ can be directly related to the current density tensor $\mathcal{J}_\gamma^{\mathcal{B}_\delta}(\mathbf{r})$ through Eqs. (2.1) and (2.2). [39]

$$\chi_{\alpha\delta} = \frac{1}{2c}\epsilon_{\alpha\beta\gamma}\int \mathrm{d}^3r\ r_\beta \mathcal{J}_\gamma^{\mathcal{B}_\delta}(\mathbf{r}) \tag{2.1}$$

$$\sigma_{\alpha\beta}^I = -\frac{1}{c}\epsilon_{\alpha\beta\gamma}\int \mathrm{d}^3r\ \frac{r_\beta - R_{I\beta}}{|\mathbf{r}-\mathbf{R}_I|^3}\mathcal{J}_\gamma^{\mathcal{B}_\delta}(\mathbf{r}) \tag{2.2}$$

In Eqs. (2.1) and (2.2), c is the speed of light. The Levi-Civita symbol $\epsilon_{\alpha\beta\gamma}$ takes the value of one for even permutations α,β,γ = (1,2,3), (3,1,2), (2,3,1), minus one for odd permutations α,β,γ = (3,2,1), (1,3,2), (2,1,3), and zero if two elements are the same, i.e., if $\alpha = \beta, \alpha = \gamma$, or $\beta = \gamma$.

An excessive electron delocalization increases the planarity of multiring hydrocarbons. It might still be quite easy to twist these molecules. For example for naphthalene, which is the simplest acene, the barrier for a twist around its 'waist' by 20^o is as low as 13.4 kJ/mol at the B3LYP/6-31G(d) level [40]. As pointed out by Haddon and Scott [41], the collinearity of the π-orbital axis vector (POAV) at adjacent atoms is a more rigorous measure of maintained conjugation than merely the geometrical torsion angle. Biphenyl, C_6H_5–C_6H_5, has a torsional angle between the two arene rings of 39° [42], but in its triplet state biphenyl is planar and the ring-current density is delocalized over the whole molecule, as shown in Paper VII.

Electron delocalization is manifested in several ways. There are therefore many different aromaticity probes that all to some extent rely on the prerequisite of an

increased delocalization of electrons. These aromaticity indices are further discussed in Subsection 2.4.

2.2 Hückel and Möbius aromaticity and antiaromaticity

The archetypal aromatic compound is benzene, first discovered by Faraday in 1825 [43]. In 1872, Kekulé explained the structure of benzene with six equivalent carbon atoms by assuming that the carbon atoms vibrated [44]. The modern understanding of the bonding situation with the six delocalized electrons was captured by Crocker in 1922 [45] and a few years later by Amit and Robinson [46]. The electronic structure of benzene was explained by Hückel in a series of papers in 1931-1932 [16–18] starting from the special stability caused by the six electrons in benzene and in related heterocycles such as furan, pyridin, pyrrole and tiophene and ending up in formulating the Hückel molecular orbital (HMO) method. The general $(4n+2)$ rule for aromaticity was also formulated by Hückel, in 1938 [47]. Von Doering found that the same stability holds also for cycloheptatrienylium oxide [48]. The term Hückel aromaticity has in recent years been extended also to non-planar conjugated systems.

The Möbius band is a well-known concept in mathematics. If one takes a strip of paper, twist its end by 180 degrees around the axis parallel with the long side of the strip, and then attaches the ends to each other, then one will have a one-sided surface — a Möbius band. It was introduced, apparently independently, by Möbius and Listing [49], in the 19th century. Heilbronner brought the concept of Möbius molecules into chemistry proposing that $4n$ π electrons would make up a filled shell in a twisted conjugated molecular ring resulting in an aromatic stabilization [50].

In conjugated molecules, the π orbitals can be thought to form a ribbon. In Hückel molecules, the ribbon has no twists and, consequently, has two sides. As proposed by Zimmermann in 1966 [51], classical Möbius molecules have one twist in the π orbital ribbon, which makes them one-sided. Zimmermann points out that there is a sign inversion in the adjacent p_z orbitals at the twist. From Heilbronner's original paper, no sign inversion is directly deducible [50]. Heilbronner showed that the unstable open-shell electron configuration which arises from $4n$ π electrons in a planar Hückel type of molecule is stabilized by a Möbius twist. The twist can be evenly distributed by tilting every p_z orbital by an angle of $\frac{\pi}{n}$, where n is the total number of p_z orbitals in the molecule. Solving the secular equation in the framework of Hückel molecular orbital theory yields a stable closed-shell configuration [50]. Another way to obtain the same result is to solve the HMO secular equation with two resonance integrals equal to $-\beta$ instead of β to account for the phase change of the orbitals [49]. The secular equations within HMO theory for annulenes with Hückel and Möbius topology

are shown in Eq. (2.3) below.

$$\text{Hückel}: \begin{vmatrix} \alpha-\mathrm{E} & \beta & \cdots & \cdots & \beta \\ \beta & \alpha-\mathrm{E} & \beta & & \vdots \\ \vdots & & \ddots & \ddots & \beta \\ \beta & \cdots & \cdots & \beta & \alpha-\mathrm{E} \end{vmatrix} ; \quad \text{Möbius}: \begin{vmatrix} \alpha-\mathrm{E} & \beta & \cdots & \cdots & -\beta \\ \beta & \alpha-\mathrm{E} & \beta & & \vdots \\ \vdots & & \ddots & \ddots & \beta \\ -\beta & \cdots & \cdots & \beta & \alpha-\mathrm{E} \end{vmatrix} \tag{2.3}$$

As the Möbius ribbon was born within the field of mathematical topology, also methods of classifying the Möbius structures have been incorporated into chemistry from mathematics. According to the Călugăreanu-White-Fuller theorem [52–55], one can define the twist T_w and the writhe W_r such that the sum is an integer, the linking number L_k.

$$L_k = T_w + W_r \tag{2.4}$$

The twisting number T_w is a measure of how much the ribbon is twisted about its own axis while the writhe indicates how much of the strain caused by the twist is compensated for by non-planarity along the ribbon [56]. For molecular rings, T_w is a sum of the local relative twists of the atoms in the molecular ring. In conjugation chemistry, the writhe is a measure of how much adjacent p_z orbitals overlap and thus compensate the strain caused by the local twists. Generally, Möbius molecules are twisted by $n\pi$ radians around the ring, where n is a non-zero integer [57, 58]. Conventional Möbius molecules are twisted only once, by π radians. If the center line lies in a plane, then the writhe is zero and the linking number will equal the twisting number, $L_k = T_w = 1$. The Möbius twist of the molecular ring significantly affects the electronic structure. As found by Heilbronner, conjugated molecules with Hückel and conventional 2D Möbius topology have different π-electron count rules for aromaticity because of the changed degeneracy of the frontier orbitals. Thus, conventional conjugated molecules follow the following π electron count rules for aromaticity [47, 48]:

$4n$ π electrons: Aromatic when $L_k = 1$

$(4n+2)$ π electrons: Aromatic when $L_k = 0$

Wannere and coworkers define conjugated π ribbons with $L_k > 1$ as higher-order Möbius structures with a non-planar three-dimensional center line. These structures will have a non-planar three-dimensional center line and are claimed to be aromatic according to: [58]

$4n$ π electrons: Aromatic when $L_k = 2n+1$

$(4n+2)$ π electrons: Aromatic when $L_k = 2n$

where n is an integer. Antiaromaticity can analogously be expected for molecular rings with $4n$ π-electrons and even L_k or when the number of π-electrons is $(4n+2)$ and L_k is odd.

2.3 Generalized Hückel rules for arbitrary spin states

Similarly to the reversed aromaticity criterion that is valid for Möbius twisted molecules, it is also possible to formulate "Hückel rules" for open-shell systems. In 1972, Baird showed by means of semiempirical calculations that there is an enhanced resonance energy in delocalized π systems with 4π electrons in the triplet state [59]. Soncini and Fowler recently generalized this rule [60]. They found that $(4n + 2)$ π electrons correspond to aromaticity when the total spin $S = \sum_i s_i$ is even, i.e., S=0,2,4,... and to antiaromaticity for odd S such as S=1,3,5,.... For delocalized systems with $4n$ π electrons, odd S yields aromaticity and even S points to antiaromaticity.

2.4 Aromaticity indices

In this Subsection, different aromaticity probes are discussed. These probes are based on geometry, energy, magnetic response, and electric response. In Subsection 2.5, the different indices are discussed in a common context.

Geometrical aromaticity indices

The geometrical criteria for aromaticity rely on the bond-length equalization that is a consequence of the electron delocalization in conjugated π systems. An intuitive measure of bond length equalization would be the bond-length alternation (BLA). The harmonic oscillator model of aromaticity (HOMA) developed by Krygowski is a popular measure of the bond-length equalization. The HOMA index is calculated using Eq. (2.6) [61], for n bonds included in the summation:

$$\mathrm{HOMA} = 1 - \frac{\alpha}{n} \sum_{i}^{n} \left(R_{\mathrm{opt-R_i}}\right)^2 \tag{2.5}$$

Bonds including heteroatoms must be taken into account separately. For a conjugated hydrocarbon that contains nitrogen atoms, such as a porphyrin, the HOMA expression becomes

$$\mathrm{HOMA} = 1 - \frac{1}{n}\left[\alpha_{\mathrm{CC}} \sum_i (R_{\mathrm{CC,opt}} - R_{\mathrm{CC,i}})^2 + \alpha_{\mathrm{CN}} \sum_i (R_{\mathrm{CN,opt}} - R_{\mathrm{CN,i}})^2\right]. \tag{2.6}$$

The optimal bond length R_{opt} and the α parameter are determined empirically for each kind of bond X-Y, where X and Y are the same or different element. In the original HOMA-paper by Krygowski [61], the parameters for common bond types X-Y in organic molecules are listed.

For aromatic rings with a small BLA, the HOMA index is about 1. Very small or negative HOMA values mean that the ring consists of localized single and dou-

ble bonds suggesting that they are non- or antiaromatic [61, 62]. Herges has shown that the aromaticity trends predicted by HOMA do not correlate with calculated nucleus-independent chemical shift (NICS) values [63]. The inability to make ultimate predictions about ring-current delocalization paths using HOMA values is also demonstrated in Paper IV and discussed in Section 4.2.4. Ring currents that are a typical feature of aromatic molecules are sustained due to electron delocalization and bond-length equalization. Thus, it is not unexpected that also antiaromatic molecules with paratropic currents often will have a HOMA value that is closer to one than zero. It has also been shown that the aromatic character of benzene and higher annulenes is largely retained also for bond-localized structures [64, 65]. The dianions of the [n]cycloparaphenylenes [Paper VI], are quinoid and have a larger BLA than the neutral ones that consist of benzenoid arene rings connected by single bonds. Arene rings with a small bond length alternation can be classified as benzenoid. The average bond order of the C–C bonds is close to 1.5. Arene rings that have C–C bonds with a high double bond character and four single C–C bonds combined with two exocyclic double bonds are classified as quinoid. The dianions are aromatic with a strong ring current delocalized along the molecular ring, while the neutral [n]CPs are more or less nonaromatic. The first triplet state of biphenyl [Paper VII] is planar and quinoid with a current-density delocalization ranging over both rings. The singlet ground state is composed of two benzenoid phenyl rings that are staggered with a torsion angle of 39°. The two phenyl rings sustain individual ring currents. For coupled arene rings the electronic structure seems to be more important for the ring currents than the geometry. In the cross-linked phenol-imidazole anion in Paper VII, elongation of the C-N cross link from 136 to 142 pm affected the current strength along the bridge by only 2%.

Energetic aromaticity indices

The aromaticity was defined as the enhanced stability of a ring-shaped electron-delocalized molecule as compared to a bond-localized aliphatic counterpart [12]. The resonance energy arises from the fact that no single Lewis structure describes the electronic structure of some molecules alone. Instead, the real structure of the molecule is a weighted average of the contributing Lewis structures. Empirically the existence of a stabilizing resonance energy can be demonstrated by comparing the measured heat of formation of a compound with the heat of formation of any single valence-bond structure of the molecule in question, calculated from tabulated bond energies. For resonance hybrids the measured heat of formation will always be greater than the calculated one [15]. By constructing a method related to the HMO theory, Pauling and Wheland were able to determine the contribution of different valence-bond structures of benzene to the total energy [14].

The aromatic stabilization energy, ASE, was proposed by Dewar and Schmeising [66] as a measure of the aromatic stabilization of benzene. In the original version, they compared the energy of aliphatic butadiene with that of benzene. Different applications of the ASE model have been developed in order to establish the aro-

matic stabilization of delocalized π systems [67, 68]. The ASE is often calculated as the energy difference between the delocalized system and the same molecular framework with an enforced localization of the π electrons, e.g., by saturation or by adding doubly-bonded atoms to the aromatic ring [67, 69]. Experimentally, the ASE is determined by homodesmotic reactions [70]. If the delocalized system is less stable than the localized reference system, the ASE will be positive and the delocalized molecule is considered antiaromatic. For aromatic systems, the ASE is negative.

The major challenges in estimating the magnitude of the stabilization of aromatic compounds due to delocalization have been discussed in reviews by George [71] and Cyrański [72]. The main issue is to find the suitable reference compound with all the features of the compound to be analyzed, but which has no π electron conjugation. Depending on method of choice, the stabilization is found to be roughly between 84 and 209 kJ/mol for benzene [72]. George [71] has summarized a wide range of experimental results yielding stabilization energies for benzene of between 134 and 205 kJ/mol. At the DFT level, Schleyer and coworkers have calculated the resonance energy to be 138 kJ/mol [73].

Havenith [65] calculated the magnetizability and the polarizability for single Kekulé structures of benzene and pyracyclene and showed that already a single Kekulé structure has the same first-order response properties as the RHF structure. Thus, a direct relationship between resonance energy and response properties was disputed.

Nuclear magnetic resonance

The first attempt to compute the ring current contribution to the NMR shielding was made by Pople in 1956 [23], and the method was shown to give satisfactory predictions for the ^{1}H NMR shieldings in benzene and condensed systems [74]. The model was based upon the approach used by Pauling 20 years earlier to compute the diamagnetic susceptibilities of a range of aromatic molecules [7].

The NMR shielding is very sensitive to molecular structure, while this is not always the case for ring current strengths [65], see also Paper VII. Therefore, relative ring-current strengths should only be deduced from nuclear shieldings within the same molecule or in similar molecules [75]. For instance, the difference in NMR chemical shifts between inner and outer protons in dehydro[n]annulenes, where n is even and ranges from 14 to 30 (except 28), correlates approximately linearly with the calculated resonance energy per π electron [76].

Apart from the existence of ring currents, by means of NMR one can obtain information about electron delocalization and bond localization specifically from the spin-spin coupling constants [75].

The use of shielding constants as a measure of ring current strengths has been criticized by pointing out that it is the out-of-plane component of the shielding tensor that is mostly effected by the magnetic field, given the magnetic field is directed perpendicularly to the molecular plane [39]. Even though the effect on the isotropic shielding constants might be of the order of one ppm, the ring current contribution to the out-of-plane component of the shielding tensor for ^{13}C is 10-15% in naphthalene

and anthracene [77].

Hall and Hardisson [33] were the first to treat the ring current effect on diamagnetic anisotropies and nuclear shieldings at the SCF level, using Coupled Hartree-Fock (CHF) perturbation theory. Amos and Roberts [34] showed that reliable results can also be obtained by the simpler Uncoupled Hartree-Fock (UCHF) perturbation theory. Lazzeretti and Taddei subsequently applied the UCHF procedure to compute the ring-current contribution to the proton NMR chemical shifts of substituted benzenes [78, 79].

The NMR shielding probes the local magnetic field and is dependent on the local current density. This makes it possible to calculate the shielding in any point of space using dummy atoms. Several methods have been built upon this feature.

The nucleus-independent chemical shift, or NICS [80], is the most widely used aromaticity index based on NMR shieldings of dummy atoms. The NICS value is the negative of the shielding at the position of a dummy atom. NICS(0) is obtained in the molecular plane, while NICS(1) is computed at 1Å above the ring, in order to probe the ring-current in the σ and the π regions. Lazzeretti has pointed out that one should be careful in using isotropic NICS values as aromaticity indices. Rather the out-of-plane component of the NICS tensor should be considered with care [39]. A negative NICS value should point to diatropic ring currents and aromaticity, but in some cases such as the hydrogen-bonded HF trimer, NICS [81] has been shown to give erroneous predictions about the ring-current strength [82, 83]. Several more elaborate NICS-based procedures have been proposed. Morao [84] and Stanger [85] computed the NICS value in several points along a line in their respective approaches to assess aromaticity. In the NICS-rate method, it is the derivative of the NICS values with respect to the z coordinate perpendicular to the aromatic ring that is computed [86].

The aromatic ring-current shieldings (ARCS) method [87] is similar to NICS, but it also gives the current strength. In the ARCS method, the NMR shielding is calculated for dummy atoms along a line, thus yielding the long-range asymptotic behavior of the shielding function. Then, the ring-current strength can be calculated from classical electrodynamics based on the Biot-Savart law using the expression [87]

$$\sigma(z) = -\frac{\mu_0}{2}\frac{\partial I_{\text{ring}}}{\partial B_{\text{ext}}}\frac{R^2}{(z^2+R^2)^{3/2}} \tag{2.7}$$

where $\frac{\partial I_{\text{ring}}}{\partial B_{\text{ext}}}$ is the ring-current susceptibility, μ_0 is the vacuum permeability, R is the radius of the molecular ring and z is the distance from the ring plane along the perpendicular z direction.

The secondary magnetic fields that arises due to the ring current in aromatic or antiaromatic molecules have been studied by Merino and coworkers [88]. The ring-current effect on the local magnetic field has also been probed by the means of nuclear magnetic shielding density maps introduced by Jameson and Buckingham [89,90]. The method has been applied to map the regions of shielding and deshielding in benzene, cyclooctatetraene and pentaprismane [91–93].

Magnetic susceptibility

In the early ring-current investigations by Pauling and Lonsdale, it was the anisotropy of magnetic susceptibility that was examined [7, 8]. Pauling computed the diamagnetic anisotropy of benzene and aromatic multiring molecules in 1936 based on the assumption that every carbon atom of benzene contribute one electron that is free to move from carbon to carbon [7]. Pauling and Lonsdale also suggested how the currents in condensed hydrocarbons would be delocalized. The ring currents affect the out-of-plane component of the magnetic susceptibility, and thus the anisotropy of the susceptibility tensor, Eq. (2.8), can be taken as a measure of the ring current strength [7, 8, 94].

$$\Delta\chi = \chi_{zz} - \frac{1}{2}(\chi_{xx} + \chi_{yy}) \tag{2.8}$$

The relationship is however not necessarily direct, since the anisotropy $\Delta\chi$ contains both local and nonlocal contributions [95]. The interpretation of the obtained anisotropies can be greatly assisted by maps of the ring-current densities [94]. The exaltation of diamagnetic susceptibility, Λ, can be calculated using Eq. (2.9)

$$\Lambda = \chi_M - \chi'_M \tag{2.9}$$

where χ_M is the measured molar magnetic susceptibility and χ'_M is the estimated susceptibility calculated from an additive formula for the non-delocalized counterpart of the molecule under scrutiny [96]. The isotropic molar magnetic susceptibility was easier to measure than the anisotropy of the magnetic susceptibility, which made the exaltation an appealing measure of ring currents. It has been shown that there is a good agreement between the magnetic exaltation and the nonlocal contributions to the magnetic susceptibility [97].

Methods to visualize the current density

During the last twenty years, theoretical methods to calculate current densities directly have been developed. The individual gauges for atoms in molecules, IGAIM, method [98] and its refinement, the continuous set of gauge transformations, CSGT, method uses multiple gauge origins [99]. The continuous transform of the current-density approach, CTOCD [27, 100–108], is related to the CSGT method. In both methods, a different gauge origin is used for every point where the current density is calculated. The applications of the CTOCD method are based on the coupled Hartree-Fock approach, and the recently developed open-shell version [60, 109] is similarly based on unrestricted Hartree-Fock. Recently, CTOCD calculations at the density-functional theory level have been reported [60]. The ACID method, anisotropy of the current-induced density [110], provides a measure of electron delocalization from the current density by plotting the anisotropic part of the current density obtained from CSGT calculations. The stagnation graph method visualizes the current density topology by identifying the points where the current density vector field is zero [27,111]. The GIMIC method falls into the same category as CTOCD, aiming at visualizing the current density, but with GIMIC the level of electronic-structure

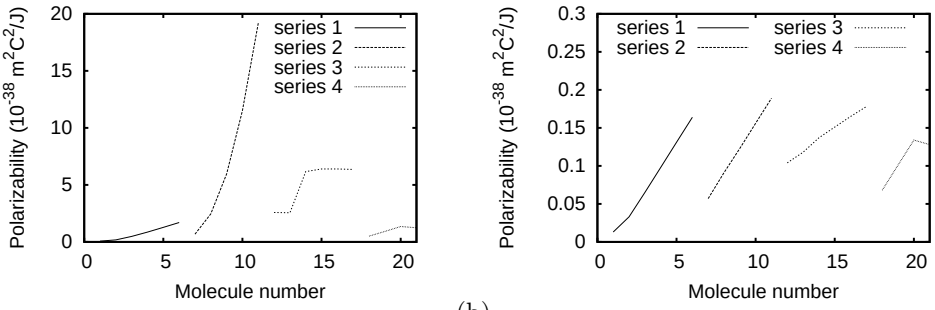

Figure 2.4: Static polarizabilities of the nanoring molecules in Paper II. (a) The in-plane polarizabilities $\alpha_{xx} = \alpha_{yy}$, (b) the out-of-plane component α_{zz}. Note the different scales of the y-axis. The in-plane polarizabilities are two orders of magnitude stronger than the out-of-plane component. The numbering of the molecules is the same as in Paper II.

theory can be extended beyond Hartree-Fock. Furthermore, GIMIC also gives the absolute strength of the ring current susceptibility. This is advantageous, since by the sole interpretation of ring-current density distributions as vector plots or isosurfaces of the moduli of the current density it is not possible to obtain a quantitative measure of the ring current strengths [39]. The GIMIC code is presently only interfaced to programs allowing non-relativistic calculations which excludes heavy-element compounds from the range of molecules that can be studied. The ring-current strengths and ring-current densities have also been calculated at the four-component relativistic level in the recent study by Bast and coworkers [112].

Electric polarizability as aromaticity index

Several suggestions about how to relate aromaticity to electric polarizability have been proposed [39]. Fowler and Soncini showed that in-plane polarizability correlates with the ring-current contribution from the π orbitals in monocycles [113]. They argue that the correlation does not hold for antiaromatic molecules. In aromatic monocyclic molecules with $(4n + 2)$ π electrons, the ring current is dominated by the same HOMO-LUMO transition as the in-plane polarizability. In antiaromatic molecules, the paratropic ring current would arise from a HOMO-LUMO transition, that is dipole forbidden and thus can not contribute to the polarizability [113, 114].

The static polarizabilities of the nanoring molecules of Paper II are shown in Figure 2.4. As typical for planar aromatic molecules, the in-plane polarizabilities, α_{xx}, α_{yy}, are larger than the out-of-plane component. The out-of-plane polarizability increases with increasing size of the molecule, while the shape of the $\alpha_{xx} = \alpha_{yy}$ curve more closely follows the same trend as the ring currents and the ^{1}H NMR shieldings. As previously pointed out [39], there is some discrepancy between the polarizability and the magnetic aromaticity criteria. The trends obtained in Paper II support the notion that the polarizability only can be used as a qualitative descriptor of aromaticity.

2.5 Aromaticity - the elephant and the blind scientists?

The lack of common acceptance of how to unequivocally define aromaticity can be described by an allegory of the Indian story about six blind men describing what an elephant is. Depending on which part of the elephant each of the men happened to find, he would give a completely different description of the animal from that of the other men. The bottom line is that an elephant has all the features that the men described [115]. The main problem stems from the fact that aromaticity is not an observable of itself, but it is more a descriptive concept. Often it is suggested that aromaticity is in reality a multidimensional property which should not be determined using only one index [116–118].

If the energetic criterion is taken as dominant, as IUPAC does [12], then aromaticity is a property of the molecule as a whole. Sometimes the geometric and magnetic criteria such as NICS and HOMA are also used to define "local aromaticity" [119]. In some condensed systems, e.g., coronene, the NICS of the central ring is affected by distant ring currents in the same molecule, which calls for care when characterizing "local aromaticity" by means of NICS calculations [120]. In synthetic organic chemistry, the aromaticity concept is used to characterize local structures that stabilize reacting species [84, 121]. In Paper II, we discuss the localization of ring-currents to "aromatic moieties" of the nanoring molecules. The polycyclic antiaromatic hydrocarbons, PAAH, are another class of condensed multi-ring molecules where the ring-current strengths of individual rings suggest local differences in aromaticity [122]. One of the PAAHs is a molecule where two hexadehdro[12]annulenes are linked by a benzene ring. Although the molecule has 26 π electrons and should be aromatic, all the three rings have paratropic ring currents. Despite the local currents that seem to give the molecule its antiaromaticity, the explanation is "global": the lack of resonance structures is suggested to yield the destabilization and antiaromaticity. The term "local aromaticity" is, as discussed by Lazzeretti [39], valid if one can obtain a certain measure of diatropicity or paratropicity, such as the ring current, and furthermore, if one defines aromaticity by the existence of a diatropic or paratropic ring currents.

3 Quantum chemical calculations

3.1 Molecular properties

In chemistry, the electrons are the main actors. Electrons are particles but due to their small mass, they also have the characteristics of waves. Thus, they obey the laws of quantum mechanics and can be described by the wavefunction ψ. The one-electron wavefunction contains all information about the state of the electron and it corresponds to the spin orbital in an atom or a molecule. The link between observables of the macroscopic and the microscopic worlds is an operator. The Hamilton operator $H = T + V$ containing the kinetic and potential terms is the most fundamental operator in quantum chemistry.

When an eigenoperator operates on the wavefunction, the outcome is a number times the same wavefunction. Solving the Schrödinger equation (3.1) means in practice finding a wavefunction that is an eigenfunction of the Hamilton operator.

$$H\psi = E\psi \tag{3.1}$$

In Equation (3.1) ψ is the wavefunction and E is the energy eigenvalue.

The operator corresponds to an observable, i.e., a measurable quantity in the macroscopic world. The outcome of a macroscopic measurement corresponds to expectation values. For a general operator Ω, the expectation value is

$$\langle\Omega\rangle = \frac{\int \psi^* \Omega \psi \; d\mathbf{r}}{\int \psi^* \psi \; d\mathbf{r}}. \tag{3.2}$$

The complex conjugate of ψ is ψ^* and the expectation values are real numbers. For normalized wavefunctions, $\int \psi^* \psi \; d\mathbf{r} = 1$.

When the Hamilton operator operates on the wavefunction, the obtained eigenvalue is the energy. Energy can be considered to be the most fundamental quantity in chemistry, as well as in other natural sciences. The chemistry of atoms and molecules is ultimately determined by energy differences and energy content.

The computation of molecular properties is lacking a universal recipe [123]. Whereas some properties such as equilibrium structures, harmonic force constants, and vibrational frequencies are obtained directly from the energy as a function of the

structure, many properties involve the interaction of the wavefunction with external magnetic or electric fields, with magnetic moments of nuclei etc.

When the molecular system is put in an external field, the response is often manifested as small changes in the total energy and the interaction can therefore be described as a perturbation that can be expanded in a Taylor series in the perturbation strength. A direct route to molecular properties is to obtain them as expectation values in the formalism of perturbation theory. Another main approach to molecular properties is to calculate them as energy derivatives of the perturbation using response theory [124].

3.2 Nuclear shieldings

3.2.1 The NMR experiment

Electrons and some nuclei possess an intrinsic magnetic moment denoted as spin. The magnitude of the spin angular momentum of the electron, m_s, along an axis is $+\frac{1}{2}\hbar$ or $-\frac{1}{2}\hbar$, where $\hbar$ is the Planck constant h divided by 2π. The electrons in these spin states are often denoted as α and β electrons, or alternatively "spin up" and "spin down" electrons, respectively. The unit of $\hbar$ is usually left out when discussing the magnitude of the spin. The spin magnetic moment of a nucleus is the sum of the contributions of the magnetic moments of the nucleons. In the following we will consider the simplest nucleus, i.e., the proton, with the spin $I = \frac{1}{2}$.

Consider a sample containing a nucleus N with a permanent magnetic moment μ_N, which requires a non-zero spin $\mathbf{I}$. The nucleus will align its magnetic moment μ_N along the magnetic field $\mathbf{B}$. More precisely, the magnetic moment vector will precess around the axis defined by the external magnetic field. The magnetic moment is proportional to the nuclear magnetic spin $\mathbf{I}_N$ and the magnetogyric ratio γ_N. The magnetic moment can also be expressed in terms of the nuclear magneton β_N and the nuclear g factor [1],

$$\mu_N = \gamma_N \hbar \mathbf{I}_N = g_N \beta_N \mathbf{I}_N. \tag{3.3}$$

The nuclear magneton in SI units JT^{-1} is defined as $\beta_N = \frac{e\hbar}{2m_p}$, where e is the elementary charge and m_p is the mass of the proton. The counterpart for the electron is the Bohr magneton, where m_p is replaced by the mass of the electron, m_e.

The interactions of the nuclear magnetic moment μ_N and the external magnetic field $\mathbf{H}$ induce a splitting of the energy levels corresponding to the nuclear spin vectors being aligned along the field such that the z component is either parallel or antiparallel with the field, assuming that the field is in the z direction. This phenomenon is known as the Zeeman effect, which similarly splits the energy levels of otherwise degenerate α and β electrons. At thermal equilibrium, the population ratio of the β and α states is given by the Boltzmann distribution $N_\beta/N_\alpha = e^{\Delta E/kT}$, where k is Boltzmann's constant, T is the temperature in K and ΔE is the energy gap between the two levels. The energy ΔE can be overcome by absorbing an energy quantum from an electromagnetic field perpendicularly to the static magnetic field. An electromagnetic field with the radio frequency ν, induces a transition between the spin levels when

the energy difference is given by

$$\Delta E = h\nu = g_N \beta_N \mathbf{B} = \mu_N \mathbf{B}. \tag{3.4}$$

The resonance frequency ν, at which the quantum is absorbed, is called the Larmor frequency. At this resonance frequency, a signal is obtained in the nuclear magnetic resonance (NMR) spectrometer.

In 1938, Rabi and coworkers reported "A New Method of Measuring Nuclear Magnetic Moment" [5]. They described the application of the NMR technique on a beam of LiCl molecules. However, there was a need to improve the theory in order to deal with complex molecules. One refinement was introduced by Lamb in 1941 [6], taking into account the secondary magnetic field induced by the electrons in the atom, whose magnetic moment one was about to measure. When an atom is exposed to an external magnetic field, the electrons will through induction make up an electric circuit around the atom thereby inducing a secondary magnetic field. This diamagnetic contribution will cause a shift in the resonance frequency at which the transition between the energy levels takes place. The nucleus becomes "shielded". This reasoning holds for spherical isotropic atoms, and also approximately for light atoms in molecules. For high accuracy and for dealing with heavier elements, this isotropic picture is not adequate. Since the shielding of the nucleus is very sensitive to the local electronic structure, a very valuable spectroscopic tool is at hand if one can get beyond the isotropic shielding picture.

Ramsey formulated in 1950 a concise theory for the nuclear magnetic shielding in molecules [125] including also the anisotropy which arises because of other atoms in the molecule. The complete shielding expression consists thus of two terms, the diamagnetic term by Lamb, and a paramagnetic term which is formally dependent on the excited states and their energies [125–127]

$$\sigma_K = \langle 0|\mathbf{h}_{\mathrm{BK}}^{\mathrm{dia}}|0\rangle - 2\sum_{n_s \neq 0} \frac{\langle 0|\mathbf{h}_{\mathrm{B}}^{\mathrm{orb}}|n_s\rangle\langle n_s|(\mathbf{h}_{\mathrm{K}}^{\mathrm{pso}})^T|0\rangle}{E_{n_s} - E_0} \tag{3.5}$$

The paramagnetic term contains the coupling of the magnetic field to the orbital motion of the electrons through the $\mathbf{h}_{\mathrm{B}}^{\mathrm{orb}}$ operator as well as the coupling of the spin and orbital motion of the electrons via the $\mathbf{h}_{\mathrm{K}}^{\mathrm{pso}}$ term.

The effect of the nuclear shielding is that the local magnetic field $\mathbf{B}_{\mathrm{loc}}$ at the nucleus will differ from the external magnetic field $\mathbf{B}_0$

$$\mathbf{B}_{\mathrm{loc}} = (1 - \sigma_K)\mathbf{B}_0 \tag{3.6}$$

In the NMR experiment, the nuclear shielding is not obtained directly, but rather as the difference between the nuclear shielding of the sample and a reference compound. This entity is called the NMR chemical shift, δ_K.

$$\delta_K = \frac{\sigma_{K,\mathrm{ref}} - \sigma_K}{1 - \sigma_{K,\mathrm{ref}}} \approx \sigma_{K,\mathrm{ref}} - \sigma_K \tag{3.7}$$

The approximation in Eq. (3.7) is $1 - \sigma_{K,\mathrm{ref}} \approx 1$, which is mostly justified since $\sigma_{K,\mathrm{ref}} \ll 1$.

3.2.2 Computing NMR shieldings

The interactions that are detected in a NMR experiment can be collected in the effective NMR spin Hamiltonian [4, 128].

$$\begin{aligned} H_{\mathrm{NMR}} &= -\frac{1}{2\pi}\sum_K \gamma_K \mathbf{I}_K \cdot (\mathbf{1} - \sigma_K) \cdot \mathbf{B}_0 \\ &+ \sum_{K<L} \mathbf{I}_K \cdot (\mathbf{D}_{KL} + \mathbf{J}_{KL}) \cdot \mathbf{I}_L \\ &+ \sum_K \mathbf{I}_K \cdot \mathbf{B}_K \cdot \mathbf{I}_K \end{aligned} \tag{3.8}$$

The first term describes the interaction between the local magnetic field, which is defined through the nuclear shielding σ and the external field $\mathbf{B_0}$, and the magnetic moments of the nuclei. The second term describes the dipole interaction between nuclear magnetic momenta. The interaction can be direct, which is described by the $\mathbf{D}_{KL}$ coupling tensor, or indirectly coupled via the electrons, as described by the $\mathbf{J}_{KL}$ coupling tensor. The third term, the nuclear quadrupole coupling, is of relevance for nuclei with spin quantum numbers larger than $\frac{1}{2}$. The chemical shift measured in an NMR experiment probes the interaction described by the first term. The forthcoming discussion will consider this term.

The NMR shielding is a second-order property arising from the response of the energy to the magnetic moment of the nucleus and to the external magnetic field. The external field and the magnetic moments are introduced into the Schrödinger equation as vector potentials $\mathbf{A}^B$ and $\mathbf{A}^{m_I}$, respectively.

$$\begin{aligned} \mathbf{A}^B &= \frac{1}{2} B \times (\mathbf{r} - \mathbf{R}_O) \\ \mathbf{A}^{m_I} &= \alpha^2 \frac{\mathbf{m}_I \times (\mathbf{r} - \mathbf{R}_I)}{|\mathbf{r} - \mathbf{R}_I|^3} \end{aligned} \tag{3.9}$$

The gauge origin $\mathbf{R}_O$ is the origin of the vector potential $\mathbf{A}^B$ describing the external magnetic field and α is the fine structure constant. Every nuclear spin $\mathbf{I} \neq 0$ positioned at $\mathbf{R}_I$ is described by a vector potential $\mathbf{A}^{m_I}$. In the following, $\mathbf{A}^m$ will be used for the sum $\mathbf{A}^m = \sum_I^N \mathbf{A}^{m_I}$ of all N nuclear magnetic moments in the molecule.

In the Hamiltonian, the vector potentials are substituted into the kinetic energy term, so that the linear momentum $\mathbf{p}$ is replaced by $\mathbf{p} + \mathbf{A}$, where $\mathbf{A} = \mathbf{A}^B + \mathbf{A}^m$.

$$\begin{aligned} E &= \langle\psi|T + V|\psi\rangle = \langle\psi|(\mathbf{p} + \mathbf{A})^2 + V|\psi\rangle \\ &= \langle\psi|\mathbf{p}^2 + \mathbf{p}\cdot\mathbf{A}^m + \mathbf{A}^m \cdot \mathbf{p} + \mathbf{p}\cdot\mathbf{A}^B + \mathbf{A}^B \cdot \mathbf{p} \\ &\quad + \mathbf{A}^m \cdot \mathbf{A}^B + \mathbf{A}^B \cdot \mathbf{A}^m + \mathbf{A}^m \cdot \mathbf{A}^m + \mathbf{A}^B \cdot \mathbf{A}^B + V|\psi\rangle \end{aligned} \tag{3.10}$$

A vector potential has its origin somewhere, and in practical applications using finite basis sets the results will depend on where this origin is situated. This leads to the

"gauge-origin problem", which will be addressed in Subsection 3.3.

The magnetic shielding tensor is obtained as the second derivative of the energy with respect to the external magnetic field B_υ and the magnetic moments of the nuclei $m_{K\tau}$. The Cartesian components (x,y,z) are denoted by υ,τ.

$$\sigma^K_{\upsilon\tau} = \frac{\partial^2 E}{\partial B_\upsilon \partial m_{K\tau}} \tag{3.11}$$

The Hellmann-Feynman theorem [129, 130] holds for optimized variational wavefunctions and also for coupled-cluster wavefunctions within the unitary coupled-cluster theory [131]. The theorem states that the derivative of the energy with respect to a parameter λ equals the expectation value of the derivative of the operator with respect to the same parameter:

$$\frac{\partial}{\partial\lambda}\langle\psi|\mathbf{H}|\psi\rangle = \langle\psi|\frac{\partial\mathbf{H}}{\partial\lambda}|\psi\rangle. \tag{3.12}$$

This is used when calculating the derivative of the energy with respect to the magnetic moments:

$$\begin{aligned}\frac{\partial \mathrm{E}}{\partial m_{K\tau}} \;=\; &\langle\psi|\mathbf{p}\cdot\frac{\partial\mathbf{A}^m}{\partial m_{K\tau}} + \frac{\partial\mathbf{A}^m}{\partial m_{K\tau}}\cdot\mathbf{p} \\ &+\frac{\partial\mathbf{A}^m}{\partial m_{K\tau}}\cdot\mathbf{A}^B + \mathbf{A}^B\cdot\frac{\partial\mathbf{A}^m}{\partial m_{K\tau}} \\ &+\frac{\partial\mathbf{A}^m}{\partial m_{K\tau}}\cdot\mathbf{A}^m + \mathbf{A}^m\cdot\frac{\partial\mathbf{A}^m}{\partial m_{K\tau}}|\psi\rangle.\end{aligned} \tag{3.13}$$

When Eq. (3.14) is subsequently differentiated with respect to the magnetic field, the Hellmann-Feynman theorem is not valid anymore, and also the $\frac{\partial\psi}{\partial B_\upsilon}$ terms have to be taken into account. The expression for the shielding constant σ then becomes

$$\begin{aligned}\sigma^K_{\upsilon\tau} \;&=\; \frac{\partial^2 \mathrm{E}}{\partial B_\upsilon \partial m_{K\tau}} \\ &=\; 2\mathrm{Re}\left[\langle\psi|\frac{\partial\mathbf{A}^m}{\partial m_{K\tau}}\cdot\frac{\partial\mathbf{A}^B}{\partial B_\upsilon}|\psi\rangle\right] + 2\mathrm{Re}\left[\langle\frac{\partial\psi}{\partial B_\upsilon}|\frac{\partial\mathbf{A}^m}{\partial m_{K\tau}}\cdot\mathbf{p}|\psi\rangle\right] \\ &+\; 2\mathrm{Re}\left[\langle\frac{\partial\psi}{\partial B_\upsilon}|\mathbf{p}\cdot\frac{\partial\mathbf{A}^m}{\partial m_{K\tau}}|\psi\rangle\right] + 2\mathrm{Re}\left[\langle\frac{\partial\psi}{\partial B_\upsilon}|\frac{\partial\mathbf{A}^m}{\partial m_{K\tau}}\cdot\mathbf{A}^B|\psi\rangle\right] \\ &+\; 2\mathrm{Re}\left[\langle\frac{\partial\psi}{\partial B_\upsilon}|\mathbf{A}^B\cdot\frac{\partial\mathbf{A}^m}{\partial m_{K\tau}}|\psi\rangle\right]\end{aligned} \tag{3.14}$$

where $\mathrm{Re}[X]$ is the real part of X. The first term on the right-hand side correspond to the diamagnetic part in Ramsey's expression for the shielding, Eq. (3.5), while the rest of the terms correspond to the paramagnetic part.

For liquid samples, only the isotropic shielding constant is obtained from the NMR experiment. The shielding constant is obtained as the average of the sum of the diagonal elements of the tensor, i.e., as one third of the trace of the tensor.

$$\sigma^K_{\mathrm{iso}} = \frac{1}{3}\left(\sigma^K_{xx} + \sigma^K_{yy} + \sigma^K_{zz}\right) \tag{3.15}$$

The open-shell case

For open-shell systems, the nuclear shielding tensor consists of three terms:

$$\sigma_{\upsilon\tau}^{K} = \sigma_{\upsilon\tau}^{\mathrm{orbital},K} + \sigma_{\upsilon\tau}^{\mathrm{contact},K} + \sigma_{\upsilon\tau}^{\mathrm{dipolar},K} \tag{3.16}$$

The contact term $\sigma_{\upsilon\tau}^{\mathrm{contact},K}$ arises from the interaction of the nuclear magnetic moment with unpaired electron spin at the position of the nucleus. The interaction is isotropic and thus only s-electrons contribute, unless the molecule has multiple centers with unpaired spin.

$$H_{FC}^{K} = \frac{4\pi}{3} g_e \alpha^2 \sum_i \delta(r_{iK})\ \mathbf{S}_i \cdot \mathbf{m}_K \tag{3.17}$$

The anisotropic interaction between the spin magnetic dipoles of the electron and the nuclei gives rise to the spin-dipole term

$$H_{SD}^{K} = \frac{1}{2} g_e \alpha^2 \sum_i \mathbf{m}_K \cdot \frac{3\ \mathbf{r}_{iK}\mathbf{r}_{iK} - \mathbf{1} r_{iK}^2}{r_{iK}^5} \cdot \mathbf{S}_i \tag{3.18}$$

The contributions of the aforementioned interactions to the nuclear shielding are within the leading-order non-relativistic theory given by

$$\sigma_{\upsilon\tau}^{\mathrm{contact},K} = \left. \frac{\partial^2 \langle H_{FC}^{K} \rangle}{\partial m_{K\upsilon} \partial B_\tau} \right|_{\substack{m_\upsilon^K = 0 \\ B_\tau = 0}} \tag{3.19}$$

$$\sigma_{\upsilon\tau}^{\mathrm{dipolar},K} = \left. \frac{\partial^2 \langle H_{SD}^{K} \rangle}{\partial m_{K\upsilon} \partial B_\tau} \right|_{\substack{m_\upsilon^K = 0 \\ B_\tau = 0}} \tag{3.20}$$

where $\langle H \rangle$ denotes the expectation value for the Hamiltonian operators. The shielding contributions in Eqs. (3.19) and (3.20) can be expressed using the isotropic hyperfine coupling constant ($A^{\mathrm{iso},K}$) and the components of the spin-dipolar hyperfine coupling tensor ($A_{\upsilon\tau}^{\mathrm{dip},K}$)

$$\sigma_{\upsilon\tau}^{\mathrm{contact},K} = -\pi A^{\mathrm{iso},K} \delta_{\upsilon\tau} g_e \frac{S(S+1)}{3kT} \tag{3.21}$$

$$\sigma_{\upsilon\tau}^{\mathrm{dipolar},K} = -\pi A_{\upsilon\tau}^{\mathrm{dip},K} g_e \frac{S(S+1)}{3kT} \tag{3.22}$$

The temperature dependence of these terms arise from a Boltzmann average of the different spin states, the degeneracy of which are split by the applied external magnetic field [132–134]. In Eqs. (3.21) and (3.22), g_e is the g value of a free electron. The orbital contribution to the nuclear magnetic shielding tensor of open-shell molecules is obtained as for closed-shell systems [133].

3.3 Gauge-including atomic orbitals

In the magnetic shielding calculations, the external magnetic field is represented by a vector potential. This vector potential must have a specified origin, and the obtained

result is dependent on where the origin is, unless the calculation is done using an infinite basis set.

To cope with this problem, London suggested [9] to use a separate vector potential for every basis function with the gauge origin included in the basis function. The London orbitals, or gauge-including atomic orbitals (GIAOs), have the form

$$\chi_\mu(\mathbf{r}) = e^{-\frac{i}{2}(\mathbf{B}\times[\mathbf{R}_\mu - \mathbf{R}_O]\cdot\mathbf{r})}\chi_\mu^{(0)}(\mathbf{r}). \tag{3.23}$$

The nucleus is situated at $\mathbf{R}_\mu$ while the gauge origin is at $\mathbf{R}_O$. The field-free basis function is $\chi_\mu^{(0)}$.

There are also other similar solutions to the gauge-origin problem. IGLO stands for "individual gauge for localized orbitals" and was proposed by Kutzelnigg [135,136]. A similar approach is LORG, "localized orbital/localized origin" by Hansen and Bouman [137]. These approaches are not used very frequently today because of the high accuracy and fast basis-set convergence that can be achieved with GIAOs.

In the GIMIC method, London orbitals are utilized in order to obtain a better convergence of the current density and to reduce errors due to lack of true gauge invariance. In common-gauge calculations there is a divergence of the current density. The divergence is significantly reduced by using London orbitals [37].

3.4 Gauge-including magnetically induced currents

In the presence of an external magnetic field, the current density $\mathbf{J}(\mathbf{r})$ in a molecular system is

$$\mathbf{J}(\mathbf{r}) = \frac{i}{2}\int d\mathbf{r}_2 \ldots d\mathbf{r}_N \left(\psi^*\nabla\psi - \psi\nabla\psi^* + 2i\mathbf{A}\psi^*\psi\right) \tag{3.24}$$

where $\mathbf{A}$ is the vector potential of Eq. (3.9).

The current density can be related to the nuclear shielding $\sigma_{\upsilon\tau}^K$ tensor through the expression [27, 37]

$$\sigma_{\upsilon\tau}^K = -\epsilon_{\upsilon\delta\gamma}\int \frac{r_\delta - R_{I\delta}}{|\mathbf{r}-\mathbf{R}_I|^3}\mathcal{J}_\gamma^{B_\tau} d\mathbf{r}. \tag{3.25}$$

In Eq. (3.25), the derivative of the current density with respect to the magnetic field, i.e., the magnetically induced current-density tensor, is expressed by [37]

$$\begin{aligned}\mathcal{J}_\gamma^{B_\tau}(\mathbf{r}) = \frac{\partial J_\gamma(\mathbf{r})}{\partial B_\tau} &= \sum_{\mu\nu} D_{\mu\nu}\frac{\partial\chi_\mu^*(\mathbf{r})}{\partial B_\tau}\chi_\nu(\mathbf{r}) \\ &+ \sum_{\mu\nu} D_{\mu\nu}\chi_\mu^*(\mathbf{r})\frac{\partial\tilde{h}}{\partial m_{K\upsilon}}\frac{\partial\chi_\nu(\mathbf{r})}{\partial B_\tau} \\ &+ \sum_{\mu\nu}\frac{\partial D_{\mu\nu}}{\partial B_\tau}\chi_\mu^*(\mathbf{r})\frac{\partial\tilde{h}}{\partial m_{K\upsilon}}\chi_\nu(\mathbf{r}) \\ &- \epsilon_{\upsilon\tau\delta}\left[\sum_{\mu\nu} D_{\mu\nu}\chi_\mu^*(\mathbf{r})\frac{\partial^2\tilde{h}}{\partial m_{K\upsilon}\partial B_\delta}\chi_\nu(\mathbf{r})\right].\end{aligned} \tag{3.26}$$

Eq. (3.26) is the working expression for the GIMIC method. Thus, to obtain the magnetically induced current density one needs the density matrix $D_{\mu\nu}$, the magnetically perturbed density matrix $\frac{\partial D_{\mu\nu}}{\partial B_\beta}$, and the derivatives of the one-electron basis functions in the AO representation $\tilde{h}$ taken with respect to the magnetic field B_β and with respect to the magnetic moments of the nuclei $m_{K\alpha}$. Magnetic-field dependent GIAOs are used in the calculation.

For visualization of the current density or for numerical integration of current strengths, the components of the magnetically induced current tensor are evaluated in discrete grid points $\mathbf{r}$. For the general open-shell case the current-density contribution of α and β electrons are treated separately. The vector expression for the spin contributions to the tensor components of the current density in each grid point ($\boldsymbol{\mathcal{J}}_\tau^{B_\upsilon,\kappa}$) is given by

$$\boldsymbol{\mathcal{J}}_\upsilon^{B_\tau,\kappa} = \mathbf{v}^\mathbf{T}\mathbf{P}_\tau^\kappa\mathbf{d}_\upsilon - \mathbf{b}_\tau^\mathbf{T}\mathbf{D}^\kappa\mathbf{d}_\upsilon + \mathbf{v}^\mathbf{T}\mathbf{D}^\kappa\mathbf{q}_{\upsilon\tau} - \epsilon_{\upsilon\tau\phi}\frac{\mathbf{1}}{\mathbf{2}}(\mathbf{v}^\mathbf{T}\mathbf{D}^\kappa\mathbf{v})\mathbf{r}_\phi. \tag{3.27}$$

where κ refers to α or β electrons, $\mathbf{D}^\kappa$ are the AO density matrices, $\mathbf{P}_\tau^\kappa$ are the corresponding perturbed AO density matrices, and $\mathbf{r}_\phi$ the Cartesian directions x, y, and z. The derivatives of the basis functions ($\mathbf{b}_\tau$, $\mathbf{d}_\upsilon$, and $\mathbf{q}_{\upsilon\tau}$) are given by

$$\mathbf{b}_\tau = \frac{\partial\mathbf{v}}{\partial\mathbf{B}_\tau}; \qquad \mathbf{d}_\upsilon = \frac{\partial\mathbf{v}}{\partial\mathbf{r}_\upsilon}; \qquad \mathbf{q}_{\upsilon\tau} = \frac{\partial^2\mathbf{v}}{\partial\mathbf{r}_\upsilon\partial\mathbf{B}_\tau}; \qquad (\upsilon,\tau = x,y,z). \tag{3.28}$$

In closed-shell molecules, the expression for the current density is the same as in Eq. (3.27), but with the α and β components equal. The working equation in vector form is then

$$\boldsymbol{\mathcal{J}}_\upsilon^{B_\tau} = \mathbf{v}^\mathbf{T}\mathbf{P}_\tau\mathbf{d}_\upsilon - \mathbf{b}_\tau^\mathbf{T}\mathbf{D}\mathbf{d}_\upsilon + \mathbf{v}^\mathbf{T}\mathbf{D}\mathbf{q}_{\upsilon\tau} - \epsilon_{\upsilon\tau\phi}\frac{\mathbf{1}}{\mathbf{2}}(\mathbf{v}^\mathbf{T}\mathbf{D}\mathbf{v})\mathbf{r}_\phi. \tag{3.29}$$

Using Eq. (3.29) one obtains the magnetically induced current density susceptibility in units of nA/T.

The GIMIC method makes it possible to represent the ring current in several ways. The integrated current strength is obtained by cutting a bond with a planar grid positioned perpendicularly to the bond half-way between the bonded atoms and then integrating the current density over the grid. The obtained current strength can be used as a qualitative yardstick for assessing aromaticity. The ring-current delocalization pathways can in principle be explored by calculating the integrated ring-current strength at several bonds. The delocalization is however more intuitively seen in graphical representations. The current density can be visualized using vector or isodensity contour plots. Since vector plots might become very crowded and hard to interpret, it is sometimes more illustrative to plot the signed modulus of the current density. The ring-current distribution in coronene and circumcoronene shown in Figure 4.12 illustrate this feature. Finally, the ring-current profile is obtained by calculating the gradient of the ring current strength with respect to the coordinate crossing a bond perpendicularly in the plane of the molecular ring. The current profile simultaneously shows the delocalization and gives the strength of the dia- and

paratropic ring current components. The ring-current profile across a C–C bond in benzene is shown in Figure 2.1.

3.5 Electron spin resonance

3.5.1 The ESR experiment

Similarly to nuclei with a non-zero spin, also the spin magnetic moment μ_e of unpaired electrons interacts with external magnetic fields. This is called the Zeeman interaction In open-shell molecules, the external magnetic field splits the energy levels of α and β electrons due to the Zeeman effect. The peaks in an ESR spectrum appear at energies equal to the Zeeman shift. In open-shell molecules, the net magnetic moment of the electrons will be non-zero. This unpaired electron spin can interact with the external magnetic field and with the magnetic moments of nuclei. These interactions give rise to the electron spin resonance (ESR) spectrum.

The spin angular momentum vector of the electron, $\hbar\mathbf{S}$ is related to the magnetic moment through the expression

$$\mu_e = -g_e\beta\mathbf{S} \tag{3.30}$$

where the Bohr magneton $\beta = \frac{e\hbar}{2m_e}$ and g_e is the electron g factor. The mass and charge of the electron are m_e and $-e$, respectively.

When an external magnetic field H is applied in the z direction and a oscillating field with the frequency ν is applied perpendicularly to this, the transitions from the lower Zeeman level to the upper take place at resonance, when

$$h\nu = g\beta H \tag{3.31}$$

The g_e value for a free electron is 2.002319. In atoms and molecules, the local electronic structure alters the energy difference between the Zeeman levels. The measure of the effect of the surroundings is the g factor, that in all atoms and molecules will differ from the free electron g value.

3.5.2 Computational ESR

The effective ESR spin Hamiltonian is often expressed with two terms [4]. These are the two first terms in Eq. (3.32). The g value determines the position of the peaks in the ESR spectrum, while the hyperfine coupling tensor, or isotropically the hyperfine coupling constant, A, is a measure of the fine structure in the spectrum. A comparison to NMR can be readily made: The g value corresponds to the chemical shift, while the hyperfine coupling constants give a similar effect as the spin-spin coupling. Since the variations in the g value with respect to the free-electron value are usually small, often the relative $\Delta g = g_e - g_{\text{measured}}$ value is reported. It is often given in parts per thousand, ppt. Taking also the zero-field splitting and the nuclear quadrupole

coupling into account, the ESR hamiltonian becomes

$$H_{\mathrm{ESR}} = \frac{1}{2}\mathbf{S}\cdot g\cdot\mathbf{B}_0 + \mathbf{S}\cdot\sum_K \mathbf{A}_K\cdot\mathbf{I}_K + \mathbf{S}_K\cdot\mathbf{D}\cdot\mathbf{S}_K + \sum_K \mathbf{I}_K\cdot\mathbf{B}_K\cdot\mathbf{I}_K \tag{3.32}$$

The first term describes the interaction between the unpaired electron spin and the magnetic field while the second term gives the coupling between the electron spin and the nuclear magnetic moments of the nuclei. The third term is the zero-field splitting which in the absence of an external magnetic field gives rise to $(2S+1)$ energy levels when the total spin $S > \frac{1}{2}$. The fourth term is the nuclear quadrupole interaction which makes a very small contribution to the ESR energy.

3.6 Electronic structure methods

In this Section, the methods used in the thesis to obtain the molecular energy by means of quantum mechanics are described. The main workhorse method is DFT, density-functional theory, which provides a cost-effective means of including the effects of electron correlation. A more systematic way of increasing the amount of dynamical electron correlation is provided by the Hartree-Fock based wavefunction methods.

The most efficient way to obtain the molecular energy in quantum chemical calculations is through the variational principle. The expectation value of the Hamilton operator calculated with Eq. (3.2) and representing the wavefunction ψ by an arbitrary function ϕ yields an energy $E(\phi)$

$$\langle H\rangle = \frac{\int \phi^* H\phi}{\int \phi^*\phi} \geq E_0. \tag{3.33}$$

The optimal representation of the wavefunction ψ is thus the function ϕ that minimizes the energy $E(\phi)$.

3.6.1 Wavefunction-based methods

Hartree-Fock self-consistent field

A hierarchy of standard quantum chemical electron-structure methods used to solve the Schrödinger equation is built upon the Hartree-Fock self-consistent field theory (HF-SCF). Within the HF-SCF framework, the eigenequation, Eq. (3.1), is recast into

$$F_i\phi_i = \epsilon_i\phi_i \tag{3.34}$$

where F_i is the so-called Fock operator, ϕ_i is the canonical molecular orbital (MO), and ϵ_i is the orbital energy. The wavefunction is within the Hartree-Fock based methods usually represented by a single Slater determinant, which for a system with

N electrons in N spin orbitals ϕ takes the form

$$\Psi(\mathbf{x}_1,\mathbf{x}_2,\ldots,\mathbf{x}_N) = (N!)^{-1/2} \begin{vmatrix} \phi_i(\mathbf{x}_1) & \phi_j(\mathbf{x}_1) & \cdots & \phi_k(\mathbf{x}_1) \\ \phi_i(\mathbf{x}_2) & \phi_j(\mathbf{x}_2) & \cdots & \phi_k(\mathbf{x}_2) \\ \vdots & \vdots & & \vdots \\ \phi_i(\mathbf{x}_N) & \phi_j(\mathbf{x}_N) & \cdots & \phi_k(\mathbf{x}_N) \end{vmatrix} \tag{3.35}$$

In practical calculations, each MO ϕ is described by a linear combination of atomic orbitals χ_α, each weighted by a factor $c_{\alpha i}$:

$$\phi_i = \sum_{\alpha}^{M} c_{\alpha i}\chi_\alpha \tag{3.36}$$

Then, the working equation of the HF-SCF theory becomes, by inserting the basis set expansion (3.36) into (3.34)

$$F_i \sum_{\alpha}^{M} c_{\alpha i}\chi_\alpha = \epsilon_i \sum_{\alpha}^{M} c_{\alpha i}\chi_\alpha \tag{3.37}$$

By multiplying from the left with a basis function χ_α, the Fock equation is obtained. In matrix form, it can be written

$$\mathbf{FC} = \mathbf{SC}\epsilon. \tag{3.38}$$

where the Fock matrix elements are $F_{\alpha\beta} = \langle\chi_\alpha|F|\chi_\beta\rangle$ and the overlap matrix elements are $S_{\alpha\beta} = \langle\chi_\alpha|\chi_\beta\rangle$.

The optimal wavefunction is then obtained by minimizing the energy with respect to the coefficients $c_{\alpha i}$. Eq. (3.37) is solved iteratively by improving the Fock matrix $\mathbf{F}_i$ and the MO coefficient vectors $c_{\alpha i}$ such that the energy ϵ_i changes by less than a preset convergence criterion in subsequent cycles.

Møller-Plesset perturbation theory

One can improve the results of the HF-SCF method by taking the difference between the true ground-state Hamiltonian and its representation in HF-SCF theory to be small and treat it as a perturbation. This is the basic idea behind the Møller-Plesset many-body perturbation theory [138]. The Schrödinger equation can then be formulated by adding a perturbation H' on top of the HF-SCF Hamiltonian H_0 and by expressing the wavefunction as a linear combination of the HF-SCF wavefunction and higher-order perturbations. Likewise, the energy E can be decomposed into the zeroth-order energy and the higher-order corrections. The λ parameter determines the strength of the perturbation. This approach is called many-body perturbation

theory.

$$H\Psi = (H_0 + H')\Psi = E\Psi \tag{3.39}$$

$$\Psi = \lambda^0\psi_0 + \lambda^1\psi_1 + \lambda^2\psi_2 + \ldots \tag{3.40}$$

$$E = \lambda^0 E_0 + \lambda^1 E_1 + \lambda^2 E_2 + \ldots \tag{3.41}$$

The Schrödinger equation then becomes

$$(H_0+H')(\lambda^0\psi_0+\lambda^1\psi_1+\lambda^2\psi_2+\ldots) = (\lambda^0 E_0+\lambda^1 E_1+\lambda^2 E_2+\ldots)(\lambda^0\psi_0+\lambda^1\psi_1+\lambda^2\psi_2+\ldots) \tag{3.42}$$

The nth order perturbation equation is obtained by collecting all terms that are up to n in the power of λ. The two first terms in the energy expansion, E_0+E_1, correspond to the Hartree-Fock energy.

Generally, the nth order wavefunction yields the energy corrections up to $(2n+1)$th order in the perturbation expansion. The second-order energy correction depends on doubly excited determinants Φ_{ij}^{ab} and the corresponding excitation energies E_{ij}^{ab}. This gives the Møller-Plesset perturbation theory of second order (MP2).

$$E_2 = \sum_{i<j}^{\text{occ}} \sum_{a<b}^{\text{virt}} \frac{\langle\Phi_0|H'|\Phi_{ij}^{ab}\rangle\langle\Phi_{ij}^{ab}|H'|\Phi_0\rangle}{E_0 - E_{ij}^{ab}} \tag{3.43}$$

In the Møller-Plesset perturbation theory of the second order, MP2, Eq. (3.43) is used to obtain a energy correction on top of the HF-SCF energy [138]. Roughly 80-90% of the correlation energy is captured at the MP2 level [124].

Coupled-cluster theory

In the coupled-cluster (CC) theory, the Schrödinger equation becomes

$$He^T\Phi_0 = Ee^T\Phi_0 \tag{3.44}$$

where the wavefunction is $\psi_{\text{cc}} = e^T\Phi_0$ and Φ_0 is a Hartree-Fock wavefunction. $T = T_1+T_2+\ldots+T_N$ is the cluster operator. When T_i operates on the reference state, i.e., on Φ_0, all the ith excited Slater determinants are generated. The general coupled-cluster theory is exact as long as the complete cluster operator is used, since it includes all excited states. This becomes utterly expensive even for small molecules, and therefore the cluster operator has to be truncated. If $T = T_1$, then the coupled-cluster singles (CCS) method would be obtained. For the ground state, CCS is however equivalent to Hartree-Fock. Including double excitations, using $T = T_1 + T_2$ gives the coupled-cluster singles and doubles method, CCSD, that can be considered the first improvement upon MP2. In MP2 theory, the single excitations T_1 are not included, and thus MP2 would be equivalent to CCD with fixed amplitudes. CCSDT is obtained by using $\mathbf{T} = \mathbf{T}_1 + \mathbf{T}_2 + \mathbf{T}_3$, etc, giving a systematic improvement of the molecular energy, but at the same time the computational cost rises, being N^6 for CCSD and N^8 for CCSDT with N the system size expressed in terms of basis functions.

One can take a short-cut in improving the accuracy by treating the highest-order excitations by means of perturbation theory. The CCSD(T) method includes the triples excitations via fourth order Møller-Plesset perturbation theory using the CCSD amplitudes for the wavefunction. The computational cost of the method is N^7, but the obtained energies are often even better than at the full CCSDT level, due to fortuitous error cancellation. Another approximate coupled-cluster method is CC2, which is an MP2-like treatment, but also the single excitations are implicitly taken into account when optimizing the wavefunction. The accuracy is slightly below that of CCSD, but the computational cost is comparable to MP2.

3.6.2 Density functional theory methods

In the studies related to this thesis we mainly used density functional theory, DFT. Instead of solving the Schrödinger equation using the N-particle wavefunction, the problem is reduced by instead taking the electron density ρ as the basic variable.

The theory relies on two theorems presented by Hohenberg and Kohn in 1964 [139] and by Kohn and Sham in 1965 [140]. The first theorem [139] states that the electron density ρ is, within a constant, a unique function of the external potential V. And since the external potential fixes the Hamiltonian $\mathbf{H}$, the electron density describes the full many-particle ground state. The second theorem [140] can be considered the variational principle for the density and states that the density that gives the true ground-state energy of the system is the true ground-state density ρ_0.

In practice, the DFT energy within the Kohn-Sham scheme is obtained in a similar fashion as in the HF-SCF framework by solving the equation

$$\mathbf{F}^{\mathrm{KS}}\phi_i = \epsilon_i\phi_i \tag{3.45}$$

where $\mathbf{F}^{\mathrm{KS}}$ is the Kohn-Sham operator and ϕ_i is the ith MO. The electron density is related to the spin orbitals $\phi(\mathbf{r},s)$ by the following relation:

$$\rho_0(\mathbf{r}) = \sum_i^N \sum_{s=\alpha,\beta} |\phi_i(\mathbf{r},s)|^2 \tag{3.46}$$

The Hartree-Fock energy E_{HF} and the DFT energy E_{DFT} can be expressed as

$$E_{\mathrm{HF}}[\phi(\mathbf{r})] = T[\phi(\mathbf{r})] + J[\phi(\mathbf{r})] + K[\phi(\mathbf{r})] + V_{\mathrm{ext}}[\phi(\mathbf{r})] \tag{3.47}$$

$$E_{\mathrm{DFT}}[\rho(\mathbf{r})] = T_{\mathrm{S}}[\rho(\mathbf{r})] + J[\rho(\mathbf{r})] + E_{\mathrm{XC}}[\rho(\mathbf{r})] + V_{\mathrm{ext}}[\rho(\mathbf{r})]. \tag{3.48}$$

The Hartree-Fock energy is a sum of kinetic energy of the electrons, the repulsive Coulombic interaction energy between electrons approximated as the one-particle interaction with the average electron distribution corresponding to one-electron states, and the quantum mechanical exchange energy between fermions of like spin. The external potential V_{ext} contains the interaction between electrons and nuclei. The main difference with respect to Hartree-Fock is that DFT includes effects of dynami-

cal correlation. In DFT, the exchange energy is replaced by the exchange-correlation energy. The kinetic energy T_S in Kohn-Sham-DFT is for a non-interacting system. The energy contributions arising from electrons interacting with each other are included in the exchange-correlation energy E_{xc}. The exchange-correlation term also corrects for the self-interaction that us due to the summation over all electrons in the Coulomb term J. The energy corresponding to the external potential is present in both theories. In the field-free case this is the attraction between electrons and nuclei.

DFT is in principle an exact theory, and it would also in practice be exact if the exact exchange-correlation functional E_{XC} would be known. All approximations in DFT are in the exchange and correlation parts of the functional. Thus, in practice one has to choose the best suited exchange-correlation functional for the problem at hand. There are at least three ways to approach this problem. I) The purist would choose the functional that has no empirical parameters. At present, PBE [141] and TPSS [142] are examples of this kind of functionals. II) The pragmatist would take any functional that is known to work for a specific kind of compound. In some cases a lot of empirical parameters are introduced and tuned until the "best" result is obtained. In this respect the pragmatic "best" is equivalent to coming as close to the experiment as possible. Some functionals have been especially tailored for certain applications, such as the KT functionals for nuclear shieldings [143, 144]. III) The careful researcher will test a range of functionals to validate the functional and basis set that will be used for the production calculations. Experience will naturally make it unnecessary to make a lot of testing for every new molecule but one can become more pragmatic and take the functional that one knows that used to work.

A hierarchy of density functionals

The most standard density functionals today are either of the generalized gradient approximation (GGA) type such as BP86 [145, 146] or hybrid functionals, such as B3LYP [147–149]. BP86 and B3LYP are used in many applications in the present thesis. The functionals can be classified according to the amount of variables in the exchange and correlation functionals. In GGA functionals the variables are the density ρ and the gradient of the density $\nabla\rho$. In meta-GGAs such as TPSS [142], also the kinetic energy density and the second-order gradient of the density are included [150].

Resolution of the identity (RI)

The calculation of the two-electron Coulomb interactions is the most time-consuming part of solving the SCF equation. Applying the resolution of the identity approach the four-center integrals can be turned into a product of three-center integrals. For large molecules, this reduces the time needed for the integral evaluation by roughly one order of magnitude [151].

For DFT calculations, the introduced errors are typically of the magnitude 10^{-4} a.u. per atom for the energies, 0.1 pm for the bond lengths and about 0.1° for the bond angles [152]. In the TURBOMOLE program package [153], the RI-approximation

is implemented for GGA and hybrid density functionals [154] as well as, in a slightly different brand, for MP2 [155, 156].

3.6.3 Nuclear shielding calculations and DFT

Efficient calculation of nuclear shieldings became possible with the implementation of GIAOs at the HF-SCF level in 1990 by Wolinski and coworkers [157]. This opened the avenue for NMR shielding calculations at accurate *ab initio* correlated levels [158–161]. The calculation of NMR shieldings and chemical shifts utilizing DFT has not been routine for a very long time. The contributions by Malkin *et al.* implementing the IGLO approach (individual gauge for localized orbitals) [162] and by Schreckenbach and Ziegler implementing GIAOs [163] into DFT calculations can be considered as initiators.

The nuclear shieldings are very sensitive to the electronic structure in the vicinity of the nucleus, and thus NMR spectroscopy is widely used as a structural probe for a wide range of molecular materials. The sensitivity of the shieldings on the structure is demonstrated on the computational side, e.g., in the benchmark work by Auer *et al.* [164]. They show that the accuracy of 1-2 ppm can be achieved for ^{13}C nuclear shieldings at the CCSD(T) level using a quadruple-ζ-valence quality basis set at geometries optimized at CCSD(T) level with triple- or quadruple-ζ basis sets. The remaining error can be due to the neglect of electron correlation effects and vibrational contributions [165]. This already hints to the fact that DFT can not really give that exact nuclear shieldings and that the functional used for optimizing the geometry might affect the shieldings.

To compare with experiments one has, however, to compute relative chemical shifts which are easier to obtain with high accuracy because of partial error cancellation. To see this, consider the Ramsey expression for the NMR shielding, Eq. (3.5). DFT methods typically overestimate the paramagnetic term and thus underestimate the shielding [166]. The error cancellation occurs when subtracting the shielding of the studied compound from that of the same nucleus in the reference compound. The main reason for DFT overestimating the paramagnetic term is the description of the denominator of the second term in Eq. (3.5), where the energy difference between virtual and occupied orbitals appears. The energy separation is not described very accurately at the DFT level, and thus several pragmatic improvements have been proposed. The so-called "Malkin-correction" introduces a level-shift into the denominator [167]. Chesnut introduced a semiempirical scaling obtained from a least square fit of the computed paramagnetic components against the difference of the experimental shieldings and the computed diamagnetic component [168]. It is expected that this procedure is only valid for similar molecules and some of the predictiveness that one would want to have in computational chemistry is lost. Yet another scaling procedure, which is perhaps more accepted also among the purist DFT-users, is to scale the amount of exact exchange. This has been done, e.g., by Helgaker *et al.* [169]. They show that using B3LYP with only 5% exact exchange yields a substantial improve-

ment of the shieldings. Aliev *et al.* fitted ^{13}C NMR chemical shifts calculated at the B3LYP level to experimental ones and found that the formula $\delta_{exp} = 0.95 \cdot \delta_{calc} + 0.30$ works rather well for main-row elements [170].

Generally, for first row elements, the hybrid functionals and GGA functionals perform equally well. In many cases hybrids are slightly better, and as noticed above, the performance can be improved further by adjusting the amount of exact exchange. For transition metal systems, B3LYP is in many cases better than the GGAs. This might partly be caused by error cancellation, but the inclusion of exact exchange seems to correct for the problems in pure functionals to account for the denominator in the paramagnetic term [171]. It seems that nonrelativistic calculations with hybrid functionals are sufficient up to 4*d*-elements, while 5*d*-elements require relativistic effects to be taken into account.

There exists a number of functionals designed for magnetic properties. Arbuznikov and Kaupp [172] have designed localized potentials to be used together with hybrid functionals where the amount of exact exchange is 40-60%, i.e., they improve the hybrids by the opposite action as compared with Helgaker's 5% -B3LYP [169]. The KT-functionals by Keal and Tozer are also designed to yield accurate shieldings [143]. The most recent functional in this family, KT3, is claimed by the authors to perform well for a wide range of properties, besides the nuclear shieldings [144]. The key behind the good magnetic shieldings is the parameterization of the exchange gradient expansion.

3.6.4 Basis sets

In practical calculations, the wavefunction is most often represented using sets of Gaussian type basis functions, or Gaussian-type orbitals (GTO). The Gaussian functions have the form:

$$\chi^{\mathrm{GTO}}(\theta,\phi,r) = Y_{lm}(\theta,\phi)\ P(r) e^{-\alpha r^2}. \tag{3.49}$$

The basis function contains an angular part that is represented as a spherical harmonics function $Y_{lm}(\theta,\phi)$ and a radial part described by a polynomial $P(r)$ in the radial coordinate r and a Gaussian-type exponential function $e^{-\alpha r^2}$. The Gaussian functions do not have the correct long-range behavior as compared to real orbitals that decay as e^{-r}. The description of the wavefunction at the nucleus is also poor as the cusp is missing. Both these defects of a GTO are corrected by Slater-type orbitals (STO) that have the general form

$$\chi^{\mathrm{STO}}(\theta,\phi,r) = Y_{lm}[\theta,\phi] P(r)\ e^{-\zeta r}. \tag{3.50}$$

However, using GTOs renders the two-electron integrals much easier to compute, due to the Gaussian product rule which states that the product of two Gaussians is another Gaussian [173]. The wrong long-range behavior of a single GTO is corrected by describing the wavefunction as a linear combination of several GTOs. Also the nuclear cusp of the *s*-functions can be largely captured by tailoring linear combina-

tions of GTOs. Consequently, most of the quantum chemistry programs of today use Gaussian-type basis sets.

Instead of working in polar coordinates, GTOs are commonly expressed in Cartesian coordinates as

$$\chi(x,y,z) = (x - A_x)^k (y - A_y)^l (z - A_z)^m e^{-\alpha(r-A)^2} \tag{3.51}$$

where $r = \left[(x - x_0)^2 + (y - y_0)^2 + (z - z_0)^2\right]^{1/2}$ and A is the center of the GTO. The advantage of the Cartesian form is that the GTO can be expressed conveniently using the seven indices (k,l,m,α,A_x,A_y,A_z).

In this thesis, the Karlsruhe basis sets are mainly used [174,175]. The most recent generation of these basis sets are denoted def2-XVP, where X=S for split valence which corresponds to double ζ accuracy for the valence electrons, and X=TZ, QZ for triple-ζ, quadruple-ζ.

Applying the resolution of the identity on the Coulomb integrals leads to a substantial speed-up in the energy calculations at the GGA-DFT level and at the MP2 level. The efficiency is gained in spite of the need for relatively large auxiliary basis sets for the Coulomb integrals in these cases. The auxiliary basis sets used in this study are all of the Karlsruhe family [156, 176–178], and they are used together with the regular Karlsruhe basis sets.

Some notes about basis sets for nuclear shielding calculations

The nuclear shieldings are semi-core properties and require a good description of the valence and semi-core region. Thus at least a triple-ζ-valence basis set should be used for quantitative results. For magnetic properties, it can be useful to apply basis sets designed for them, such as the EPR basis sets [179] or the IGLO basis sets [180, 181]. EPR-III or IGLO-III are in most cases sufficient for chemical shifts.

The Karlsruhe basis sets are well-suited for the calculation of ^{13}C and ^{1}H NMR shieldings. It was previously found [32] that they converge more quickly than Dunning's correlation-consistent basis sets [182, 183] and a bit more systematically than Jensen's polarization consistent basis sets [184, 185]. Since large basis sets are needed for accurate shieldings [164], a fast basis set convergence is required in order to be able to treat big molecules.

3.7 Software used

In practice, all the structure optimizations, the closed-shell nuclear shielding calculations, calculations of analytical and numerical vibrational frequencies and the molecular dynamics are done with TURBOMOLE [153]. The open-shell NMR shieldings for the GIMIC calculations on open-shell systems were computed with ACES II and the newer generation of the same code, called CFOUR [186,187]. The current susceptibility strengths were calculated with GIMIC, using as input the perturbed and unperturbed one-electron densities obtained from nuclear shielding calculations with TURBOMOLE or ACES II/CFOUR. The EPR A-tensors in Paper I were partially calculated with

GAUSSIAN [188]. The pNMR shieldings and the spin-orbit contribution to the EPR A-tensor as well as the g-tensor of the endohedral fullerene $Sc_3C_2@C_{80}$ were obtained with a local version of DeMon [189]. The molecular structures and density isosurfaces are visualized using JMOL [190], XMAKEMOL [191], GNUPLOT [192], VMD [193], and MOLDEN [194].

4 Results

In the following Section the molecular systems that are investigated in Papers I-VIII are presented. The results are analyzed and discussed in Section 4.2

4.1 Investigated systems

4.1.1 The endohedral fullerene $Sc_3C_2@C_{80}$

When reporting the discovery of the fullerene C_{60}, Kroto and coworkers characterized the buckyball as appearing to be aromatic. The interior of the fullerene was expected to be strongly deshielded because of the ring currents on the surface [195]. By the ring current criterion, C_{60} in fact appears to be very weakly aromatic [196]. The first endohedral fullerene was observed and identified as a lanthanum monocation encapsulated inside C_{60} [197]. This endohedral fullerene is denoted as $La@C_{60}$, and generally $M@C_n$ indicates that the cluster M is encapsulated inside the fullerene C_n.

The dynamical nature of atoms encapsulated into fullerenes was demonstrated in a Car-Parrinello Molecular Dynamics (CPMD) simulation of $La@C_{82}$ by Laasonen and coworkers in 1992 [198]. Since there are many equivalent bonding sites for a metal ion inside a fullerene, it is a delicate problem to determine a definite equilibrium structure, especially at elevated temperatures. The symmetry point group of endohedral metallofullerenes may appear different in NMR and Raman experiments. For example, the ^{13}C NMR spectrum of $Sc_3N@C_{80}$ points to an average I_h symmetry and a loose coupling between the endohedral cluster and the cage [199]. A lower C_{2v} symmetry is interpreted from the Raman spectrum [200]. Similar Raman patterns were observed for $Sc_3N@C_{78}$ and $Sc_2C_2@C_{84}$ [201, 202]. Thus, the internal dynamics has a time scale comparable to or longer than the time-resolution of Raman spectroscopy, i.e., of the magnitude of femtoseconds, while the motion is averaged over the nanosecond time scale of NMR.

The endohedral fullerene $Sc_3C_2@C_{80}$, studied in Paper I, is an illustrative example of how difficult it is to experimentally determine the molecular structure of the endohedral guest and the fullerene host. The Sc_3C_{82} molecule was initially thought to be $Sc_3@C_{82}$ based on synchrotron powder diffraction [203] and EPR [204] experiments. The correct structure was found by means of NMR studies on the closed-shell anion [205]. The ^{13}C NMR spectrum has two peaks corresponding to an I_h symmetric C_{80} cage. Subsequently, two stable isomers of the molecule were found, denoted as **1a** and **2a**, shown in Figure 4.1.

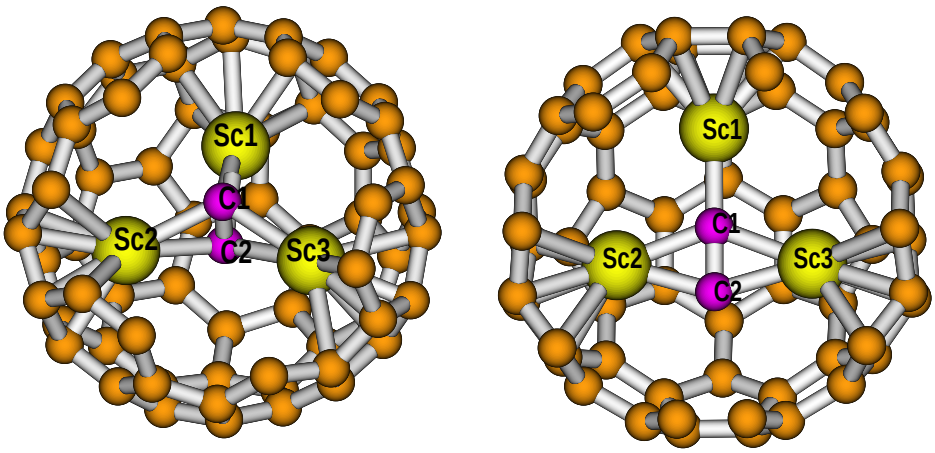

(a) (b)

Figure 4.1: (a) **1a** and (b) **2a** isomers of $Sc_3C_2@C_{80}$. For improved visibility of the confined moiety, part of the cage wall has been cut out.

4.1.2 Nanorings

The "nanorings" constitute a series of 21 polycyclic conjugated hydrocarbons building up a main ring with benzene, naphthalene, and anthracene-like groups along the edges and with benzene, triphenylene and pyrene groups in the corners. The molecules are all planar and could potentially be placed on a surface and be used as part of electric circuits. The structures are shown in Figures 4.2-4.5. In Paper II, the current delocalization pathways of the nanorings were determined by explicitly calculating the ring-current strengths at selected bonds. The in-plane and out-of-plane components of the static polarizability, as well as the ^{1}H NMR chemical shifts were also calculated. The results were analyzed for correlations between ring-current strengths, NMR shieldings, and polarizabilities.

The in-plane electric polarizability of conjugated molecules might be related to their aromaticity [113, 114]. In planar hydrocarbons with many delocalized electrons, the in-plane polarizability is expected to be of considerable magnitude. Comparing the polarizabilities to the induced current densities is expected to give insight into the connection between delocalization, conjugation, and aromaticity.

4.1.3 [n]Cycloparaphenylenes

The [n]cycloparaphenylenes ([n]CP) are, as the name suggests, cyclic molecules made up of phenylene rings connected to each other at the para-position. The optimized structures of the [n]CPs with $n = 6, \ldots, 11$ and the corresponding dianions are shown in Figures 4.6 and 4.7. Thus, the π orbitals are largely pointing to the center of the

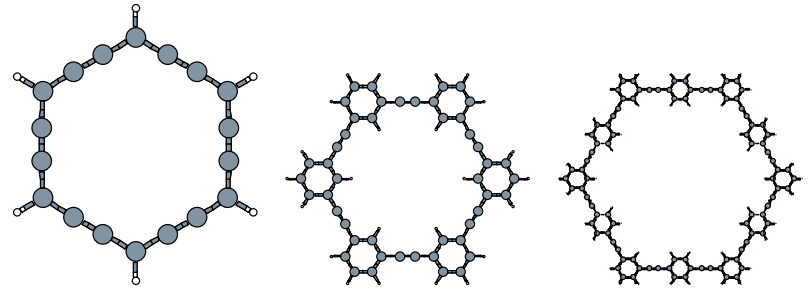

(a) **[m1]** ($C_{18}H_6$, a) (b) **[m2]** ($C_{48}H_{24}$, at) (c) **[m3]** ($C_{96}H_{48}$, at)

(d) **[m4]** ($C_{144}H_{72}$, at) (e) **[m5]** ($C_{192}H_{96}$, at) (f) **[m6]** ($C_{240}H_{120}$, at)

Figure 4.2: The first series of molecules consisting of fused benzene rings in the molecular macro cycle. The used abbreviations, the chemical brutto formula, and the expected aromaticity according to Hückel's rule is given (a = aromatic, at = antiaromatic).

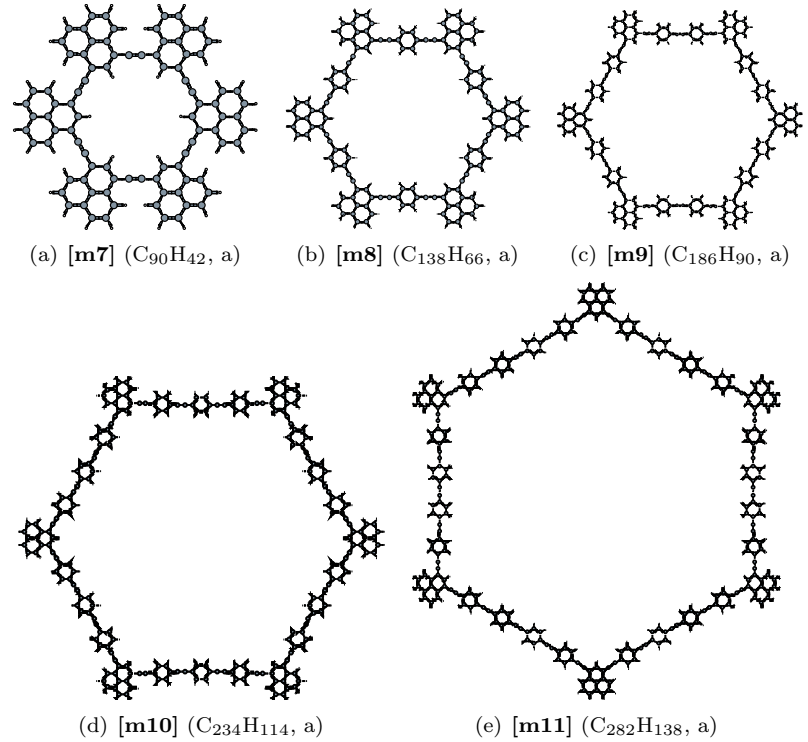

(a) **[m7]** ($C_{90}H_{42}$, a) (b) **[m8]** ($C_{138}H_{66}$, a) (c) **[m9]** ($C_{186}H_{90}$, a)

(d) **[m10]** ($C_{234}H_{114}$, a) (e) **[m11]** ($C_{282}H_{138}$, a)

Figure 4.3: The second series of molecules consisting of six fused phenalenyl groups in the corners of the macro ring and fused benzene rings along the edges of the molecular macro cycle. The used abbreviations, the chemical brutto formula, and the expected aromaticity according to Hückel's rule is given (a = aromatic, at = antiaromatic).

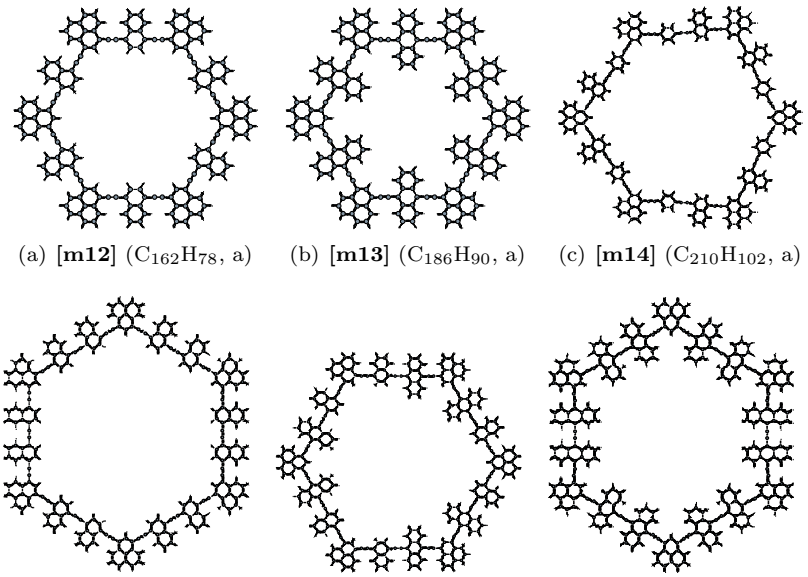

(a) **[m12]** ($C_{162}H_{78}$, a) (b) **[m13]** ($C_{186}H_{90}$, a) (c) **[m14]** ($C_{210}H_{102}$, a)

(d) **[m15]** ($C_{234}H_{114}$, a) (e) **[m16]** ($C_{258}H_{126}$, a) (f) **[m17]**($C_{282}H_{138}$, a)

Figure 4.4: The third series of molecules consisting of six fused phenalenyl groups in the corners of the macro ring and fused benzene, naphthalene, and anthracene groups along the edges of the molecular macro cycle. The used abbreviations, the chemical brutto formula, and the expected aromaticity according to Hückel's rule is given (a = aromatic, at = antiaromatic).

hoop and towards the outer surface of the wheel-shaped molecules. The synthesis of these molecules was attempted by Parekh and Guha in 1934 [206] but was not accomplished until 2008 when Jasti and coworkers synthesized the [n]CPs with 9, 12, and 18 phenylene rings. Takaba *et al.* managed to selectively synthesize [12]CP in 2009 [207]. The cycloparaphenylenes have peculiar optical properties. The Stokes shift is defined as the energy difference between the absorption and emission for a specific electronic transition in the UV-Vis spectrum and arise because the structure of the excited state differs from that of the ground state. The Stokes shift becomes larger with a decreasing diameter of the nanohoop [208,209]. The phenylene rings are benzenoid in the ground state and become quinoid in the first exited state [209]. In Paper VI we find that also the anions have a more quinoid bond length alternation than the neutral counterpart. In the dianions, the torsion angles between adjacent phenylene rings are small or zero as also observed for the first exited state. In Paper VI, the ring-current densities and ring-current strengths in the neutral and dianionic [n]CPs are related to the bond length alternation along the nanohoops.

4.1.4 Bianthraquinodimethane-stabilized [16]annulene

A π conjugated molecule with $4n$ π electrons is predicted to be antiaromatic if the conjugation pathway is untwisted and aromatic when it is twisted to a Möbius stripe, as discussed previously in Section 2.2. Herges and co-workers reported the synthesis of a Möbius-shaped [16]annulene, that was suggested to be aromatic based on aro-

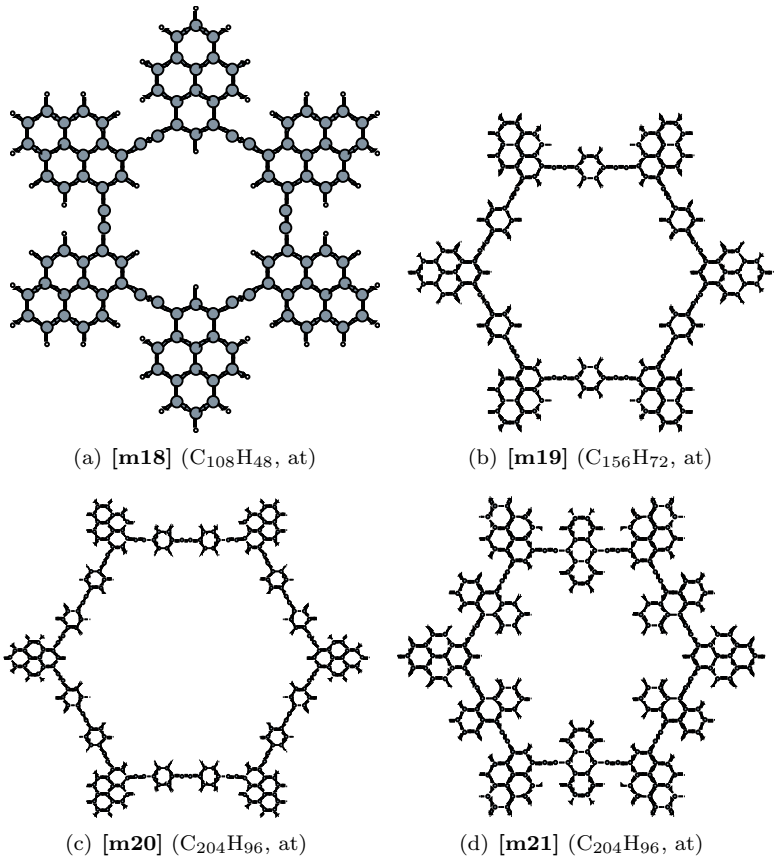

(a) **[m18]** ($C_{108}H_{48}$, at) (b) **[m19]** ($C_{156}H_{72}$, at)

(c) **[m20]** ($C_{204}H_{96}$, at) (d) **[m21]** ($C_{204}H_{96}$, at)

Figure 4.5: The fourth series of molecules consisting of six fused pyrene groups in the corners of the macro ring and fused benzene or anthracene groups along the edges of the molecular macro cycle. The used abbreviations, the chemical brutto formula, and the expected aromaticity according to Hückel's rule is given (a = aromatic, at = antiaromatic).

matic stabilization energies (ASE) [210]. Subsequently, NICS calculations suggested the [16]annulene studied is nonaromatic [211] and in an extended study of energetics some aromaticity was thereafter suggested again [212]. Since NICS alone does not necessarily give decisive information about the ring currents [22, 39], we investigated the ring currents of this molecule in Paper III in order to assess the degree of aromaticity of the bianthraquinodimethane-stabilized 4π Möbius annulene, as well as the possible antiaromaticity of the Hückel counterpart. The molecular structures are shown in Figure 4.8.

4.1.5 Hexaphyrins

In the porphyrins, four pyrrole rings linked by methine (–CH=) bridges make up a macroring. In expanded porphyrins, more than four pyrrole rings are analogously linked together. Another member of such a class of compounds is the hexaphyrins where six pyrrole rings are linked together and constitute the macroring. In Paper V, the ring-current pathways in hexaphyrins with different degree of protonation at the pyrrole nitrogen atoms were investigated. The investigated molecules **1**, **2**, **3**, **4**, and **5** correspond to [n]hexaphyrins with n =24, 26, 26, 28, and 30, respectively.

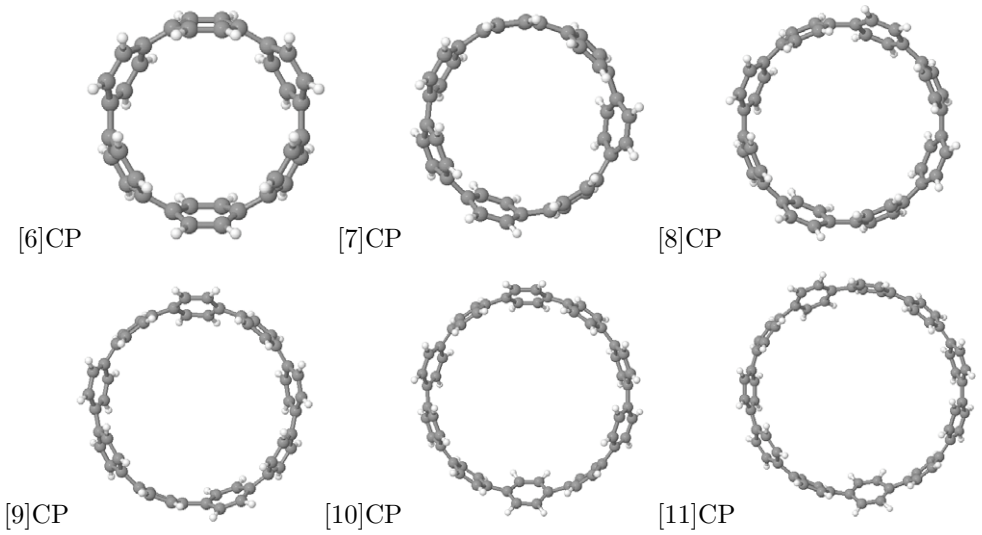

Figure 4.6: The neutral [n]CPs, n=6–11. Please note that the molecules have different diameter but they are plotted with same size and hence the atom balls appear larger for [6]CP and smaller for [11]CP. The Figure is plotted with Jmol. [190]

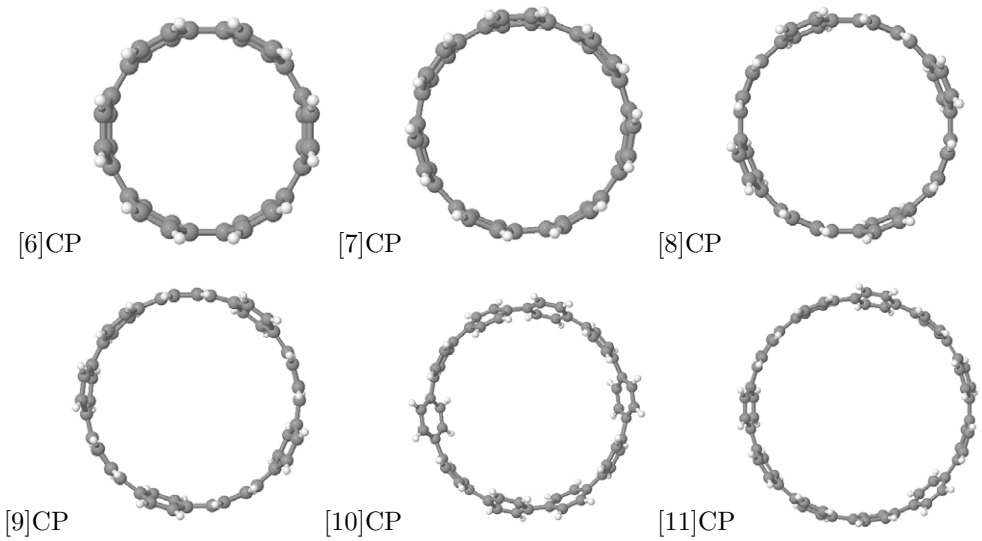

Figure 4.7: The dianionic nanohoops [n]CP^{2-}, n=6–11. *Cf.* Figure 4.6. The Figure is plotted with Jmol. [190]

Molecules **2** and **3** are isomers of the [26]hexaphyrin that differ only in the positions of the NH protons. The molecules are depicted schematically in Figure 4.9.

Proton NMR spectra of doubly twisted [26]hexaphyrin and [28]hexaphyrin showed that the NH protons pointing inside the main ring were shielded in both molecules [213]. According to the generalized Hückel rule, 26 π electrons along the conjugation pathway point to net diatropic currents whereas 28 π electrons should indicate antiaromaticity for a doubly twisted Möbius molecule. The aromaticity of the doubly-

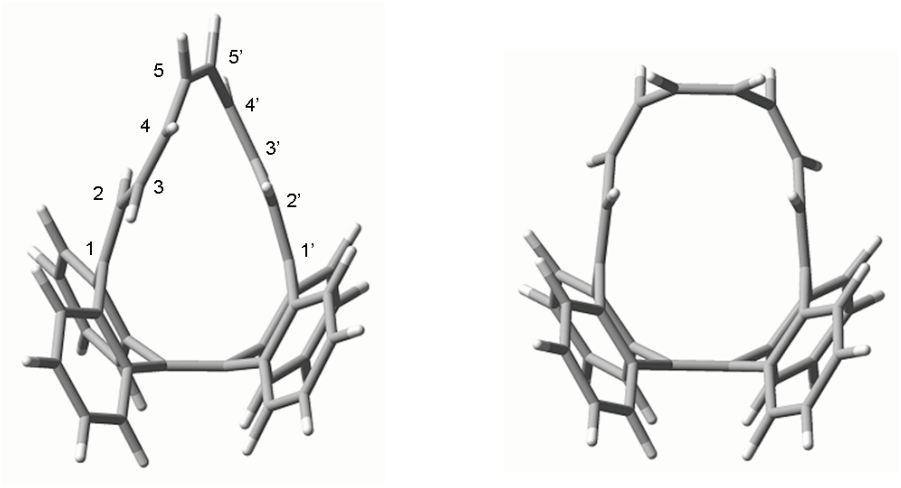

(a) (b)

Figure 4.8: The optimized structures of the bianthraquinodimethane-stabilized [16]annulene. (a) Möbius isomer (b) Hückel isomer.

twisted [26]hexaphyrins and [28]hexaphyrins were previously investigated based on the topological twist and writhe indices, computed ^{1}H NMR chemical shifts and NICS constants as well as topological atoms in molecules (AIM) and electron localization function (ELF) analysis [57, 214, 215]. The [26]hexaphyrin was concluded to be aromatic and the [28]hexaphyrin was antiaromatic.

4.1.6 Open-shell applications

Biphenyl and related bi-ring molecules

The simplest examples of multiring molecules consist of two rings connected with a C–C bond. Biphenyl, C_6H_5–C_6H_5, is in its singlet ground state in practice two independent coupled benzene rings in a staggered conformation with the torsional angle of 44.4° [216]. At the CCSD(T) level the angle is 39°, and the discrepancy with respect to experiment is due to vibrational and temperature effects [42]. In Paper VII we study biphenyl, bicyclobutadiene, and phenylcyclobutadiene together with related biochemically relevant bi-ring molecules at the MP2 and at the B3LYP levels of theory. In the lowest-lying triplet state, biphenyl is planar with a bridging C–C bond length of 140 pm. Despite the fact that the BLA in the individual benzene rings is large as compared to the spin-singlet ground state, the planarity and the short C–C bridge point to delocalization of electrons over the whole molecule. Bicyclobutadiene is planar both in its spin-singlet ground state and in its first triplet state, but the bridging C–C bond is shortened from 136.6 to 134.2 pm, at the MP2 level. While MP2 and B3LYP more or less agree on the bond lengths for C_6H_5–C_6H_5

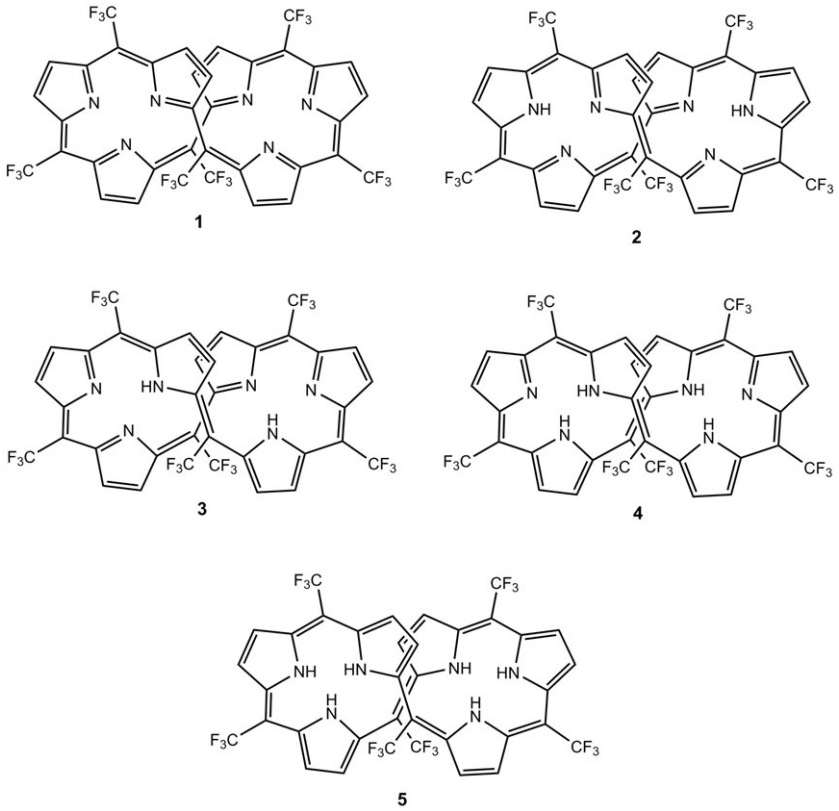

Figure 4.9: Two-dimensional projections of the doubly twisted hexaphyrins. The numbering of the molecules is the same as in Paper V.

and C_4H_3–C_4H_3, the results differ for the "mixed" phenylcyclobutadiene molecule, C_6H_5–C_4H_3. At the B3LYP level, the C–C cross-link is 143.7 pm for the singlet and 141.9 pm for the triplet state, while MP2 yields 143.5 and 145.3 pm, respectively. As bicyclobutadiene, the phenylcyclobutadiene molecule is planar. The structures of these bi-ring molecules point to changes in the delocalization upon the singlet – triplet transition. In Paper VII, the magnetically induced currents in biphenyl, bicyclobutadiene, and phenylcyclobutadiene are calculated in order to probe for these effects. A further objective of the study was to model the ring-current delocalization in models for the coupled phenol-imidazole pair which is taken as a model system for the histidine-tyrosine (His-Tyr) unit in heme-copper oxidases. It has been suggested that the aromatic stabilization of the His-Tyr moiety would increase the electron affinity and decrease the proton affinity of the tyrosine [217].

Cyclobutadiene

Cyclobutadiene, C_4H_4, poses a difficult case for computational chemistry. The ground state is an open-shell singlet with the square D_{4h} symmetry that would require a multi-reference method such as Complete active space self-consistent field, CASSCF [218]. The lowest-lying triplet state has a well-behaved single-reference wavefunction and can be studied with correlated methods such as MP2 and coupled cluster. The triplet

state has 4π electrons and is according to the modified Hückel rule [59, 60] expected to be aromatic.

B_3 and Al_3 and their monoanions

It is known that the anions of the boron and aluminum trimers exhibit aromatic patterns. They have regular triangular shapes and equalized bond lengths. The HOMO and HOMO−1 are delocalized across all the bonds and could be described as two-electron three-center bonds [21, 219, 220]. The NICS(0) values in the plane of the rings and the NICS(1) values at 1Å above the rings are large and negative. This has been described as "double aromaticity" [221]. The neutral B_3 and Al_3 molecules that are spin-doublets also possess three equally long bonds, and the topologies of the frontier orbitals is similar to those their anions. These molecules are small and provide a good test case for the open-shell implementation of GIMIC, since CCSD calculations with large basis sets are feasible. The ring-current investigations of the B_3 and Al_3 radicals and the corresponding closed-shell anions are reported in Paper VIII. The ring currents of the neutral radicals can give a further dimension to aromaticity considerations since these molecules do not fulfill the generalized Hückel rule with their odd number of valence electrons. However, the two "π" electrons in HOMO−1 might enable a ring current.

4.2 Analysis and discussion of the results

In the following, the results from the Papers I-VIII included in the Thesis are summarized, together with some unpublished results. The intention is on the one hand to present characteristic results for specific molecules, and on the other hand to make general conclusions about the characteristics of ring current densities in multi-ring molecules and about the connection between ring-current strengths and observables such as chemical shifts and molecular geometries.

4.2.1 Dynamics and magnetic properties of $Sc_3C_2@C_{80}$

The motivation of Paper I was twofold: The main goal was to computationally determine the EPR and pNMR properties of the neutral spin-doublet species as well as the NMR chemical shifts for the closed-shell monoanion. Since the chemical shifts of the cage carbon atoms were known from experiment, the closed-shell NMR shieldings can be calculated to validate the density functional theory calculations for the present case. The NMR shieldings of the confined carbide carbon atoms were not known experimentally, neither were there any pNMR spectra published, and to this part our calculations were intended to be predictive. The machinery for computing pNMR shieldings for open-shell systems has recently been developed [133, 134, 222]. Another purpose was to investigate the short-term dynamics of the confined Sc_3C_2 cluster as a first step in modelling the dynamical effects on the magnetic properties. Apart from a tight-binding density functional (DFTB) study on $Sc_3N@C_{80}$ by Heine *et al.* [223], no recent molecular dynamics studies at the *ab initio* or first-principles

level on endohedral fullerenes has to our knowledge been reported. In particular, it was of interest to determine whether either of the two isomers would dominate at elevated temperatures.

The short molecular dynamics trajectory of 7 picoseconds for the neutral $Sc_3C_2@C_{80}$ reported in Paper I shows several features of the dynamics of the confined Sc_3C_2 cluster. Dynamically, there is an equilibrium between the isomers **1a** and **2a**, and in the MD trajectory obtained at the BP86/def2-SVP level, the **2a** isomer dominates. The motion of the C_2 moiety is faster than that of the Sc atoms, suggesting that the interaction is rather ionic than covalent. The Sc_3 triangle ratchets fast back and forth several times even on the picosecond time scale, and the motion will be averaged out on the time scale of NMR.

The results from the simulation are thus in concordance with the experimental observations. The existence of only two peaks in the ^{13}C NMR spectrum [205] also points to one average structure, at least on the NMR time scale. The measured ^{13}C NMR spectrum of the endohedral C_2 moiety contains only one peak, proving the rapid dynamical motion of the carbide dimer [224].

The arithmetic average of the ^{13}C NMR chemical shifts for the confined carbon atoms unit in the anions of **1a** and **2a** is 390 ppm at the BP86/def2-TZVP level, which can be compared with the measured 328.3 [224].

The molecular dynamics results show that it might be of importance to calculate dynamically averaged NMR chemical shifts in order to make comparisons to experiment. The results in Paper I also show the challenges for density-functional theory calculations: The obtained nuclear shieldings are heavily dependent on the functional used.

The magnetic properties of the two isomers differ more for the neutral radical species than for the anions. There are qualitative differences in the spin density distributions on the Sc_3C_2 cluster. The ^{13}C pNMR chemical shifts of the confined carbon atoms vary heavily between the isomers, being -1257 ppm in **1a** and -1429 and -2498 ppm for **2a**. The influence of changes in the spin density on the open-shell magnetic properties is reflected in the ^{13}C pNMR resonances for the cage carbon atoms. In **2a**, the resonances are at 109.1 ppm for the strong peak and 105.8 ppm for the weak peak, while the corresponding pNMR chemical shifts in **1a** are 99.5 and 241.2 ppm. The large difference in the position of the weak peak is almost completely due to the Fermi-contact contribution that is 146.8 ppm in isomer **1a**. Thus, pNMR could be used as a sensitive probe for the detailed structure of endohedral fullerenes with open-shell electronic structure.

The inside of the fullerenes is strongly deshielded, as is seen by the small nuclear shieldings or large chemical shifts of confined carbon atoms. On the fullerene, several possible ring-current paths fulfilling the $(4n+2)$ rule can be found, but as previously observed for the C_{60} fullerene and for the golden fullerene Au_{32}, it is probably the global sphere currents of the fullerene that cause the deshielding [20, 196]. The signed modulus of the ring-current density of the **1a** anion of $Sc_3C_2@C_{80}$ is shown in Figure 4.10. The diatropic current on the outside of the fullerene is compensated by a paratropic current on the inside, and consequently the net current is small. The

top view (Figure 4.10 a) shows that the global ring currents flow around the sphere at the pole and at the equator. In the side view (Figure 4.10 b), the ring-current delocalization around the equator is emphasized. It is not evident from the picture that the bonding between the endohedral cluster and the cage would cause localization of electrons to aromatic pathways, as suggested in $Sc_3N@C_{68}$ and $Sc_3N@C_{78}$ [225].

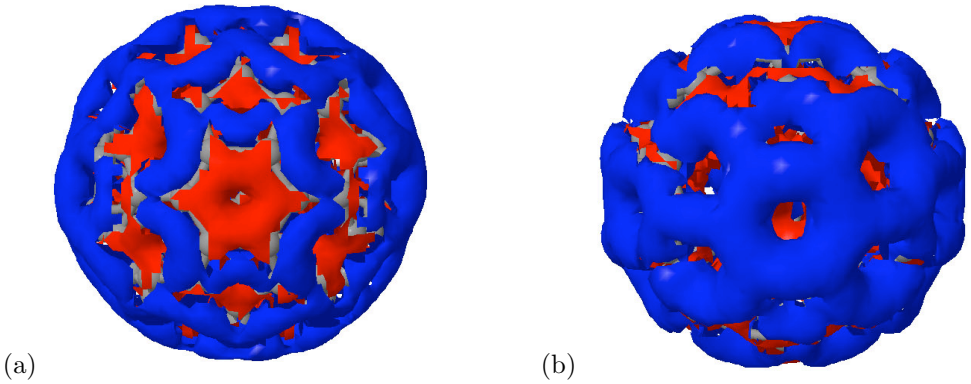

(a) (b)

Figure 4.10: The signed modulus of the ring-current density in the anion of $Sc_3C_2@C_{80}$, isomer **1a**. (a) Top view, with the magnetic field perpendicular to the page. (b) Side view, with the magnetic field in the plane of the page, directed from the bottom up. The diatropic current density is blue and the paratropic current density is red. The isocontour values for the densities are ± 0.02.

4.2.2 Aromatic, antiaromatic, and homoaromatic systems from the ring-current point of view

By the ring-current criterion, molecules that sustain a ring current when exposed to a magnetic field might be aromatic, if the ring current is diatropic and or they might be antiaromatic if the net ring current is paratropic. Bearing in mind that aromaticity can be expressed in different dimensions using geometric, energetic, or magnetic criteria, the existence of a ring current is not necessarily the ultimate proof for aromaticity [117, 118, 226, 227]. For instance, the ring current of cyclopropane is, as discussed below, not a proof of the aromaticity of the molecule. The ring currents of a range of monocyclic hydrocarbons listed in Table 4.1 agree with the Hückel rules on the aromaticity for most of the molecules.

Cyclopropane, C_3H_6, appears aromatic based on the ring current. The NICS value at the center of the ring is also large, but surprisingly it is dominated by the in-plane component [228]. The ring current is most probably a consequence the forced overlap of the bonding orbitals in the C–C bonds in the highly strained molecular structure. The ^{1}H NMR shieldings of cyclopropane are in the typical range for aliphatic hydrocarbons and do not point to aromaticity. A modest ring-current strength adds only little to the ^{1}H NMR shieldings, which are mainly governed by the molecular structure, i.e., by the hybridization.

In the homoaromatic molecules, the conjugation pathway is interrupted by satu-

rated carbon atoms [229]. The 1-3-5-cycloheptatriene, C_7H_8 is obtained by inserting a CH_2 group between two carbon atoms in benzene. This does reduce the ring current to about half of the ring current strength in benzene, but the molecule can still be regarded as somewhat aromatic. The homotropylium anion, $C_8H_9^+$, can be considered as the archetypical homoaromatic molecule [230]. By the ring-current criterion, it is aromatic with a ring-current strength of 12.9 nA/T.

Table 4.1: The diatropic and paratropic contributions to the net ring current (in nA/T) of some aromatic, antiaromatic and nonaromatic molecules calculated at the B3LYP/def2-TZVP level.

Molecule	Diatropic	Paratropic	Total
C_3H_6	11.4	–1.4	10.0
C_4H_4	3.5	–23.4	–19.9
C_5H_6	11.0	–5.6	5.4
C_6H_6	16.7	–4.9	11.8
C_6H_{12}	7.6	–7.4	0.2
C_7H_8	13.1	–7.0	6.1
$C_8H_9^+$	18.1	–5.2	12.9

4.2.3 Current localization and delocalization in multiring molecules

In the nanorings of Paper II, the ring current is prone to be localized in isolated pathways that fulfill the Hückel $(4n+2)$ π electron rule. The delocalization in the kind of multiring molecules that we studied was also explained through graph theoretical arguments by Monaco and Zanasi [231].

The nanoring molecules are classified by the Hückel rule as overall aromatic if they have $(4n+2)$ π electrons and as antiaromatic of they have a total of $4n$ π electrons. In the overall aromatic molecules, the electron delocalization was global, spreading over the main ring. The large electron delocalization in these molecules, denoted as series 2 and 3, causes a steady increase of the in-plane polarizability with increasing diameter of the main ring, as seen in Figure 2.4. The benzene, naphthalene and anthracene groups along the edges cause the current to split. The total current is conserved at the junctions, but otherwise there is no obvious pattern. In the overall antiaromatic molecular series 1 and 4, excluding **[m1]**, the main ring sustains no net current. Ring currents with the strength of 12-14 nA/T are localized to the benzene and pyrene groups in the corner as well as to the benzene and anthracene groups along the edges.

The dianionic [n]CPs are all aromatic according to the ring-current criterion. The diatropic ring-currents of 24–35 nA/T are delocalized over the whole nanohoop. The current density distribution in [6]CP and its dianion is shown in Figure 4.11 as an illus-

trative example. Most of the dianions of the nanohoops built up from $n = 6,7,\ldots,11$ arene rings have a highly symmetrical shape. The ring-current is therefore split equally along both edges of the arene rings. The [10]CP dianion is an exception, being more irregularly shaped, and explicit calculations are needed to obtain the ring-current strengths along the edges of the individual arene rings.

A common feature of many multiring molecules is that the ring-current loops are isolated by C–C bonds with a considerable amount of single-bond character. In the nanoring molecule [**m7**], the C–C bond distance between the naphthalene moieties in the corners and the main ring is 147 pm, and there is no net current along this bond. The C–C bond length alternation is small along the naphthalene perimeter, with bond lengths between 139 and 143 pm. In the neutral [n]CPs [Paper VI], the arene rings are structurally benzene-like, with equalized bond lengths, whereas the C–C cross links between the rings are 148 pm. In practice no net current passes around most of the neutral [n]CPs. Also in biphenyl [Paper VII], the bridging C–C bond is 148 pm and the ring currents are localized in the arene rings.

It has been suggested that also coronene has two individual current loops. A weakly paratropic ring current would circulate around the central ring while a stronger diatropic current would flow along the perimeter [232, 233]. Unlike the individual ring-current paths in the nanorings, in biphenyl and in the [n]CPs, the suggested ring currents of coronene are not isolated by elongated C–C bonds. The radial C–C bonds of coronene are 142.6 pm at the BP86/def2-TZVP level [234]. The ring-current density plot in Figure 4.12 shows the ring-current pathways in coronene and circumcoronene. There is a diatropic ring-current along the outer edge of the coronene molecule. Along the inner ring, there is a paratropic ring-current of -5 nA/T, in line with previous results. Circumcoronene has a similar ring-current delocalization as coronene along the periphery, and in the inner parts of the molecule there is an alternating pattern of paratropic and diatropic ring currents.

4.2.4 Möbius molecules

Bianthraquinodimethane-stabilized [16]annulene

The bianthraquinodimethane-stabilized [16]annulene [Paper III] is in practice nonaromatic by the ring-current criterion. The ring current is composed of a diatropic current along the outer edge of the annulene, and a paratropic current of approximately the same size on the inside, yielding a zero net current. The Möbius isomer is favored over the Hückel isomer by 13, 28, and 31 kJ/mol at the B3LYP, MP2, and CC2 levels, respectively. The stabilizing effect of the inclusion of electron correlation in the post-HF methods points to intramolecular weak forces stabilizing the Möbius isomer, where the opposite edges of the elliptic [16]annulene are closer due to the Möbius twist than in the Hückel counterpart. The paratropic current density at the edge further away from the bianthraquino-dimethane moiety is more outspread in the Möbius isomer. In the same region, the AIM analysis shows intramolecular CH$\cdots\pi$ inter-

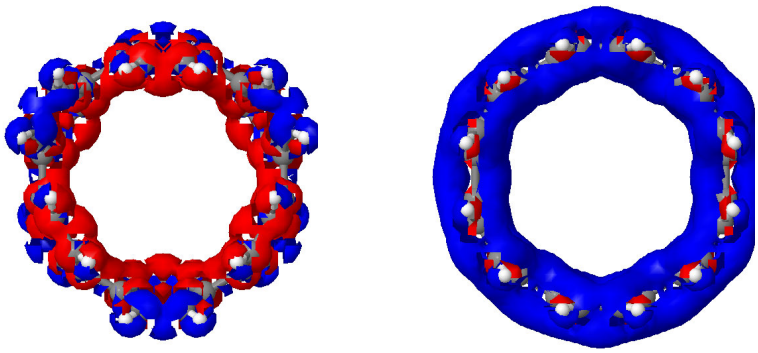

(a) (b)

Figure 4.11: The ring-current densities in the [6]CP at the BP86/def2-TZVP level. (a) Neutral [6]CP and (b) diaionic $[6]CP^{2-}$. The diatropic current density is blue and the paratropic current density is red. The isocontour values for the densities are ±0.03.

actions. As shown by Fliegl and coworkers [235], the hydrogen bond strengths are correlated with increased current strengths on one side of the hydrogen bond. Thus, nonbonded intramolecular interactions might explain the stabilization of the Möbius isomer. The diatropic ring current along the outside of the annulene almost exactly cancels out the paratropic ring-current component on the inside. The ring-current density distribution is shown in Figure 4.13. Since the net ring-current strength of the [16]annulene is practically zero, the Hückel rule for Möbius-twisted molecules does not give a definitive indication of aromaticity.

Hexaphyrins

The aromatic pathways of Möbius twisted [n]hexaphyrins with n = 24,26,28,30 with the linking number $L_k = 2$ are unraveled in Paper VI. These doubly twisted Möbius molecules are expected to be aromatic when the conjugation path contains 26 or 30 π electrons, whereas 24 and 28 π electrons should yield antiaromaticity by the generalized Hückel rule. Figure 4.14 shows the ring currents circulating along the expanded porphyrins as a function of the angle of the magnetic field. Hexaphyrin **1** sustains almost no net current and is practically nonaromatic, whereas there is a net paratropic current circulating around the [28]hexaphyrin, molecule **4**, which consequently is antiaromatic. The hexaphyrins **2**, **3**, and **5**, i.e., the two [26]hexaphyrins and the [30]hexaphyrin are aromatic by the ring-current criterion.

In complex three-dimensional structures like the Möbius-twisted hexaphyrins it is not straightforward to deduce the ring-current strengths directly from the ^{1}H NMR chemical shifts. For the hexaphyrins, intramolecular interactions, in particular involv-

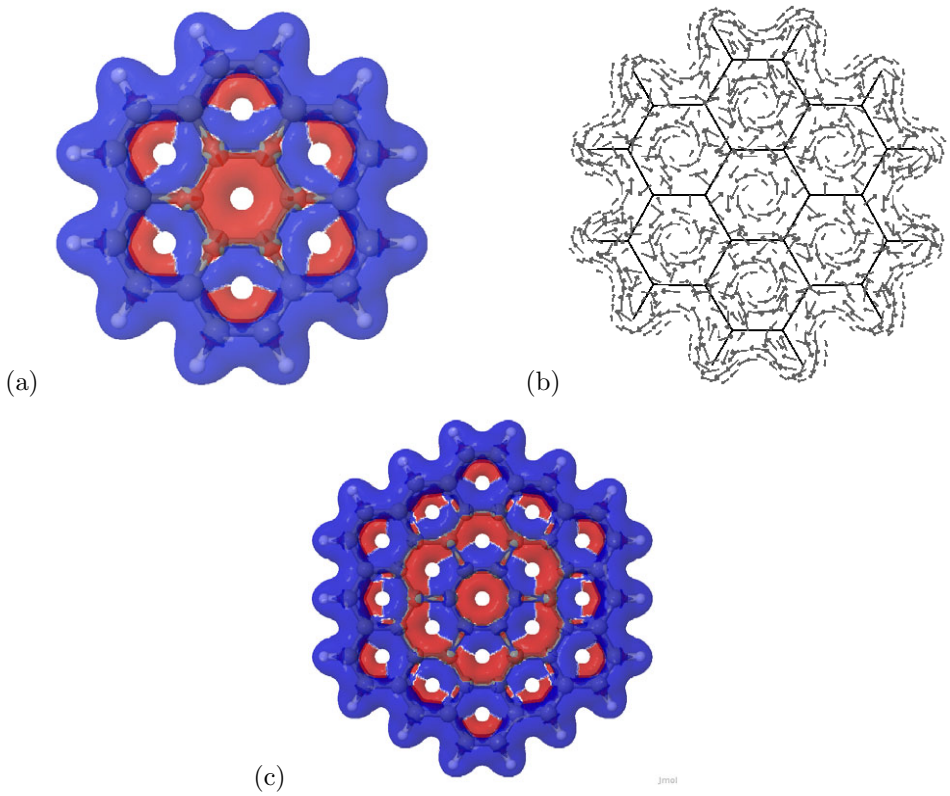

Figure 4.12: The ring-current densities in coronene and circumcoronene at the BP86/def2-SV(P) level. (a) The signed modulus of the ring-current density in coronene. The diatropic current density is blue and the paratropic current density is red. (b) Vector plot of the ring current in coronene. The diatropic current flows clockwise. (c) The signed modulus of the ring-current density in circumcoronene. The isocontour values for the densities are ± 0.02.

ing hydrogen bonds, have a much larger effect than the ring currents on the NMR shieldings of the inner NH protons.

The ring-current delocalization paths of the hexaphyrins cannot be deduced only by considering the ^{1}H NMR chemical shifts of the inner NH hydrogen atoms, neither by analyzing the HOMA index of different pathways around the expanded porphyrin ring [Paper IV]. It is equally difficult to decide whether the net current is diamagnetic or paramagnetic by analyzing NMR chemical shifts or HOMA indices. Herges found that [16]annulene isomers having large positive nucleus independent chemical shifts (NICS), i.e., antiaromatic molecules according to the magnetic criterion, exhibit a smaller BLA than molecules with vanishingly small NICS values [63]. An aromatic or an antiaromatic molecular ring needs a continuous electron delocalization in order to sustain a ring current. It does not matter whether the ring current is diatropic or paratropic. The studied molecules sustaining paratropic ring currents also exhibit a reduced BLA as demonstrated by the small differences in the HOMA indices of the hexaphyrins (**2**), (**3**), and (**4**). Explicit GIMIC calculations are required in order to map the preferred current pathway at the pyrrole ring junctions.

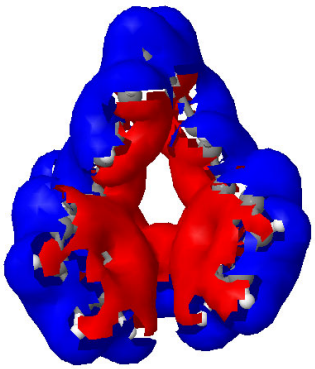

Figure 4.13: The signed modulus of the ring-current density of the Möbius shaped [16]annulene. The diatropic current density is blue and the paratropic current density is red. The isocontour values for the densities are ±0.01.

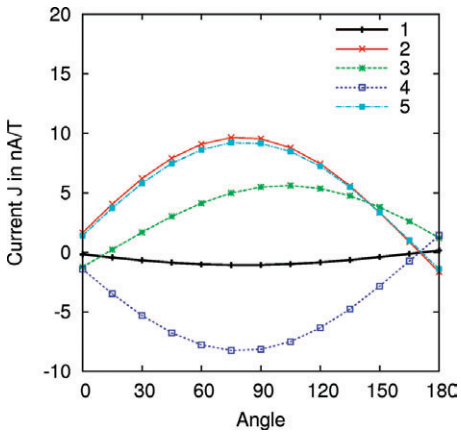

Figure 4.14: The current strength along the main porphyrin ring of the [n]hexaphyrins **1**–**5** as a function of the angle of the magnetic field.

4.2.5 Ring currents and spin currents in open-shell molecules

Cyclobutadiene and bi-ring molecules

The ring currents in the lowest-lying closed-shell singlet state and in the first triplet state of cyclobutadiene follow the generalized Hückel rule [59, 60]. With its 4π electrons, the spin-singlet should be antiaromatic while the triplet state is expected to be aromatic. At the MP2/def2-QZVP level, the ring-current strengths are -21.2 and 4.1

nA/T [Paper VIII], respectively. For the closed-shell singlet, the def2-TZVPP basis set yields converged ring-current strengths at the MP2 level. At the B3LYP/def2-TZVP level, the ring-current strength of the spin-singlet is −19.9 nA/T, in line with the MP2 results. Soncini and coworkers have argued that a good description of the paratropic contribution to the ring current can only be obtained at electron-correlated levels [236]. At the SCF-HF/def2-TZVP level, the ring-current strength of spin-singlet cyclobutadiene is −20.6 nA/T, indicating that the electron correlation does not play a crucial role for that molecule. For the triplet, the def2-QZVPP basis set still adds 12% to the total current while the spin current is reduced by 12% as compared to the def2-TZVPP results. At the CCSD level, the quadruple-ζ basis adds 28% to the total current but lowers the spin current by 8%, with respect to the triple-ζ results. Also Hartree-Fock gives qualitatively correct current strengths for the triplet state of cyclobutadiene. In open-shell molecules the correlation effects might be strong, as discussed below, and the ring-current strengths obtained at the HF-SCF level should be validated at a correlated level.

Phenylcyclobutadiene consists of a phenyl ring and a cyclobutadienyl ring connected by a single C–C bond, see Figure 4.15. Both the singlet ground state and the first triplet state are planar with a C–C bond length at the bridge of 143.5 and 145.3 pm, respectively, at the MP2/def2-SVP level [Paper VII]. In the singlet state, the two rings have individual ring currents with almost the same strength as benzene and cyclobutadiene. In the triplet state, the phenyl ring has a ring current strength of 9.7 nA/T at the MP2/def2-SVP level and 8.3 nA/T at the CCSD/def2-SVP level, which compares to 11.5 nA/T in the singlet state. Since the ring current in the arene is not much different in the two spin states, the unpaired spin resides more on the cyclobutadienyl ring. At the MP2 level, the current strength of −2.5 nA/T in the cyclobutadienyl ring is slightly paratropic while the CCSD ring-current strength is 7.2 nA/T and diatropic, as would be expected for the triplet state of cyclobutadiene. These results suggest that there can be a "local aromaticity" of individual rings in multi-ring molecules, at least within the ring-current framework.

The importance of including electron correlation into the current density calculations is shown by the GIMIC calculations on the lowest-lying triplet state of biphenyl. The structure of biphenyl is shown in Figure 4.15 and the current densities for the singlet ground state and the first triplet state are shown in Figure 4.16. The singlet ground state is a twisted molecule with a single C–C bond of 147 pm at the bridge (B3LYP/def2-TZVP; MP2/def2-SVP gives 148 pm) and conjugated C–C bonds in the arene rings. The lowest lying triplet state is planar and quinoid with alternating single and double bond character. The bond length of the C–C cross-link is 140 pm at the MP2/def2-SVP level. The ring-current densities at the MP2 and CCSD level are similarly distributed, but the net currents are qualitatively different. At the CCSD level, the delocalized current along the cross-link is 2.0 nA/T while MP2 predicts −10.9 nA/T. As for the phenylcyclobutadiene, MP2 and CCSD predict opposite ring-current character. The improved electron correlation treatment at the CCSD level is needed to obtain the aromaticity pattern predicted by the generalized Hückel rule.

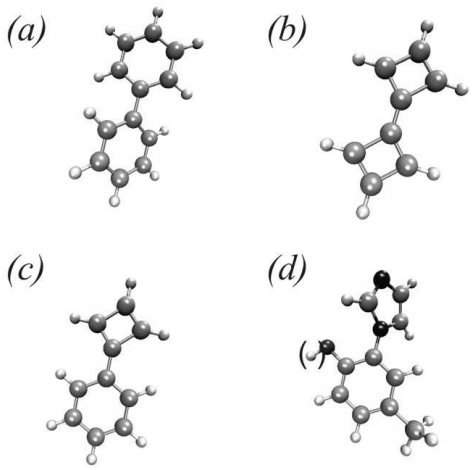

Figure 4.15: The molecular structures of the studied systems: (a) biphenyl, (b) bicyclobutadiene, (c) phenyl-cyclobutadiene, and (d) phenol-imidazole. The parentheses indicates that the hydrogen is not present in the anion and in the radical. The molecular structures were visualized with VMD [193].

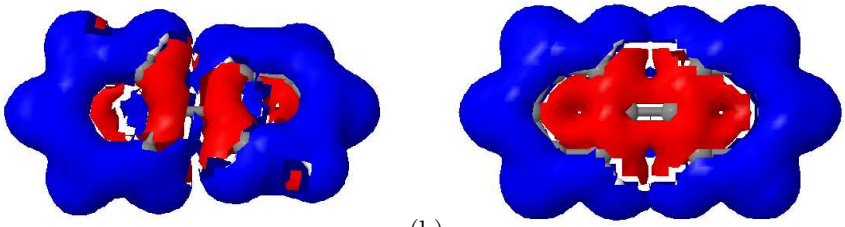

Figure 4.16: The current densities of biphenyl. (a) The total current of the singlet ground state calculated at the B3LYP/def2-TZVP level (b) total ring current of the first triplet state calculated at the MP2/def2-SVP level. An excess of α electrons is assumed for the triplet. The isocontour values for the densities are ± 0.005. The Figure is plotted with jmol [190].

Aromatic B_3 and Al_3 clusters

The anions B_3^- and Al_3^- are aromatic by the ring-current criterion, as can be assumed based on their delocalized HOMO and HOMO-1 orbitals. A ring current with the strength 15.3 nA/T circulates around the boron trimer anion while the ring-current strength in Al_3^- is 13.7 nA/T, at the CCSD/def2-TZVP level. In these closed-shell molecules, the correlation effects are small. At the Hartree-Fock level, the ring-currents are 0.3 and 1.0 nA/T larger for B_3^- and Al_3^-, respectively. Also the neutral boron and aluminum trimers have diatropic ring currents, as suggested by the similarity of the geometric and electronic topologies with those of the anionic counterparts. The total ring-current strengths at the CCSD/def2-TZVPP level are 18.2 and 11.3 nA/T for B_3 and Al_3, respectively. Although qualitatively correct total current strengths are again obtained at the SCF-HF level, the spin current is greatly overes-

timated. At the MP2 level, the all-electron calculation yields the same total current strength as CCSD, while the spin current is slightly too large. With a frozen core, MP2 gives the correct spin current, but the total current strength becomes a bit too low. See Table 4.2.

Table 4.2: The ring-current contributions of α and β electrons, and the total ring currents (in nA/T) for Al_3 and B_3 as well as the total ring current for the corresponding Al_3^- and B_3^- anions calculated at different levels of theory. The def2-TZVPP basis set is used.

Level	Al_3				Al_3^-	B_3				B_3^-
	α	β	Spin	Total	Total	α	β	Spin	Total	Total
HF-SCF	3.2	10.2	−7.0	13.5	12.7	5.7	8.3	−2.6	14.0	15.6
BP86					13.7					14.6
B3LYP					13.3					15.1
MP2^{fc}	5.7	5.5	0.2	11.3	15.9	9.9	8.3	1.6	18.2	15.2
MP2	5.9	4.9	1.0	10.8	15.6	9.9	8.3	1.6	18.2	15.1
CCSD^{fc}	5.6	5.8	−0.2	11.4	14.0	7.6	10.6	−3.0	18.2	15.4
CCSD	5.5	5.8	−0.3	11.3	13.7	7.6	10.6	−3.0	18.2	15.3

fc = frozen core; the 1s electrons in boron, and the 1s, 2s, and 2p electrons in aluminum are uncorrelated.

4.2.6 Ring currents and ^{1}H NMR shieldings

The NMR shielding of protons is rather sensitive to ring-current strengths. In Table 4.3 the ^{1}H NMR shieldings in some of the molecules discussed in the thesis are listed together with the calculated strengths of the net ring current passing the atom that the hydrogen atom in question is bonded to. The ^{1}H NMR shieldings are also strongly affected by the molecular structure, and therefore they can only provide a measure of the ring-current strengths in structurally and chemically similar molecules. Among the small hydrocarbon molecules, the fairly strong ring current of 10 nA/T in cyclopropane can not be deduced from the isotropic ^{1}H NMR shielding constant which is in the range typical for aliphatic hydrocarbon protons. The ring-current strength in cyclopropene is only about half of that in benzene, but the ^{1}H NMR shieldings differ only by 0.2 ppm. The nuclear shielding is strongly dependent on the hybridization; the carbon atoms participating in the C–C double bond in cyclopropene are sp^2 hybridized as compared to the sp^3 hybridization of the carbon atoms in cyclopropane.

In the hexaphyrins, the local ring-current strength is not decisive for the ^{1}H NMR shieldings of the inside NH protons. In Table 4.3, the local current strengths passing the NH protons are listed. Neither is there any clear correlation between the magnitude of the NMR shieldings of the NH protons and the total ring current in the expanded porphyrin ring. The global ring-current strengths of 9.6 and 5.6 nA/T in the two different aromatic [26]hexaphyrins (molecules **2** and **3** in Section 4.1.5) correspond to ^{1}H NMR shieldings of about 26 and 21 ppm. It is important to note that the ^{1}H NMR shieldings of 21 ppm would point to antiaromaticity, but the ring current is diatropic. In the likewise aromatic [30]hexaphyrin, the inside protons are shielded as expected inside a diatropic ring-current pathway. The ^{1}H NMR shieldings are between 26.5 and 29.2 ppm. In the antiaromatic [28]hexaphyrin with a net parat-

ropic ring current, the inside protons are similarly deshielded. The deshielding of the NH protons in [28]hexaphyrin as well as and in the [26]hexaphyrin is likely to be a consequence of intramolecular hydrogen bonding rather than to be caused primarily by the ring currents.

The inner hydrogen at the corner groups in the nanorings investigated in Paper II has a very similar environment in all the molecules, and a close correlation between ring-current strengths and ^{1}H NMR shieldings is obtained, as seen in Figure 2.3. It is expected that the shieldings of the inner hydrogens in the nanorings will be large, since the hydrogen atoms reside in the shielded region inside the current loop, and consequently the NMR shielding will be larger.

Coronene, circumcoronene, circumcircumcoronene, and the [**m1**] nanoring make up a series similar to the nanorings [**m2**]–[**17**], but the protons whose ^{1}H NMR shieldings are listed in Table 4.3 are on the outside of the main molecular ring in the deshielded region. Consequently, the NMR shielding constants of the protons decrease with increasing ring-current strengths. The bonding is different at the periphery of the coronene series of molecules and in [**m1**], which probably explains the different relationship between the current strength and the ^{1}H NMR shieldings. In the [**m1**] nanoring there are triple bonds along the edges of the hexagon and therefore more π electrons are available per bond as compared to the periphery of coronene which is made up of conjugated single and double bonds. In the nanorings [**m2**]–[**17**] there is a direct relationship between ring currents and isotropic ^{1}H NMR shieldings. This is expected since the bonding in these molecules is very similar.

In the dianions of the [n]cycloparaphenylenes there is some correlation between the ring current and the proton NMR shieldings, but because of the quite small range of ring-current strengths, the correlation is not as striking as for the nanorings. In the [n]CPs, the C–H bonds are roughly parallel to the magnetic field, which is probably the reason why the protons are deshielded in spite of the diatropic net current. In benzene, the shielded region inside the diatropic ring-current loop is cone-shaped and above the ring plane also some of the outside region can be shielded [88].

In the nonaromatic [16]annulene, the ^{1}H NMR shieldings are closer to those of the conjugated hydrocarbon molecules benzene and cyclobutadiene than to those of the aliphatic cyclohexane. This is expected, since the ring-current contribution to the magnetic nuclear shieldings should be negligible.

Taken together, the ^{1}H NMR shieldings can be used with some caution as a probe for ring currents, but the relative comparison of the shieldings of different protons is only valid within the same molecule and to some extent in similar molecules. This conclusion is in line with the remarks by Mitchell [75]. A more direct relationship between the nuclear shielding and the current strengths might be found by considering the out-of-plane component of the shielding tensor instead of the isotropic shielding, as pointed out by Lazzeretti and coworkers [39, 77, 228].

Table 4.3: ^{1}H NMR shieldings (σ in ppm) compared to ring-current strengths (J in nA/T) in different closed-shell molecules. σ_{in} are shieldings for protons inside the ring-current loop, σ_{out} are the shieldings for protons on the outside, and σ_{oop} are shieldings of protons that are directed out of the plane defined by the ring current.

Molecule	Computational level	J	σ_{out}	σ_{in}	σ_{oop}
C_3H_4	B3LYP/def2-TZVP	6.7	24.5		
C_3H_6	B3LYP/def2-TZVP	10.0	31.7		
C_4H_4	B3LYP/def2-TZVP	−19.9	25.5		
C_6H_6	B3LYP/def2-TZVP	11.8	24.3		
C_6H_{12}	B3LYP/def2-TZVP	0.2	30.2-30.6		
[26]hexaphyrin	B3LYP/def2-TZVP	2.0	25.7		
[26]hexaphyrin	B3LYP/def2-TZVP	6.8	25.6		
[26]hexaphyrin	B3LYP/def2-TZVP	−0.7	20.6		
[26]hexaphyrin	B3LYP/def2-TZVP	6.3	21.1		
[28]hexaphyrin	B3LYP/def2-TZVP	−7.2; −2.9	12.2		
[28]hexaphyrin	B3LYP/def2-TZVP	−9.0; 0.3	17.1		
[30]hexaphyrin	B3LYP/def2-TZVP	−0.7-+7.7	26.5-29.2		
Coronene	BP86/def2-SVP	17	22.4		
Circumcoronene	BP86/def2-SVP	26	20.0-20.5		
Circumcircumcoronene	BP86/def2-SVP	22	20.0-21.1		
[**m**1]	BP86/def2-SVP	33	20		
[**m**6]	BP86/def2-SVP	0		24	
[**m**7]	BP86/def2-SVP	25		38	
[**m**8]	BP86/def2-SVP	50		50	
[**m**14]	BP86/def2-SVP	61		54	
[**m**17]	BP86/def2-SVP	88		67	
[6]CP^{2-}	B3LYP/def2-TZVP	14			25.8-28.0
[8]CP^{2-}	B3LYP/def2-TZVP	17-18			27.2-29.6
[16]annulene, Hückel	B3LYP/def2-TZVP	0.2			25.3-26.1
[16]annulene, Möbius	B3LYP/def2-TZVP	0.3			25.6-26.5

5 Conclusions

This thesis consists of case studies on the magnetically induced currents and the NMR chemical shifts of molecules made up of one or several rings. Although the issue of aromaticity is not settled by the presented results, some conclusions can be made.

The existence of a diatropic ring current seems to be a necessary requirement for aromaticity, but as a consequence of strain, ring currents can exist in nonaromatic molecules such as cyclopropane. A paratropic ring current is indicative for antiaromaticity, but molecules with paratropic ring currents might nevertheless have a similar bond length alternation as aromatic molecules with diatropic ring currents. On the other hand, a certain amount of bond length alternation is present in multiring molecules with strong diatropic ring currents. Therefore, structural criteria for aromaticity do not always agree with the ring current criterion. Ring-current delocalization paths can not be deduced merely by inspection of bond length alternation. In fact, stretching bonds do not easily cut the current path, but the electronic structure seems to be decisive for the existence of ring currents.

The advantage of the GIMIC method with respect to other methods to visualize the current density is that both ring-current strengths and ring-current density distributions are obtained. This makes the interpretation of the aromatic pathways easier in multiring molecules. Furthermore, a quantitative description of the ring-current distribution strengths is possible when both the ring-current distribution and the ring-current strengths are at hand.

The gauge-including magnetically induced currents can be obtained with a reasonable computational cost even for hydrocarbons with hundreds of atoms. For closed-shell molecules, the basis-set requirements are modest and reliable ring currents are often obtained already at the Hartree-Fock level and with double-ζ basis sets. Density functional theory includes dynamical electron correlation at a small computational cost and is probably the best alternative for closed-shell cases. The electron correlation can be important in open-shell molecules. Therefore Hartree-Fock results should always be validated at an electron-correlated level such as many-body perturbation theory or coupled cluster theory, using basis sets of at least triple-ζ-valence quality.

The ^{1}H NMR chemical shifts are directly related to the ring-current strengths, but this correlation holds only for protons in equivalent positions and with the same bonding character. The NMR shieldings should be interpreted with care, and the influence of further interactions such as hydrogen bonds must be taken into account. In the hydrocarbon nanorings, the correlation is valid for certain hydrogen nuclei, but

in the hexaphyrins the intramolecular interactions have a far larger effect on the ^{1}H NMR shieldings than the ring currents.

The Hückel $(4n + 2)$ π rule is strongly predictive for the aromaticity of planar, non-twisted molecules. In multi-ring molecules, the Hückel rule can be used to find paths where ring currents might tend to localize. The generalized Hückel rules for open shell molecules and for Möbius topologies do not always agree with the ring-current criterion on the aromaticity. Also molecules with odd number of delocalized electrons, such as the Al_3 and B_3 radicals can have ring currents and appear aromatic.

In multi-ring molecules the ring current delocalization is not intuitively predictable, nor can the preferred delocalization paths necessarily be deduced by geometrical indices such as HOMA. It also is not easy to find the strengths of the ring-currents taking different routes at a junction in the molecular delocalization framework by inspection of nuclear shieldings of protons nor through NICS analysis. At junctions, the total current will be preserved, but explicit calculations of the ring-current strengths across specific bonds are needed to deduce the ring current strength along different pathways.

The molecules discussed above have been studied without accounting for dynamical effects. In endohedral fullerenes, the dynamics need to be taken into account when calculating the magnetic properties. The relatively novel pNMR method might be a sensitive experimental method to probe detailed structure of endohedral systems with open shells.

Chemistry is a rich science in terms of the number of phenomena that give molecules their character. The limitations of the applicability of the GIMIC code depends on which program packages it is interfaced to. In order to be able to determine the current susceptibilities in any molecule, the density and the perturbed density should to be obtained from program packages that can handle relativistic effects, e.g., using effective core potentials (ECPs) as well as to codes including multiconfigurational schemes such as multiconfigurational self-consistent field (MCSCF) and complete active space-SCF and -perturbation theory (CASSCF, CASPT2).

Concluding, in this thesis it has been shown that the GIMIC method can be utilized to assess the degree of aromaticity of molecules on a semi-quantitative level. An aromaticity scale can be constructed with zero current strength as the borderline between aromatic and antiaromatic molecules and with the ring-current strength in benzene of about 12 nA/T as a qualitative yardstick.

Aromaticity aside, the knowledge about how the charge and spin current densities are prone to be localized and delocalized might be valuable information in designing molecules for nanoscale electronics. Another immediate application of a tool such as GIMIC could be found in the interpretation of experimentally measured NMR chemical shift tensors. The possibility to calculate the ring-current strength in nearly any molecular structure that the nuclear shieldings can be computed for, enables the NMR experimentalist to immediately either exclude or confirm the ring-current effect on observed anomalous peaks in the spectrum. Further innovations, such as estimating the strength of hydrogen bonds by means of GIMIC might also be of considerable value in many fields of science.

Bibliography

[1] A. Carrington and A. D. McLachlan, *Introduction to Magnetic Resonance With Applications to Chemistry and Chemical Physics*, Harper & Row, New York, Evanston and London, 1967.

[2] P. Pyykkö in *Calculation of NMR and EPR Parameters – Theory and Applications*, ed. M. Kaupp, M. Bühl, and V. Malkin; Wiley-VCH, Weinheim, Germany, 2004; pp. 7–19.

[3] F. Neese and M. Munzarová in *Calculation of NMR and EPR Parameters – Theory and Applications*, ed. M. Kaupp, M. Bühl, and V. Malkin; Wiley-VCH, Weinheim, Germany, 2004; pp. 21–32.

[4] G. H. Lushington in *Calculation of NMR and EPR Parameters – Theory and Applications*, ed. M. Kaupp, M. Bühl, and V. Malkin; Wiley-VCH, Weinheim, Germany, 2004; pp. 33–41.

[5] I. I. Rabi, J. R. Zacharias, S. Millman, and P. Kusch, *Phys. Rev.*, 1938, **53**, 318.

[6] W. E. Lamb, Jr, *Phys. Rev.*, 1941, **60**, 817–819.

[7] L. Pauling, *J. Phys. Chem.*, 1936, **4**, 673–677.

[8] K. Lonsdale, *Proc. R. Soc. (London) A*, 1937, **159**, 149–161.

[9] F. London, *J. Phys. Radium*, 1937, **8**, 397–309.

[10] F. London, *J. Chem. Phys.*, 1937, **7**, 837–838.

[11] J. A. Pople, *Mol. Phys.*, 1958, **1**, 175–180.

[12] IUPAC. Compendium of Chemical Terminology, 2nd ed. (the 'Gold Book'). Compiled by A. D. McNaught and A. Wilkinson. Blackwell Scientific Publications, Oxford (1997). XML on-line corrected version: http://goldbook.iupac.org (2006-) created by M. Nic, J. Jirat, B. Kosata; updates compiled by A. Jenkins. ISBN 0-9678550-9-8. doi:10.1351/goldbook.A00442.

[13] J. C. Slater, *Phys. Rev.*, 1931, **37**, 481–489.

[14] L. Pauling and G. W. Wheland, *J. Chem. Phys.*, 1960, **1**, 362–374.

[15] L. Pauling, *The Nature of the Chemical Bond*, Cornell University Press, Ithaca, New York, 3rd ed., 1960.

[16] E. Hückel, *Z. Physik*, 1931, **70**, 204–286.

[17] E. Hückel, *Z. Physik*, 1931, **72**, 310–337.

[18] E. Hückel, *Z. Physik*, 1932, **76**, 628–648.

[19] Y. C. Lin, J. Jusélius, D. Sundholm, and J. Gauss, *J. Chem. Phys.*, 2005, **122**, 214308:1–9.

[20] M. P. Johansson, D. Sundholm, and J. Vaara, *Angew. Chem. Int. Ed.*, 2004, **43**, 2678–2681.

[21] A. I. Boldyrev and L. S. Wang, *Chem. Rev.*, 2005, **105**, 3716–3757.

[22] M. P. Johansson, *J. Phys. Chem. C*, 2009, **113**, 524–530.

[23] J. A. Pople, *J. Chem. Phys.*, 1956, **24**, 1111.

[24] J. I. Musher, *J. Chem. Phys.*, 1965, **43**, 4081–4083.

[25] J. I. Musher, *J. Chem. Phys.*, 1966, **46**, 1219–1221.

[26] U. Fleischer, W. Kutzelnigg, P. Lazzeretti, and V. Mühlenkamp, *J. Am. Chem. Soc.*, 1994, **116**, 5298–5306.

[27] P. Lazzeretti, *Progr. NMR Spectr.*, 2000, **36**, 1–88.

[28] C. S. Wannere and P. von Ragué Schleyer, *Org. Lett.*, 2003, **5**, 605–608.

[29] C. S. Wannere, C. Corminboeuf, Z. X. Wang, M. D. Wodrich, R. B. King, and P. von Ragué Schleyer, *J. Am. Chem. Soc.*, 2005, **127**, 5701–5705.

[30] R. G. Viglione, R. Zanasi, and P. Lazzeretti, *Org. Lett.*, 2004, **6**, 2265–2267.

[31] R. A. Klein, *J. Comput. Chem.*, 2003, **24**, 1120–1131.

[32] S. Taubert, H. Konschin, and D. Sundholm, *Phys. Chem. Chem. Phys.*, 2005, **7**, 2561–2569.

[33] G. G. Hall and A. Hardisson, *Proc. R. Soc. Lond. A*, 1962, **268**, 328–338.

[34] A. T. Amos and H. G. Roberts, *J. Chem. Phys.*, 1969, **50**, 2375–2381.

[35] R. C. Haddon, *Tetrahedron*, 1972, **28**, 3613–3633.

[36] R. C. Haddon, *Tetrahedron*, 1972, **28**, 3635–3655.

[37] J. Jusélius, D. Sundholm, and J. Gauss, *J. Chem. Phys.*, 2004, **121**, 3952–3963.

[38] J. McMurry, *Organic Chemistry*, Brooks/Cole, Pacific Grove, CA, United States of America, 2000.

[39] P. Lazzeretti, *Phys. Chem. Chem. Phys.*, 2004, **6**, 217–223.

[40] R. A. Pascal, Jr., *Chem. Rev.*, 2006, **106**, 4809–4819.

[41] R. C. Haddon and L. T. Scott, *Pure & Appl. Chem.*, 1986, **58**, 137–142.

[42] M. P. Johansson and J. Olsen, *J. Chem. Theory Comput.*, 2008, **4**, 1460–1471.

[43] M. Faraday, *Phil. Trans. R. Soc. Lond.*, 1825, **115**, 440–466.

[44] A. Kekulé, *Justugs Liebigs Annalen der Chemie*, 1872, **162**, 77–124.

[45] E. C. Crocker, *J. Am. Chem. Soc.*, 1922, **44**, 1618–1630.

[46] J. W. Amit and R. Robinson, *J. Chem. Soc., Trans.*, 1925, **127**, 1604–1618.

[47] E. Hückel, *Grundzüge der Theorie ungesättigter und aromatischen Verbindungen*, Verlag Chemie, Berlin, 1938.

[48] W. von E. Doering and F. L. Detert, *J. Am. Chem. Soc.*, 1951, **73**, 876–877.

[49] R. Herges, *Chem. Rev.*, 2006, **106**, 4820–4842.

[50] E. Heilbronner, *Tetrahedron Lett.*, 1964, **5**, 1923–1926.

[51] H. E. Zimmermann, *J. Am. Chem. Soc.*, 1966, **88**, 1564–1567.

[52] G. Călugăreanu, *Czech. Math. J.*, 1961, **11**, 588–625.

[53] W. F. Pohl, *Indiana Univ. Math. J.*, 1968, **17**, 975–985.

[54] J. H. White, *Am. J. Math.*, 1969, **91**, 693–728.

[55] F. B. Fuller, *Proc. Natl. Acad. Sci.*, 1971, **68**, 815–819.

[56] M. R. Dennis and J. H. Hannay, *Proc. R. Soc. A*, 2005, **461**, 3245–3254.

[57] S. M. Rappaport and H. S. Rzepa, *J. Am. Chem. Soc.*, 2008, **130**, 7613–7619.

[58] C. S. Wannere, H. S. Rzepa, B. C. Rinderspacher, A. Paul, C. S. M. Allan, H. F. Schaefer III, and P. von Ragué Schleyer, *J. Phys. Chem. A*, 2009, **113**, 11619–11629.

[59] N. C. Baird, *J. Am. Chem. Soc.*, 1972, **94**, 4941–4948.

[60] A. Soncini and P. W. Fowler, *Chem. Phys. Lett.*, 2008, **450**, 431–436.

[61] T. M. Krygowski, *J. Chem. Inf. Comput. Sci.*, 1993, **33**, 70–78.

[62] M. K. Cyrański, T. M. Krygowski, M. Wisiorowski, N. J. R. van Eikema Hommes, and P. von Ragué Schleyer, *Angew. Chem. Int. Ed.*, 1998, **37**, 177–180.

[63] R. Herges, *Chem. Rev.*, 2006, **106**, 4820–4842.

[64] J. Aihara and T. Ishida, *J. Phys. Chem. A*, 2010, **114**, 1093–1097.

[65] R. W. A. Havenith, *J. Org. Chem.*, 2006, **71**, 3559–3563.

[66] M. J. S. Dewar and H. N. Schmeising, *Tetrahedron*, 1959, **5**, 166–178.

[67] P. von Ragué Schleyer and F. Pühlhofer, *Org. Lett.*, 2002, **4**, 2873–2876.

[68] Y. Wang, I. Fernández, M. Duvall, J. I. Wu, G. Frenking, and P. von Ragué Schleyer, *J. Org. Chem.*, 2010, **75**, 8252–8257.

[69] B. Kiran and M. T. Nguyen, *Chem. Phys. Lett.*, 2001, **349**, 307–312.

[70] W. C. Herndon and N. S. Mills, *J. Org. Chem.*, 2005, **70**, 8492–8496.

[71] P. George, *Chem. Rev.*, 1975, **75**, 85–111.

[72] M. K. Cyránski, *Chem. Rev.*, 2005, **105**, 3773–3811.

[73] P. von Ragué Schleyer, M. Manoharan, H. Jiao, and F. Stahl, *Org. Lett.*, 2001, **3**, 3643–3646.

[74] H. J. Bernstein, W. G. Schneider, and J. A. Pople, *Proc. R. Soc. Lond. A*, 1956, **256**, 515–528.

[75] R. H. Mitchell, *Chem. Rev.*, 2001, **101**, 1301–1315.

[76] B. A. Hess, Jr., L. J. Schaad, and M. Nakagawa, *J. Org. Chem.*, 1977, **42**, 1669–1670.

[77] I. G. Cuesta, A. Sánches de Merás, S. Pelloni, and P. Lazzeretti, *J. Comput. Chem.*, 2009, **30**, 551–564.

[78] P. Lazzeretti and F. Taddei, *Mol. Phys.*, 1971, **22**, 941–943.

[79] P. Lazzeretti, *Mol. Phys.*, 1974, **28**, 1389–1395.

[80] P. von Ragué Schleyer, C. Maerker, A. Dransfeld, H. Jiao, and N. J. R. van Eikema Hommes, *J. Am. Chem. Soc.*, 1996, **118**, 6317–6318.

[81] A. Rehaman, A. Datta, S. S. Mallajosyula, and S. K. Pati, *J. Chem. Theory Comput.*, 2006, **2**, 30–36.

[82] R. Islas, G. Martínez-Guajardo, J. O. C. Jiménez-Halla, M. Solá, and G. Merino, *J. Chem. Theory Comput.*, 2010, **6**, 1131–1135.

[83] Y. C. Lin, J. Jusélius, D. Sundholm, L. F. Cui, X. Li, H. J. Zhai, and L. S. Wang, *J. Phys. Chem. A*, 2006.

[84] I. Morao, B. Lecea, and F. P. Cossío, *J. Org. Chem.*, 1997, **62**, 7033–7036.

[85] A. Stanger, *J. Org. Chem.*, 2006, **71**, 883–893.

[86] S. Noorizadeh and M. Daradab, *Chem. Phys. Lett.*, 2010, **493**, 376–380.

[87] J. Jusélius and D. Sundholm, *Phys. Chem. Chem. Phys.*, 1999, **1**, 3429–3435.

[88] G. Merino, T. Heine, and G. Seifert, *Chem. Eur. J.*, 2004, **10**, 4367–4371.

[89] C. J. Jameson and A. D. Buckingham, *J. Phys. Chem.*, 1979, **83**, 3366–3371.

[90] C. J. Jameson and A. D. Buckingham, *J. Chem. Phys.*, 1980, **73**, 5684–5692.

[91] M. B. Ferraro, P. Lazzeretti, R. G. Viglione, and R. Zanasi, *Chem. Phys. Lett.*, 2004, **390**, 268–271.

[92] A. Soncini, P. W. Fowler, P. Lazzeretti, and R. Zanasi, *Chem. Phys. Lett.*, 2005, **401**, 164–169.

[93] S. Pelloni, R. Carion, V. Liégeois, and P. Lazzeretti, *J. Comput. Chem.*, 2011, **32**, 1599–1611.

[94] I. García Cuesta, R. Soriani Jartín, A. Sánches de Merás, and P. Lazzeretti, *J. Chem. Phys.*, 2003, **119**, 5518–5526.

[95] R. C. Benson and W. H. Flygare, *J. Am. Chem. Soc.*, 1970, **92**, 7523–7529.

[96] H. J. Dauben Jr., J. D. Wilson, and J. L. Laity, *J. Am. Chem. Soc.*, 1968, **90**, 811–813.

[97] A. K. Burnham, J. Lee, T. G. Schmalz, P. Beak, and W. H. Flygare, *J. Am. Chem. Soc.*, 1977, **99**, 1836–1844.

[98] T. A. Keith and R. F. W. Bader, *Chem. Phys. Lett.*, 1992, **194**, 1–8.

[99] T. A. Keith and R. F. W. Bader, *Chem. Phys. Lett.*, 1993, **210**, 223–231.

[100] R. F. W. Bader and T. A. Keith, *J. Chem. Phys.*, 1993, **99**, 3683–3693.

[101] P. Lazzeretti, M. Malagoli, and R. Zanasi, *Chem. Phys. Lett.*, 1994, **220**, 299–304.

[102] S. Coriani, P. Lazzeretti, M. Malagoli, and R. Zanasi, *Theor. Chim. Acta*, 1994, **89**, 181–192.

[103] R. Zanasi, P. Lazzeretti, M. Malagoli, and F. Piccinini, *J. Chem. Phys.*, 1995, **102**, 7150–7157.

[104] R. Zanasi, *J. Chem. Phys.*, 1996, **105**, 1460–1469.

[105] P. W. Fowler, R. Zanasi, B. Cadioli, and E. Steiner, *Chem. Phys. Lett.*, 1996, **251**, 132–140.

[106] R. Zanasi, P. Lazzeretti, and P. W. Fowler, *Chem. Phys. Lett.*, 1997, **278**, 251–255.

[107] P. W. Fowler, E. Steiner, B. Cadioli, and R. Zanasi, *J. Phys. Chem. A*, 1998, **102**, 7297–7302.

[108] P. Lazzeretti in *Encyclopedia of Computational Chemistry*, ed. P. von Ragué Schleyer, N. L. Allinger, T. Clark, J. Gasteiger, P. A. Kollman, H. F. Schaefer III, and P. R. Schreiner, Vol. 3; Wiley, 1998; p. 1659.

[109] A. Soncini, *J. Chem. Theory Comput.*, 2007, **3**, 2243–2257.

[110] R. Herges and D. Geuenich, *J. Phys. Chem. A*, 2001, **105**, 3214–3220.

[111] S. Pelloni and P. Lazzeretti, *J. Chem. Phys.*, 2008, **128**, 194305:1–10.

[112] R. Bast, J. Jusélius, and T. Saue, *Chem. Phys.*, 2009, **356**, 187–194.

[113] P. W. Fowler and A. Soncini, *Chem. Phys. Lett.*, 2004, **383**, 507–511.

[114] E. Steiner and P. W. Fowler, *Chem. Commun.*, 2001, 2220–2221.

[115] See e.g. http://www.jainworld.com/education/stories25.asp for a Jainistic version of the story. Link retreaved 10.1.2011.

[116] A. R. Katritzky, P. Barczyński, G. Musumarra, D. Pisano, and M. Szafran, *J. Am. Chem. Soc.*, 1989, **111**, 7–15.

[117] M. K. Cyrański, T. M. Krygowski, and P. von Ragué Schleyer, *J. Org. Chem.*, 2002, **67**, 1333–1338.

[118] M. Alonso and B. Herradón, *J. Comput. Chem.*, 2010, **31**, 917–928.

[119] J. Poater, X. Fradera, M. Duran, and M. Solá, *Chem. Eur. J.*, 2003, **9**, 1113–1122.

[120] S. Fias, S. van Damme, and P. Bultinck, *J. Comp. Chem.*, 2010, **31**, 2286–2293.

[121] C. Corminboeuf, T. Heine, and J. Weber, *Org. Lett.*, 2003, **5**, 1127–1130.

[122] J. Jusélius and D. Sundholm, *Phys. Chem. Chem. Phys.*, 2008, **10**, 6630–6634.

[123] W. Kutzelnigg, *Z. Phys. D*, 1989, **11**, 15–28.

[124] F. Jensen, *Introduction to Computational Chemistry*, Wiley, Chichester, 1999.

[125] N. F. Ramsey, *Phys. Rev.*, 1950, **78**, 699–703.

[126] N. F. Ramsey, *Phys. Rev.*, 1953, **91**, 303–307.

[127] T. Helgaker, M. Jaszuński, and K. Ruud, *Chem. Rev.*, 1999, **99**, 293–352.

[128] J. Vaara, *Phys. Chem. Chem. Phys.*, 2007, **9**, 5399–5418.

[129] P. Güttinger, *Z. Physik A*, 1932, **73**, 169–184.

[130] R. P. Feynman, *Phys. Rev.*, 1939, **56**, 340–343.

[131] R. J. Bartlett, S. A. Kucharski, and J. Noga, *Chem. Phys. Lett.*, 1989, **155**, 133–140.

[132] I. Bertini, C. Luchinat, and G. Parigi, *Solution NMR of Paramagnetic Molecules*, Elsevier, Amsterdam, 2001.

[133] Z. Rinkevicius, J. Vaara, L. Telyatnik, and O. Vahtras, *J. Chem. Phys.*, 2003, **118**, 2550–2561.

[134] T. O. Pennanen and J. Vaara, *Phys. Rev. Lett.*, 2008, **100**, 133002:1–4.

[135] M. Schindler and W. Kutzelnigg, *J. Chem. Phys.*, 1982, **76**, 1919–1933.

[136] W. Kutzelnigg, *J. Mol. Struct. (THEOCHEM)*, 1989, **202**, 11–61.

[137] A. E. Hansen and T. D. Bouman, *J. Chem. Phys.*, 1985, **82**, 5035–5047.

[138] C. Møller and M. S. Plesset, *Phys. Rev.*, 1934, **46**, 618–622.

[139] P. Hohenberg and W. Kohn, *Phys. Rev. B*, 1964, **136**, 864–871.

[140] W. Kohn and L. J. Sham, *Phys. Rev. A*, 1965, **140**, 1133–1138.

[141] J. P. Perdew, K. Burke, and M. Ernzerhof, *Phys. Rev. Lett.*, 1996, **77**, 3865–3868.

[142] J. Tao, J. P. Perdew, V. N. Staroverov, and G. E. Scuseria, *Phys. Rev. Lett.*, 2003, **91**, 146401:1–4.

[143] T. W. Keal and D. J. Tozer, *J. Chem. Phys.*, 2003, **119**, 3015–3024.

[144] T. W. Keal and D. J. Tozer, *J. Chem. Phys.*, 2004, **121**, 5654–5660.

[145] A. D. Becke, *Phys. Rev. A*, 1988, **38**, 3098–3100.

[146] J. P. Perdew, *Phys. Rev. B*, 1986, **33**, 8822–8824.

[147] A. D. Becke, *J. Chem. Phys.*, 1993, **98**, 5648–5652.

[148] C. Lee, W. Yang, and R. G. Parr, *Phys. Rev. B*, 1988, **37**, 785–789.

[149] P. J. Stephens, F. J. Devlin, C. F. Chabalowski, and M. J. Frisch, *J. Phys. Chem.*, 1994, **98**, 11623–11627.

[150] W. Koch and M. C. Holthausen, *A Chemist's Guide to Density Functional Theory*, Viley-VCH, Weinheim, 2001.

[151] R. A. Kendall and H. A. Fruchtl, *Theor. Chem. Acc.*, 1997, **97**, 158–163.

[152] K. Eichkorn, O. Treutler, H. Öhm, M. Häser, and R. Ahlrichs, *Chem. Phys. Lett.*, 1995, **240**, 283–289.

[153] R. Ahlrichs, M. Bär, M. Häser, H. Horn, and C. Kölmel, *Chem. Phys. Lett.*, 1989, **162**, 165–169.

[154] F. Weigend, A. Köhn, and C. Hättig, *J. Chem. Phys.*, 2002, **116**, 3175–3183.

[155] F. Weigend and M. Häser, *Theoret. Chem. Acc.*, 1997, **97**, 331–340.

[156] F. Weigend, M. Häser, H. Patzelt, and R. Ahlrichs, *Chem. Phys. Lett.*, 1998, **294**, 143–152.

[157] K. Wolinski, J. F. Hinton, and P. Pulay, *J. Am. Chem. Soc.*, 1990, **112**, 8251–8260.

[158] J. Gauss, *Chem. Phys. Lett.*, 1992, **191**, 614–620.

[159] K. Ruud, T. Helgaker, R. Kobayashi, P. Jørgensen, K. L. Bak, and H. J. A. Jensen, *J. Chem. Phys.*, 1994, **100**, 8178–8185.

[160] J. Gauss and J. F. Stanton, *J. Chem. Phys.*, 1995, **102**, 251–253.

[161] J. Gauss and J. F. Stanton, *J. Chem. Phys.*, 1996, **104**, 2574–2583.

[162] V. G. Malkin, O. L. Malkina, and D. R. Salahub, *Chem. Phys. Lett.*, 1993, **204**, 87–95.

[163] G. Schreckenbach and T. Ziegler, *J. Phys. Chem.*, 1995, **99**, 606–611.

[164] A. A. Auer, J. Gauss, and J. F. Stanton, *J. Chem. Phys.*, 2003, **118**, 10407–10417.

[165] D. Sundholm, J. Gauss, and A. Schäfer, *J. Chem. Phys.*, 1996, **105**, 11051–11059.

[166] G. Magyarfalvi and P. Pulay, *J. Chem. Phys.*, 2003, **119**, 1350–1357.

[167] V. G. Malkin, O. L. Malkina, M. E. Casida, and D. R. Salahub, *J. Am. Chem. Soc.*, 1994, **116**, 5898–5908.

[168] D. B. Chesnut, *Chem. Phys. Lett.*, 2003, **380**, 251–257.

[169] T. Helgaker, P. J. Wilson, R. D. Amos, and N. C. Handy, *J. Chem. Phys.*, 2000, **113**, 2983–2989.

[170] A. E. Aliev, D. Courtier-Murias, and S. Zhou, *J. Mol. Struct. (THEOCHEM)*, 2009, **893**, 1–5.

[171] M. Bühl, M. Kaupp, O. L. Malkina, and V. G. Malkin, *J. Comp. Chem.*, 1999, **20**, 91–105.

[172] A. V. Arbuznikov and M. Kaupp, *Int. J. Quantum Chem.*, 2005, **104**, 261–271.

[173] T. Helgaker, P. Jørgensen, and J. Olsen, *Molecular Electronic-Structure Theory*, Wiley, West Sussex, England, 2000.

[174] A. Schäfer, H. Horn, and R. Ahlrichs, *J. Chem. Phys.*, 1992, **97**, 2571–2577.

[175] F. Weigend and R. Ahlrichs, *Phys. Chem. Chem. Phys.*, 2005, **7**, 3297–3305.

[176] K. Eichkorn, O. Treutler, H. Öhm, M. Häser, and R. Ahlrichs, *Chem. Phys. Lett.*, 1995, **242**, 652–660.

[177] K. Eichkorn, F. Weigend, O. Treutler, and R. Ahlrichs, *Theoret. Chem. Acc.*, 1997, **97**, 119–124.

[178] F. Weigend, *Phys. Chem. Chem. Phys.*, 2006, **8**, 1057–1065.

[179] V. Barone, *Recent Advances in Density Functional Methods, Part I*, World Scientific Publ. Co., Singapore, 1996.

[180] S. Huzinaga, *Approximate Atomic Functions*, University of Alberta, Edmonton, 1971.

[181] W. Kutzelnigg, U. Fleischer, and M. Schindler, *NMR basic principles and progress. Vol 23*, Springer, Berlin, 1990.

[182] T. H. Dunning Jr., *J. Chem. Phys.*, 1989, **90**, 1007–1023.

[183] D. E. Woon and T. H. Dunning Jr., *J. Chem. Phys.*, 1993, **98**, 1358.

[184] F. Jensen, *J. Chem. Phys.*, 2001, **115**, 9113–9125.

[185] F. Jensen and T. Helgaker, *J. Chem. Phys.*, 2004, **121**, 3463–3470.

[186] ACES II is a program product of the Quantum Theory Project, University of Florida. Authors: J. F. Stanton, J. Gauss, S. A. Perera, J. D. Watts, A. D. Yau, M. Nooijen, N. Oliphant, P. G. Szalay, W. J. Lauderdale, S. R. Gwaltney, S. Beck, A. Balková, D. E. Bernholdt, K. K. Baeck, P. Rozyczko, H. Sekino, C. Huber, J. Pittner, W. Cencek, D. Taylor, and R. J. Bartlett. Integral packages included are VMOL (J. Almlöf and P. R. Taylor); VPROPS (P. Taylor); ABACUS (T. Helgaker, H. J. Aa. Jensen, P. Jørgensen, J. Olsen, and P. R. Taylor); HONDO/GAMESS (M. W. Schmidt, K. K. Baldridge, J. A. Boatz, S. T. Elbert, M. S. Gordon, J. J. Jensen, S. Koseki, N. Matsunaga, K. A. Nguyen, S. Su, T. L. Windus, M. Dupuis, J. A. Montgomery).

[187] J. F. Stanton, J. Gauss, M. E. Harding, and P. G. Szalay, CFOUR, Coupled Cluster techniques for Computational Chemistry, a quantum-chemical program package also with contributions from A .A. Auer, R. J. Bartlett, U. Benedikt, C. Berger, D. E. Bernholdt, Y. J. Bomble, O. Christiansen, M. Heckert, O. Heun, C. Huber, T-C. Jagau, D. Jonsson, J. Jusélius, K. Klein, W. J. Lauderdale, D. A. Matthews, T. Metzroth, D. P. O'Neill, D. R. Price, E. Prochnow, K. Ruud, F. Schiffmann, S. Stopkowicz, M. E. Varner, J. Vázquez, F. Wang, J. D. Watts and the integral packages MOLECULE (J. Almlöf and P. R. Taylor), PROPS (P. R. Taylor), ABACUS (T. Helgaker, H. J. Aa. Jensen, P. Jørgensen, and J. Olsen), and ECP routines by A. V. Mitin and C. van Wüllen. For the current version, see http://www.cfour.de., 2009.

[188] M. J. Frisch, G. W. Trucks, H. B. Schlegel, G. E. Scuseria, M. A. Robb, J. R. Cheeseman, T. V. J. A. Montgomery, Jr., K. N. Kudin, J. C. Burant, J. M. Millam, S. S. Iyengar, J. Tomasi, V. Barone, B. Mennucci, M. Cossi, G. Scalmani, N. Rega, G. A. Petersson, H. Nakatsuji, M. Hada, M. Ehara,

K. Toyota, R. Fukuda, J. Hasegawa, M. Ishida, T. Nakajima, Y. Honda, O. Kitao, H. Nakai, M. Klene, X. Li, J. E. Knox, H. P. Hratchian, J. B. Cross, V. Bakken, C. Adamo, J. Jaramillo, R. Gomperts, R. E. Stratmann, O. Yazyev, A. J. Austin, R. Cammi, C. Pomelli, J. W. Ochterski, P. Y. Ayala, K. Morokuma, G. A. Voth, P. Salvador, J. J. Dannenberg, V. G. Zakrzewski, S. Dapprich, A. D. Daniels, M. C. Strain, O. Farkas, D. K. Malick, A. D. Rabuck, K. Raghavachari, J. B. Foresman, J. V. Ortiz, Q. Cui, A. G. Baboul, S. Clifford, J. Cioslowski, B. B. Stefanov, G. Liu, A. Liashenko, P. Piskorz, I. Komaromi, R. L. Martin, D. J. Fox, T. Keith, M. A. Al-Laham, C. Y. Peng, A. Nanayakkara, M. Challacombe, P. M. W. Gill, B. Johnson, W. Chen, M. W. Wong, C. Gonzalez, and J. A. Pople, Gaussian 03, Revision C.02, Gaussian, Inc., Wallingford CT, 2004.

[189] V. G. Malkin, O. L. Malkina, L. A. Eriksson, and D. R. Salahub in *Modern Density Functional Theory; A Tool for Quantum Chemistry Vol. 2.*, ed. J. M. Seminario and P. Poltzer; Elsevier, Amsterdam, 1995.

[190] JMOL: an open-source Java viewer for chemical structures in 3D., http://www.jmol.org.

[191] http://www.nongnu.org/xmakemol/.

[192] http://www.gnuplot.info/.

[193] VMD is developed with NIH support by the Theoretical and Computational Biophysics group at the Beckman Institute, University of Illinois at Urbana-Champaign, 1996.

[194] G. Schaftenaar and J. Noordik, *J. Comput.-Aided Mol. Design*, 2000, **14**, 123–134.

[195] H. W. Kroto, J. R. Heath, S. C. O'Brien, R. F. Curl, and R. E. Smalley, *Nature*, 1985, **318**, 162–163.

[196] M. P. Johansson, J. Jusélius, and D. Sundholm, *Angew. Chem. Int. Ed.*, 2005, **44**, 1843–1846.

[197] J. R. Heath, S. C. O'Brien, Q. Zhang, Y. Liu, R. F. Curl, H. W. Kroto, F. K. Tittel, and R. E. Smalley, *J. Am. Chem. Soc.*, 1985, **107**, 7779–7780.

[198] K. Laasonen, W. Andreoni, and M. Parrinello, *Science*, 1992, **258**, 1916–1918.

[199] S. Stevenson, G. Rice, T. Glass, K. Harich, F. Cramer, M. Jordan, J. Craft, E. Hadju, R. Bible, M. M. Olmstead, K. Maitra, A. J. Fischer, and A. L. Balch, *Nature*, 1999, **401**, 55–57.

[200] M. Krause, H. Kuzmany, P. Georgi, L. Dunsch, K. Vietze, and G. Seifert, *J. Chem. Phys.*, 2001, **115**, 6596–6605.

[201] M. Krause, M. Hulman, H. Kuzmany, O. Dubay, G. Kresse, K. Vietze, G. Seifert, C. Wang, and H. Shinohara, *Phys. Rev. Lett.*, 2004, **93**, 137403: 1–4.

[202] M. Krause, A. Popov, and L. Dunsch, *ChemPhysChem*, 2006, **7**, 1734–1740.

[203] M. Takata, E. Nishibori, M. Sakata, M. Inakuma, E. Yamamoto, and H. Shinohara, *Phys. Rev. Lett.*, 1999, **83**, 2214–2217.

[204] J. Rahmer, L. Dunsch, H. Dorn, J. Mende, and M. Mehring, *Magn. Reson. Chem*, 2005, **43**, S192–S198.

[205] Y. Iiduka, T. Wakahara, T. Nakahodo, T. Tsuchiya, A. Sakuraba, Y. Maeda, T. Akasaka, K. Yoza, E. Horn, T. Kato, M. T. H. Liu, N. Mizorogi, K. Kobayashi, and S. Nagase, *J. Am. Chem. Soc.*, 2005, **127**, 12500–12501.

[206] V. C. Parekh and P. C. Guha, *J. Indian Chem. Soc.*, 1934, **11**, 95–100.

[207] H. Takaba, H. Omamoto, J. Bouffard, and K. Itami, *Angew. Chem. Int. Ed.*, 2009, **48**, 6112–6116.

[208] R. Jasti, J. Bhattacharjee, J. B. Neaton, and C. R. Bertozzi, *J. Am. Chem. Soc.*, 2008, **130**, 17646–17647.

[209] D. Sundholm, S. Taubert, and F. Pichierri, *Phys. Chem. Chem. Phys.*, 2010, **12**, 2751–2757.

[210] D. Ajami, O. Oeckler, A. Simon, and R. Herges, *Nature*, 2003, **426**, 819–821.

[211] C. Castro, Z. Chen, C. S. Wannere, H. Jiao, W. L. Karney, M. Mauksch, R. Puchta, N. J. R. van Eikema Hommes, and P. von Ragué Schleyer, *J. Am. Chem. Soc.*, 2005, **127**, 2425–2432.

[212] D. Ajami, K. Hess, F. Köhler, C. Näther, O. Oeckler, A. Simon, C. Yamamoto, Y. Okamoto, and R. Herges, *Chem. Eur. J.*, 2006, **12**, 5434–5445.

[213] S. Shimizu, N. Aratani, and A. Osuka, *Chem. Eur. J.*, 2006, **12**, 4909–4918.

[214] H. S. Rzepa, *Org. Lett.*, 2008, **10**, 949–952.

[215] C. S. M. Allan and H. S. Rzepa, *J. Org. Chem.*, 2008, **73**, 6615–6622.

[216] A. Allmenningen, O. B. L. Fernholt, B. N. Cyvin, S. J. Syvin, and S. Samdal, *J. Mol. Struct.*, 1985, **128**, 59–76.

[217] V. R. I. Kaila, M. P. Johansson, L. Laakkonen, and M. Wikström, *Biochim. Biophys. Acta*, 2009, **1787**, 221–233.

[218] P. B. Karadakov, *J. Phys. Chem. A*, 2008, **112**, 7303–7309.

[219] A. N. Alexandrova, A. I. Boldyrev, H. J. Zhai, and L. S. Wang, *Coord. Chem. Rev.*, 2006, **250**, 2811–2866.

[220] K. K. Baeck and R. J. Bartlett, *J. Chem. Phys.*, 1998, **109**, 1334–1342.

[221] M. D. Wodrich, C. Corminboeuf, S. S. Park, and P. von Ragué Schleyer, *Chem. Eur. J.*, 2007, **13**, 4582–4593.

[222] T. O. Pennanen and J. Vaara, *J. Chem. Phys.*, 2005, **123**, 174102:1–10.

[223] T. Heine, K. Vietze, and G. Seifert, *Magn. Reson. Chem.*, 2004, **42**, 199–201.

[224] Y. Yamazaki, K. Nakajima, T. Wakahara, T. Tsuchiya, M. O. Ishitsuka, Y. Maeda, T. Akasaka, M. Waelchli, N. Mizorogi, and S. Nagase, *Angew. Chem. Int. Ed.*, 2008, **47**, 7905–7908.

[225] D. Liu, F. Hagelberg, and S. S. Park, *Chem. Phys.*, 2006, **330**, 380–386.

[226] F. Feixas, E. Matito, J. Poater, and M. Sola, *J. Comput. Chem.*, 1998, **29**, 1543–1554.

[227] A. Stanger, *Chem. Commun.*, 2009, 1939–1947.

[228] S. Pelloni, P. Lazzeretti, and R. Zanasi, *J. Phys. Chem. A*, 2007, **111**, 8163–8169.

[229] S. Winstein, *J. Am. Chem. Soc.*, 1959, **81**, 6524–6525.

[230] R. F. Childs, *Acc. Chem. Res.*, 1984, **17**, 347–352.

[231] G. Monaco and R. Zanasi, *J. Chem. Phys.*, 2009, **131**, 044126:1–10.

[232] S. Fias, P. W. Fowler, J. L. Delgado, U. Hahn, and P. Bultinck, *Chem. Eur. J.*, 2008, **14**, 3093–3099.

[233] A. T. Balaban, D. E. Bean, and P. W. Fowler, *Acta Chim. Slov.*, 2010, **57**, 507–512.

[234] S. Ikäläinen, P. Lantto, P. Manninen, and J. Vaara, *Phys. Chem. Chem. Phys.*, 2009, **11**, 11404–11414.

[235] H. Fliegl, O. Lehtonen, D. Sundholm, and V. R. I. Kaila, *Phys. Chem. Chem. Phys.*, 2011, **13**, 434–437.

[236] A. Soncini, A. M. Teale, T. Helgaker, F. De Proft, and D. J. Tozer, *J. Chem. Phys.*, 2008, **129**, 074101:1–15.